State of Health Estimation and Prediction for Lithium-ion Batteries Based on Transfer Learning

Che, Yunhong

DOI (link to publication from Publisher):
10.54337/aau679680715

Publication date:
2023

Document Version
Publisher's PDF, also known as Version of record

STATE OF HEALTH ESTIMATION AND PREDICTION FOR LITHIUM-ION BATTERIES BASED ON TRANSFERLEARNING

BY
YUNHONG CHE

DISSERTATION SUBMITTED 2023

AALBORG UNIVERSITY
DENMARK

STATE OF HEALTH ESTIMATION AND PREDICTION FOR LITHIUM-ION BATTERIES BASED ON TRANSFER LEARNING

by

Yunhong Che

AALBORG UNIVERSITY
DENMARK

Dissertation submitted

.

Dissertation submitted:	December 2023
PhD supervisor:	Professor Remus Teodorescu Aalborg University
Co-supervisor:	Dr. Xin Sui Aalborg University
PhD committee:	Professor Huai Wang (chairman) Aalborg University, Denmark Associate Professor Changfu Zou Chalmers University of Technology, Sweden Associate Professor Chresten Træholt Technical University of Denmark, Denmark
PhD Series:	Faculty of Engineering and Science, Aalborg University
Department:	AAU Energy

ISSN (online): 2446-1636
ISBN (online): 978-87-7573-582-2

Published by:
Aalborg University Press
Kroghstræde 3
DK – 9220 Aalborg Ø
Phone: +45 99407140
aauf@forlag.aau.dk
forlag.aau.dk

Printed in Denmark by Stibo Complete, 2023

CV

Yunhong Che received the B.E. and M.S. degrees from the College of Mechanical and Vehicle Engineering, Chongqing University, Chongqing, China, in 2019 and 2021, respectively. He is currently pursuing the Ph.D. degree with the Department of Energy, Aalborg University, Aalborg, Denmark. He was a visiting student researcher with the Institute of Civil Engineering at Swiss Federal Institute of Technology in Lausanne (EPFL), Lausanne, Switzerland, and the Department of Energy Science & Engineering at Stanford University, Stanford, CA, USA, in 2023.

He won the 2023 Automotive Innovation Best Paper Award. He serves as a special session chair in ECCE-Asia 2024, and reviewer for more than 15 top-tier journals. His research interests include battery health estimation and prediction, fault diagnostics, physics-informed machine learning in modeling and prognostics, and intelligent control and management for energy storage systems.

ENGLISH SUMMARY

Emerging developments in electrified transportation and renewable energy storage promote large-scale applications of lithium-ion batteries. It is significant and practically demanded to model and monitor the states of batteries in battery management systems since internal states cannot be measured directly. Health states are of vital importance to ensure safe operations and guide optimal control and management. On the other hand, the rapid development of artificial intelligence brings new opportunities for data-driven health prognostics for batteries despite complex electrochemical modeling. However, most of the works rely heavily on large amounts of training datasets and have poor generalization abilities, which motivates this Ph.D. project to develop advanced transfer learning-based battery health prognostics with limited labels to improve model performances under various application scenarios.

Aging experiments are conducted to test the degradation behaviors of different battery types with various loadings and temperature conditions including dynamic loading profiles and variable temperatures. Both fresh batteries and second-life batteries are used for testing and the aging behaviors under different conditions are analyzed. To consider practical application requirements, partial curves are used for feature extractions. Data cleaning strategy is investigated to ensure the features can be effectively extracted under different loading profiles. The fine-tuning strategy, which only uses sparsely labeled data from the testing batteries, helps improve estimated accuracy and reliability. This is valuable for industrial applications where only limited and sparse labeled data can be obtained during maintenance. In addition, by leveraging the pretext-learning only using unlabeled operating data, the downstream health estimation task obtains satisfactory results by fine-tuning the model with only a few sparse labeled samples.

Regarding the unlabeled data, another strategy named domain adaptation is investigated for performance improvement. In this regard, labels from the target batteries are not necessarily required, while the model generalization can be improved by reducing the domain discrepancies based on aligning the learned domain invariant features. Another main problem of conventional machine learning is catastrophic forgetting, which is solved by the proposed domain adaptative continual learning. The model is improved continuously during applications under various working conditions by only using sparsely labeled data. The model can be interpreted by the post-hoc analysis of the domain invariant features under different current rates and temperature conditions. Therefore, only one model initiated from one condition is used for the generalization improvement to satisfy the estimation under various application scenarios.

Health prediction with transfer learning is also investigated to be proven performance improvement. Reconstrued pseudo capacities support the fine-tuning of the

degradation trajectory prediction model. Therefore, the degradation of battery capacity can be predicted with sequential predictions without the requirement of continuous labeled capacities for modeling. In addition, domain adaptation is also integrated with a multi-task framework to predict the future trajectory with the extrapolation of features without capacity labels. Furthermore, a long-term regularization penalty is investigated to ensure stable predictions, solving the challenge of accumulated errors during recursive predictions.

Finally, the predictive health assessment strategy is proposed to detect accelerating aging. Probabilistic point and sequence predictions collaborated to judge the accelerating aging stages that help guide predictive management. In addition, different prognostic tasks, such as lifetime prediction, knee prediction, as well as onboard health status and aging rate predictions are integrated by the multi-task learning. The model integration is improved while different prognostics can be obtained via one model to reduce the requirement of resources of storage and computation, thus promoting practical applications. The concept of cloud-edge is also adopted for the base model training using cloud and updating on the edge device.

Overall, by investigating the roles of advanced transfer learning strategies in battery health prognostics, the accuracy, reliability, and generalization of machine learning models are improved while the requirement of labeled data is reduced. Therefore, the findings from this Ph.D. project will help promote the next generation of intelligent battery management.

DANSK RESUME

Udviklingen inden for elektrificeret transport og lagring af vedvarende energi fremmer omfattende vedtagelse af lithium-ion-batterier. Det er betydningsfuldt og praktisk nødvendigt at modellere og overvåge batteriers tilstande i batteristyringssystemer, da interne tilstande ikke kan direkte måles. Tilstanden af batterier er af vital betydning for at sikre sikker drift samt optimal kontrol og styring. På den anden side bringer den hurtige udvikling af kunstig intelligens nye muligheder for data-drevne sundhedsprognoser for batterier på trods af kompleks elektrokemisk modellering. Dog baserer de fleste værker sig i høj grad på store mængder træningsdatasæt og har dårlige generaliseringsfærdigheder, hvilket motiverer dette ph.d.-projekt til at udvikle avancerede transfer learning-baserede batterisundhedsprognoser kun ved hjælp af begrænsede etiketter for at forbedre modelpræstationerne under forskellige anvendelsesscenarier.

Aldringseksperimenter udføres for at teste nedbrydningsadfærdene af forskellige batterityper under forskellige belastninger og temperaturforhold, herunder dynamiske belastningsprofiler og variable temperaturer. Både nye batterier og batterier med andet liv anvendes til test, og aldrende adfærd under forskellige betingelser analyseres. For at tage hensyn til praktiske anvendelseskrav bruges delkurver til feature-ekstraktion. Der undersøges en strategi for datarensning for at sikre, at funktionerne kan ekstraheres effektivt under forskellige belastningsprofiler. Finjusteringsstrategien, der kun bruger sparsomt etiketterede data fra testbatterierne, hjælper med at forbedre den estimerede nøjagtighed og pålidelighed. Dette er værdifuldt for industrielle anvendelser, hvor kun begrænsede og sparsomt etiketterede data kan opnås under vedligeholdelse. Derudover opnår sundhedsestimeringsopgaven tilfredsstillende resultater ved at finjustere modellen med kun få sparsomt etiketterede prøver ved at udnytte for-læringsmetoden kun ved hjælp af ikke-etiketterede driftsdata.

Hvad angår de ikke-etiketterede data, undersøges en anden strategi ved navn domæneadaptation for ydeevneforbedring. I denne henseende er etiketter fra målbatterierne ikke nødvendigvis påkrævet, mens modellens generalisering kan forbedres ved at reducere domæneforskelle baseret på at justere de indlærte domæneinvariante funktioner. Et andet hovedproblem ved konventionel maskinlæring er katastrofal glemsel, hvilket løses ved den foreslåede domæne af adaptiv kontinuerlig læring. Modellen forbedres kontinuert under anvendelser under forskellige arbejdsbetingelser ved kun at bruge sparsomt etiketterede data. Modellen kan fortolkes ved den post-hoc analyse af de domæneinvariante funktioner under forskellige strømniveauer og temperaturforhold. Derfor bruges kun én model, der er startet fra én betingelse, til at forbedre generaliseringen og opfylde estimatet under forskellige anvendelsesscenarier.

Sundhedsprediktion med transfer learning undersøges også for at bevise præstationsforbedring. Genopbyggede pseudokapaciteter understøtter finjustering af modellen til forudsigelse af nedbrydningsbanen. Derfor kan kapacitetens nedbrydning forudsiges med sekventielle forudsigelser uden krav om kontinuerligt etiketterede kapaciteter til modellering. Derudover integreres domæneadaptation også med en multitask ramme for at forudsige den fremtidige bane med ekstrapolering af funktioner uden kapacitetsetiketter. Desuden undersøges en langsigtet reguleringssanktion for at sikre stabile forudsigelser og løse udfordringen med akkumulerede fejl under rekursive forudsigelser.

Endelig foreslås strategien for forudsigelig sundhedsvurdering for at registrere accelererende aldring. Sandsynlige punkt- og sekvensforudsigelser samarbejder om at bedømme de accelererende aldrende stadier, der hjælper med at guide forudsigelig ledelse. Derudover integreres forskellige prognostiske opgaver, såsom levetidsforudsigelse, knæforudsigelse samt prognose for on-board sundhedstilstand og aldringshastighed ved hjælp af multitask læring. Modelintegrationen forbedres, mens forskellige prognoser kan opnås via én model for at reducere kravet til lagring og beregning af ressourcer og dermed fremme praktiske anvendelser. Konceptet med cloud-edge anvendes også til grundmodeltræning ved hjælp af cloud og opdatering på kantenheden. Samlet set forbedres nøjagtigheden, pålideligheden og generaliseringen af maskinlæringsmodeller ved at undersøge rollerne af avancerede transfer learning-strategier inden for batterisundhedsprognoser, mens kravet til etiketterede data reduceres. Derfor vil resultaterne fra dette ph.d.-projekt bidrage til at fremme næste generation af intelligent batteristyring.

ACKNOWLEDGEMENTS

I would like to express my deepest gratitude to all those who have provided assistance and advice to me during the completion of my doctoral research and dissertation. I would like to begin by expressing my heartfelt gratitude to my wife, who has been the unwavering pillar of support that has allowed me to persist in my research and exploration. Whenever I faced challenges, moments of low spirits, or even contemplated giving up, it was her unwavering encouragement that propelled me forward. Even though we have been separated by great distances, you have remained the sanctuary of my soul. I am also grateful for your patience and understanding during times when my temper got the better of me. You have shouldered the responsibilities of our home and daily life, even while managing your own demanding career, and for this, I am deeply appreciative. I commit to assuming more responsibilities in our future life together, believing that, with each other's company, we can create a brighter future. Your love, support, and understanding have been the driving force behind my journey, and I cherish the life we have built together. Thank you for being my rock and my guiding light. My parents and all of my family members have also provided me with abundant care and assistance on my educational journey, supporting me as I persevered with determination.

Next, I want to express my gratitude to my advisor, Prof. Remus Teodorescu, who is a mentor I deeply admire. From the very first day of my enrollment, you have shown a personal interest in my research, regularly engaging in discussions about my progress, and providing the best technical and hardware support to ensure I could confidently tread the right path. You are not only a dedicated guide but also a caring elder. You have shown genuine concern for my well-being, worrying about whether I was under excessive stress, in need of more rest and holidays, and even facilitating opportunities for me to engage in academic exchanges elsewhere, which has had a significant impact on my professional development. I would also like to extend my heartfelt appreciation to my mentors during my academic exchanges at Stanford University, Prof. Simona Onori, and at the Swiss Federal Institute of Technology in Lausanne (EPFL), Prof. Olga Fink. I am immensely grateful for the opportunities you provided me to study at some of the world's top institutions. During my time there, I acquired invaluable skills, achieved personal growth, and enriched my research, which has been a lasting benefit to me. These experiences have left an indelible mark on my academic and professional journey. Prof. Xiaosong Hu, whom I have always needed to thank. It is your guidance and assistance that have afforded me the opportunity to be on the verge of completing my doctoral degree today. You have been the guiding light throughout my research career, leading the way and directing my path towards success.

I also would like to thank the Villum Foundation, which supports me to accomplish my Ph.D. project, attend research conferences, publish papers, and study abroad. It is your support that I can successfully finish my thesis. I also want to express my gratitude to the finial support from AAU doctoral school and OTTO Foundation to support these activities. I also would like to thank my co-supervisor Dr. Xin Sui, my friend Yusheng Zheng and all my colleagues from AAU Smart Battery group. Thanks for the support for my research and valuable comments to help me finish my thesis. Hope we can promote the advanced development of our group together in the future. In addition, it is my pleasure to meet my friends from Be Mars group. We are like-minded friends, and it's been a pleasure working and struggling with you, and I hope we can accomplish our goals together!

Lastly, I want to express my gratitude to all the friends and colleagues who have been with me every step of the way. Your support has been invaluable in my academic pursuits, research endeavors, and daily life, enabling me to thrive and grow in a foreign land. We have worked hard together, shared our thoughts and dreams, celebrated together, and explored the world together, and these moments have been the most precious part of my international student experience. I hope that each and every one of you, my friends and colleagues, will have a bright future, shining brightly in your respective places all around the world. I would like to express my heartfelt gratitude to the three esteemed professors on the defense committee. Thank you for taking time out of your busy schedules to review my thesis and for offering invaluable insights that will significantly improve the quality of the dissertation.

Yunhong Che   Yunhong Che

Winter 2023 at Stanford

TABLE OF CONTENTS

LIST OF ABBREVIATIONS

ANN	Artificial neural network
BMSs	Battery management systems
BNN	Bayesian neural network
CNN	Convolutional neural network
CI	Confidence interval
CL	Continual learning
DT	Differential temperature
DL	Deep learning
DA	Domain adaptation
EOL	End of life
ECM	Equivalent circuit model
EM	Electrochemical model
EMD	Empirical Mode Decomposition
EEM	Empirical Exponential Model
GA	Genetic algorithm
GPR	Gaussian process regression
GRU	Gated recurrent unit
HIs	Health indicators
IC	Incremental capacity
KF	Kalman filter
LS	Least square
LR	Linear regression
LSTM	Long-short-term-memory
MHE	Moving horizon estimation
MMD	Maximum mean discrepancy
MLP	Multilayer perceptron
MTL	Multi-task learning
ML	Machine learning
MAE	Mean absolute error
MSE	Mean square error
MaxAE	Maximum Absolute Error
PHM	Prognostics and health management
PF	Particle filter
PSO	Particle swarm optimization
PCC	Pearson correlation coefficient
Q-V	Capacity-voltage
RUL	Remaining useful life
RF	Random forest
RVR	Relevant vector regression
RNN	Recurrent neural network
RMSE	Root-mean-square error

R2	Coefficient of determination
RKHS	Reproducing kernel Hilbert space
SOH	State of health
SOC	State of charge
SVR	Support vector regression
STS	Sequence-to-sequence
STP	Sequence-to-point
SSSL	Semi-supervised self learning
SD	Source domain
TD	Target domain
TL	Transfer learning

LIST OF FIGURES

LIST OF TABLES

PART I REPORT

CHAPTER 1. INTRODUCTION

Publications J1 and J2 contribute to the background and state of the art in this chapter.

1.1. BACKGROUND

Lithium-ion batteries, being a primary energy storage source, have posed constraints on the progress of electric vehicles, electric ships, and electric aircraft [1], [2]. Electrification of transportation plays a pivotal role in reducing exhaust emissions, alleviating the concerns of overreliance on fossil fuels, energy scarcity, and environmental pollution [3], [4]. Furthermore, lithium-ion batteries find extensive application in commercial satellites, portable electric devices, smart grids, etc. [5]–[8]. However, due to the dynamic, time-varying, and nonlinear characteristics of lithium-ion batteries, their internal electrochemical mechanism continues to be complex [9], [10]. Alongside the primary reactions for charging and discharging, side reactions associated with aging transpire simultaneously [11]. The battery capacity experiences gradual degradation, while internal resistance increases with storage and usage [12], [13]. Constrained battery lifespan stands as a pivotal obstacle that hinders the widespread commercial adoption across the aforementioned applications and battery aging may even trigger safety issues [14]. However, battery failures or end-of-life (EOL) can be extended with optimal management as well as ensure safe operations [15]. Hence, the development of battery management systems (BMSs) aims to achieve accurate and reliable health estimation and prediction. Additionally, prognostics and health management (PHM) as one main function of BMSs seeks to diagnose and prognose the health of batteries and devise optimization strategies that effectively prolong the operational lifespan [16], [17].

Nonetheless, lithium-ion batteries remain somewhat enigmatic, often labeled as "black boxes" due to the challenge of directly measuring their internal aging states. Consequently, the internal states necessitate estimation through algorithms reliant on measured parameters. Battery health prognostics predominantly encompass estimations of State of Health (SOH) and predictions of lifetime or Remaining Useful Life (RUL). SOH generally refers to the ratio of the currently available capacity to the nominal or fresh capacity [18]. RUL or lifetime is determined by the remaining operational cycles prior to reaching EOL, which is commonly associated with the cycle at which SOH falls to 80% or 70% [19], [20]. In recent years, health prognostics for batteries have garnered wide interest and substantial significance. By thoroughly investigating degradation mechanisms and extracting valuable aging features, it becomes possible to develop real-time and non-destructive and health prognostic methods for lithium-ion batteries. For detailed aging mechanisms, please refer to the J1 and J2 published by the author. Accurate and reliable battery health prognostics offer effective means to establish timely maintenance strategies, which help ensure safe and reliable operations [21].

1.2. BATTERY HEALTH PROGNOSTICS

Various methodologies exist for battery health prognostics, typically categorized as model-based, data-driven, or hybrid methods [22]. In this chapter, we first introduce different objectives, namely SOH estimation, EOL point prediction, and degradation trajectory predictions. The specific methods within each objective are described. The distinct aims of these three objectives, as depicted on one representative capacity curve, can be visualized in Fig. 1-1. At the current *k*th cycle, SOH estimation concentrates on estimating the current available capacity, performing as a short-term prognostic task. Conversely, EOL prediction pertains to the eventual cycle point when the battery reaches its EOL, encompassing a long-term point predictive goal. Degradation trajectory prediction is primarily concerned with forecasting future degradations until EOL, representing long-term sequence prediction.

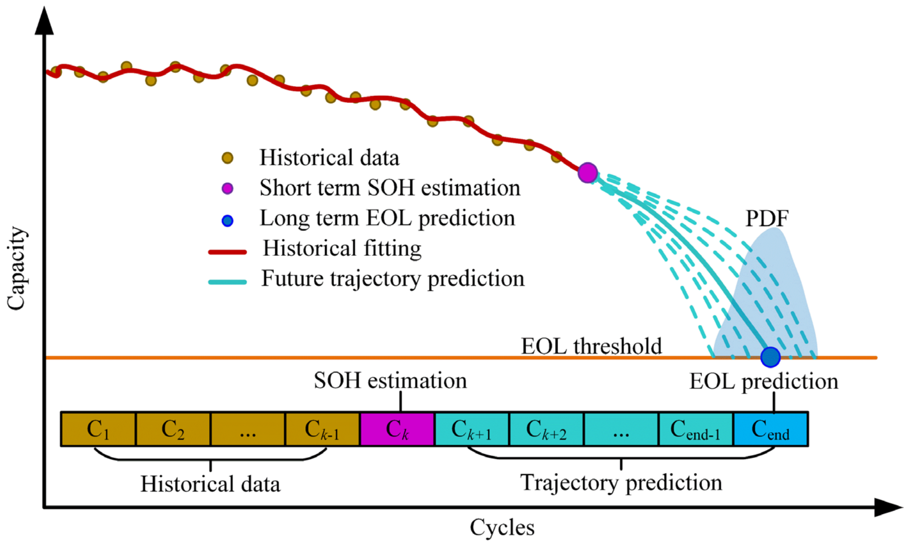

Figure 1-1 Illustration of three main battery health prognostic objectives. Source: [J1]

The comprehensive categorization of battery health prognostics is visualized in Fig. 1-2. Within SOH estimation, two method types are encompassed: model parameter optimization and machine learning (ML). For EOL prediction, the prevalent usage involves data-driven methods, which are subsequentially subdivided into feature-based and deep learning (DL), differing based on the manual or automatic extraction of features. Lastly, degradation trajectory prediction is comprised of three distinct methods: curve fitting, model generation, and sequence prediction. Within this categorization framework, people could initially identify their prognostic objective and then consult the corresponding methods.

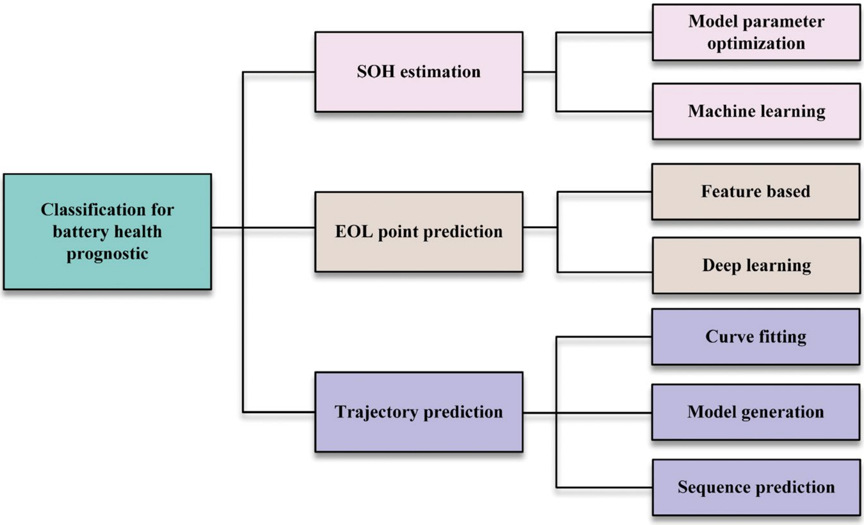

Figure 1-2 Battery health prognostic objectives and methodologies. Source: [J1]

1.2.1. SOH ESTIMATION.

Short-term capacity or resistance estimations are the main concern in SOH estimation. Estimating SOH accurately offers insights into the battery's health status at the present moment and updates critical parameters for other state estimations, such as state of charge (SOC), aiding in the design of optimal management strategies, and so on [23]. Model parameter optimization and ML are the two mainstream SOH estimation methods. The overall procedure of these two methods for battery SOH estimation is visualized in Fig. 1-3. SOH is defined as the ratio of the current available capacity (C_k) to the fresh capacity (C_0) in this thesis [24], which is given below.

$$\mathrm{SOH}=C_k / C_0 \tag{1.1}$$

1.2.1.1 Model parameter optimization

Model parameter optimization method typically involves integrating a battery model with a parameter identification/estimation algorithm to assess the health status. Models employed for such estimation encompass the empirical model, equivalent circuit model (ECM), and electrochemical model (EM). An expression capturing quantifiable relationships between affecting factors and SOH is generally built by the empirical model, determined through experimental fitting [25]. ECM is constructed using representative electrical components to elucidate battery behavior [26], while EM is founded on fundamental principles, depicting dynamics of internal electrochemical reactions by partial differential equations [27], [28]. It is generally agreed upon that as one moves from the empirical model to ECM and then to EM, accuracy has improved gradually while complexity has increased. Within empirical models, parameters to be estimated generally comprise fitting coefficients, whereas the other two involve specific physical/electrochemical parameters to be determined [29]. The most popular and well-developed methods for parameter identification/estimation are the Kalman filter (KF), particle filter (PF), and their respective derivatives [30]–[32]. Variants of KF encompass the extended, unscented, sigma point, cubic, and their amalgamation with adaptive frameworks. Improved performances are also observed with techniques like unscented PF and adaptive PF. Comparatively less frequently used but still, effective methods include least square (LS), sliding mode observer, genetic algorithm (GA), H-infinity filter, moving horizon estimation (MHE), particle swarm optimization (PSO), etc. [33]–[35]. Despite the diverse algorithm ranges, the common goal is to accurately estimate/identify the relevant parameters to facilitate precise SOH estimation. To conclude, the general procedure for SOH estimation with parameter optimization can be demonstrated in Fig. 1-3.

1.2.1.2 Machine learning

Nonetheless, striking a balance between model complexity and accuracy proves industrial application challenges of model-based methods. As a result, ML-based approaches, devoid of explicit models, have gained substantial traction in recent times [36]. These methods seek to establish nonlinear relationship mappings between the chosen inputs and desired SOH. However, the absence of a physical explanation stands out as a significant limitation. The typical procedure for battery SOH estimation with ML encompasses data preprocessing, model training, and validation [37], as depicted in Fig. 1-3. According to the inputs, existing methodologies can be categorized into feature-based and feature-free methods, as both aim to provide the SOH as output.

Feature-based methods entail the manual extraction of features, also referred to as health indicators (HIs) [38]. HIs are features derived from measured or estimated parameters to represent battery aging [39]. HIs extraction can be categorized into direct extraction from measured parameters [40]–[42], and indirect calculated data [43]–[45]. In addition to time series HIs, histogram data-based HIs are also effective, especially for field data [46]. Correlation coefficient analysis is a prevalent method for selecting effective HIs for the input of ML-based SOH estimation model [47]. However, HIs selected solely based on correlation analysis can be highly redundant, necessitating the removal of some redundant HIs from the subset [37]. Methods involve employing optimal search approaches to select HIs, like the wrapper method. Linear regression (LR) and multi-linear regression (MLR) methods are appropriate choices for modeling, given that HIs generally exhibit high linear correlations with SOH [48]. Moreover, various nonlinear mapping algorithms perform better, including support vector regression (SVR), random forest (RF) regression, and various artificial neural networks (ANN). In addition, gaussian process regression (GPR) and relevant vector regression (RVR) are commonly utilized to provide probabilistic estimations with Bayesian theories [49]–[52]. The constructed model is finally used to estimate SOH of the testing batteries for the evaluation of accuracy, reliability, and onboard application ability.

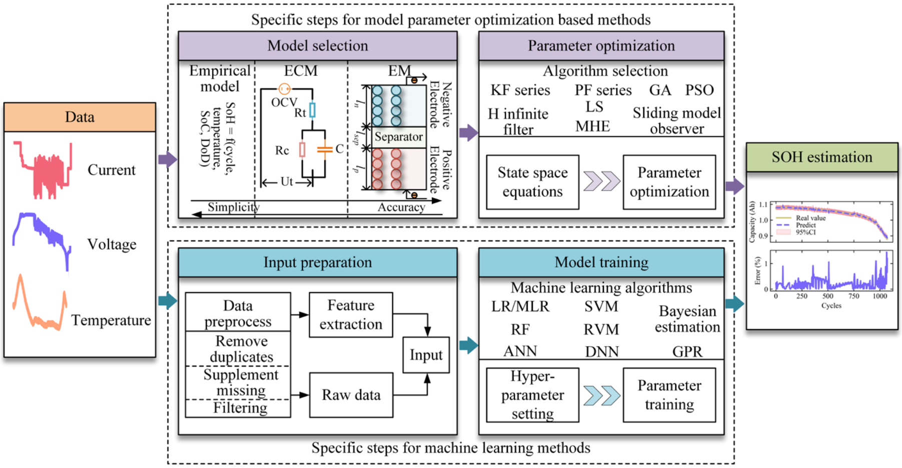

Figure 1-3 Methods and general framework for battery SOH estimation. Source: [J1]

Feature-free methods denote data-driven battery SOH estimations without involving manual HIs extraction and selection. HIs based on manual extraction methods are often sensitive to certain parameters and can struggle with generalization across various testing conditions. Furthermore, the variability of HIs from one condition to another can lead to poor generalization. Additionally, finding ideal HIs can be challenging. To mitigate these issues, researchers opt to employ measured data directly for ML, enabling the model to autonomously uncover relative features, which necessitate robust nonlinear capabilities, making DL methods the favored option [53]. Autoencoders and multi-layer decoders are prominent for this purpose. In addition, recurrent neural networks (RNN) and convolutional neural networks (CNN) have demonstrated satisfactory capabilities in this context [54]. In this approach, the model is trained directly using measured parameters to estimate SOH. However, the computational burden is generally higher than those of feature-based methods.

1.2.2. END OF LIFE PREDICTION.

In the context of long-term predictions, the first category is referred to EOL prediction, which aims at predicting the EOL/lifetime. Two kinds of ML methods including feature-based and DL, whose process diagrams are displayed in Fig. 1-4. Given that EOL prediction typically involves multiple batteries, the majority of methods employed fall under the data-driven category. The key distinction lies in whether manual feature engineering is conducted and the subsequent use of ML models.

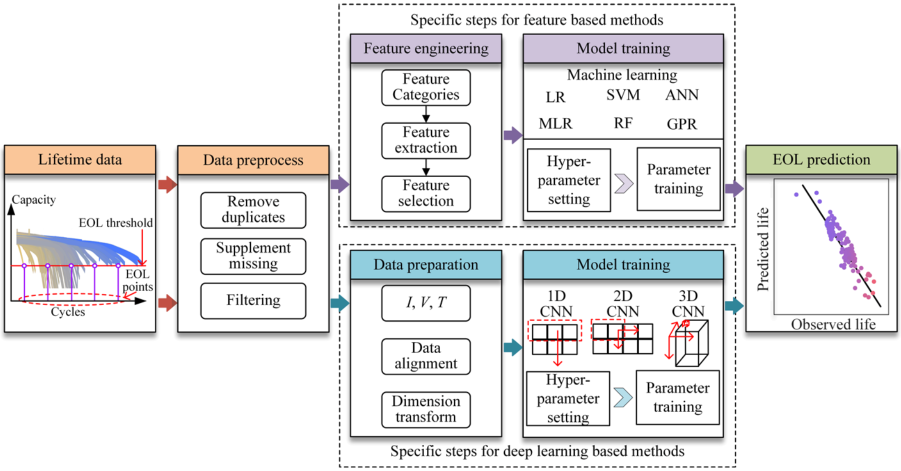

Figure 1-4 Methods and general framework for battery EOL point prediction. Source: [J1]

1.2.2.1 Feature-based

The fundamental concept behind feature-based methods is to initially extract specific HIs. Subsequently, these extracted features are employed to model the mapping with battery lifetime using ML [55], [56]. The comprehensive framework for this approach is depicted in Fig. 1-4, encompassing five essential steps. Firstly, battery data collected is pre-processed to ensure quality and consistency. Then, diverse features are extracted, guided by aging correlation analysis of parameters. Common extraction methods extract features from voltages, currents, internal resistance, capacities, and temperatures. Nevertheless, the resulting feature matrix is often multi-dimensional, leading to some exhibiting weak correlations with battery lifetime and others demonstrating high redundancy [37]. Therefore, the third step is aiming at selecting an optimal subset of features. Four popular methods for feature selection include filter-based, wrapper-based, embedded-based, as well as fusion-based techniques [57]. Subsequently, selected features are used to construct a mapping with battery lifetime through various ML models, where the above SOH estimation techniques are also suitable [58]. Finally, the data-driven model is evaluated using testing datasets. Feature-based ML methods for EOL prediction and SOH estimation appear analogous. The key distinction lies in the source of the data for feature extraction. Features are extracted from data of one battery within each cycle in SOH estimation. In contrast, features are derived from numerous batteries in their early cycles under similar working conditions when considering EOL predictions. In essence, SOH estimation involves mapping the relationships between features and SOH across multiple cycles for an individual battery, while EOL prediction maps the connection between features and EOL for a particular battery type aging under comparable operational conditions.

1.2.2.2 Deep learning approaches

EOL prediction with feature-based approaches necessitates specific feature extraction, which significantly influences accuracy and generalization. However, these extracted features are notably influenced by battery types and operational scenarios. Hence, prediction methods based on DL approaches aim to automatically derive features from measured parameters utilizing deep neural networks [59], [60]. The foundational structure for DL-enabled EOL prediction is depicted in Fig. 1-4. The steps resemble those of feature-based methods, with the exception of feature engineering and ML models. This approach can be conceptualized as an end-to-end prediction, wherein measured data is directly and autonomously learned for the prediction of the target outcomes. The distinction between deep-learning-enabled SOH and EOL predictions lies in the nature of the data sources: either one battery running multiple cycles or multiple batteries (each with a single value), along with the nature of the output.

1.2.3. DEGRADATION TRAJECTORY PREDICTION.

While EOL prediction yields promising outcomes for early predictions, the acquired insights remain somewhat limited, lacking specifics about the degradation process at distinct aging stages. To address this limitation, degradation predictions aim to forecast future trajectory curves, thereby furnishing more comprehensive information for predictive maintenance. The three principal methods can be categorized as curve fitting, model generation, and sequence predictions. The typical processes for each of them are illustrated in Fig. 1-5.

1.2.3.1 Curve fitting of degradation trajectories

Curve fitting offers a straightforward approach to predicting battery trajectory and lifetime [61]. Typically, key influential factors on battery aging including operating cycles, current rates, temperature, depts of discharge, mean SOC, etc. are quantitively analyzed with battery aging experiments [62]. The mapping linking operating cycles and capacity is constructed. Frequently employed equations include exponential, polynomial, logarithmic functions, etc. Fitting parameters within these expressions are updated using historical available data. Common methods for this parameter update involve the PF series, KF series, GA, PSO, GA, etc. [63], [64]. The constructed model is then extrapolated with the increasing number of operating cycles to predict future capacities or resistances until a predefined threshold. Trajectory prediction with curve-fitting bears resemblance to empirical model-based SOH estimation. The distinction lies in the requirement for an extrapolation process to forecast future degradations. As a result, the primary focus of the model is to establish the correlation between operating cycles and factors such as capacity or power fade. Conversely, in the context of SOH estimation, the model encompasses additional information that can be gathered in each cycle, extending beyond these simple measurements. Furthermore, in addition to mathematical expressions used to depict battery degradation trajectories, data-driven techniques are also employed to establish the mappings between capacity or power degradation and the cycle number [65]. This mapped implicit model is subsequently extrapolated by incrementally increasing the number of cycles for the input, enabling the prediction of future capacity values within the context of degradation trajectory projection.

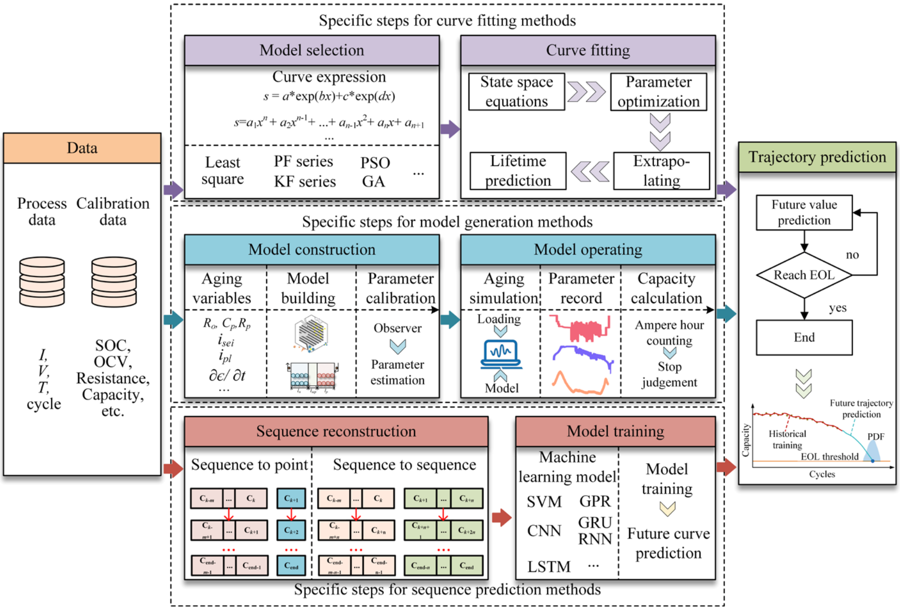

Figure 1-5 Methods and general framework for battery degradation trajectory predictions. Source: [J1]

1.2.3.2 Model generation-based methods

The core concept behind trajectory predictions with model generation is the construction of an EM or ECM that effectively represents actual batteries, enabling the simulation of future aging [66]. Typical procedures are illustrated in Fig. 1-5. Calibration of the model parameters must be conducted beforehand, where the parameter optimization methods discussed above can also be applied here. After calibrating the parameters, the model can be simulated with running cycles to generate synthetic data for future degradations. Consequently, both capacity degradation and operating data can be available [67], [68]. It's important to note that the generated data may differ based on varying aging conditions. The accuracy of the calibration significantly influences the models' performance and predictive accuracy. In contrast to model parameter optimization-based SOH estimation where acquired data is employed to identify parameters, the model generation approach utilizes the model to generate data for future cycles. The parameter variations over operating cycles are presumed to be known by experts. This methodology is often employed to support battery aging simulation. The future capacity trajectory and operating data can be simulated with the preset loading profiles, significantly reducing the labor and time consumption of real aging tests.

1.2.3.3 Sequence prediction based on machine learning

Battery degradation possesses a significant sequential relationship, which has paved the way based on sequence prediction techniques [69]. This approach can be further categorized into two sub-methods: recursive sequence-to-point (STP) prediction, and sequence-to-sequence (STS) prediction. The initial step involves reconstructing the original curve to create input and output sequences for both of the two methods. The fundamental procedure is depicted in Fig. 1-5. The underlying principle capitalizes on the inherent sequential variation properties of battery degradation [70]. ML or DL techniques are subsequently employed to establish the input-output relationships. For making future curve predictions, the recursive procedure is used in the STP prediction. In contrast, STS prediction framework utilizes one-shot prediction [71]. It's worth noting that the iterative method is also suitable for STS prediction when one prediction doesn't cover the whole demanded cycle. Given the challenge of measuring capacity directly in the real world, SOH estimation is often integrated before the sequence predictions. All the previously introduced SOH estimation methods can be applied to meet the requirements.

1.3. RESEARCH MOTIVATIONS

The general processes for each kind of methodology in each health prognostic objective have been summarized above. More detailed representative works and comprehensive comparisons among these methods can be found in J1. Although existing works show satisfactory prognostic effectiveness, there are still many challenges remaining in data preprocessing, feature extraction, ML model construction, as well as model generalization and implementation. The detailed research questions that motivated this project are summarized below.

Q1: Feature extraction is only specific for each kind of objective in the health prognostics while the general extraction method for all the three objectives is required. In addition, conventional feature extraction is not widely applicable with different loading profiles. Therefore, can we develop methods for general feature extraction for different battery types working with different loadings?

Q2: ML usually requires a huge amount of data for model training. However, it is very challenging to obtain sufficient labeled data in the real world while most of them are without labels. Furthermore, the model transferability and generalization ability are low, especially for different battery types and working conditions. Therefore, the next question is that can we improve model generalization under different scenarios with limited labeled data for model construction?

Q3: How battery SOH estimation benefits long-term SOH trajectory prediction is worth investigating to build the relationship between the two objectives. Similarly, the unlabeled data make it difficult for the capacity extrapolation method for future trajectory predictions. Furthermore, the recursive prediction is hard to be stable which may cause ineffective trajectory predictions. Therefore, the third question is what can we do to develop advanced strategies to eliminate the high reliance on labeled capacities and ensure long-term prediction abilities?

Q4: Predictive strategies are desired for guiding the early maintenance and health management of batteries that suffer from accelerating aging. However, the collaborative strategy for predictive health management considering both point and sequence predictions is still missing. That is, the implementation of battery health prognostics is not clear. Furthermore, ML model is supposed to be suitable for different health prognostics and contains various prediction tasks, which can be helpful for integrated algorithms implementation in BMSs. So, the last question is how to provide health assessment based on the SOH predictions?

1.4. RESEARCH CONTRIBUTIONS AND LIMITATIONS

1.4.1. RESEARCH OBJECTIVES

Motivated by the above-analyzed research questions, this project aims to improve health prognostics under various scenarios via advanced transfer learning (TL) strategies and designing predictive health assessment strategies. The main objectives are summarized as follows.

O1: General feature extraction methods are investigated for all three health prognostic objectives. The features can be extracted effectively with batteries having different types and working under different loading and temperature scenarios. To ensure practical applications, feature extraction is conducted using partial capacity-voltage (Q-V) curves. The data cleaning process is studied to ensure the features can be extracted using different charging policies. With this objective, the general feature extraction is supposed to develop for different batteries working under various conditions.

O2: Model training and transferring using limited labeled data for fine-tuning and the unsupervised domain adaptation (DA) are comprehensively studied. The general idea and strategy of using different TL strategies under each kind of application scenario are proposed. The systematic experiments are conducted for the demonstration and verification of each kind of TL for battery health prognostics. With the comprehensive investigation, the general framework is supposed to be proposed which will be one guidance of TL-based battery health estimation and prediction in this field.

O3: The semi-supervised learning idea with the TL strategy is proposed for battery health prediction without heavy reliance on capacity labels. Only several checkpoints can support the accurate and reliable prediction of the whole degradation curve. In addition, to solve the ineffective prediction caused by the gradient vanishing and deterioration, long-term regularization is proposed to ensure effective prediction during the recursive process. The DA and feature extrapolation strategies are also proposed to predict future SOH without the requirement of capacity labels. This objective helps solve the problem of limited labeled data and unstable predictions to ensure more effective SOH predictions.

O4: Predictive health assessment with accelerating aging detection is proposed. The collaboration of point and sequence predictions is investigated to guide the predictive maintenance with the aging stage deviation based on the probabilistic predictions. The integration of different prediction tasks is studied by multi-task learning (MTL) and the implementation strategies are prospected with the cloud-edge framework. Both point and sequence predictions are achieved by the same model structure, improving the model integration effectively. A new framework for the health assessment will be produced with this objective to guide the application of battery SOH predictions.

1.4.2. RESEARCH LIMITATIONS

Although comprehensive SOH estimations and predictions using TL techniques are investigated in this project. There are still some limitations such as the following two aspects.

L1: The algorithm developments are still on personal computers, while the implementation of the prognostic algorithms will be facing more challenges. In addition, the proposed cloud-edge framework is still waiting for the implementation of the onboarding BMS system. The effectiveness of the proposed models is waiting for validation.

L2: The proposed methods are evaluated using experimental data. Although the experiments are tried to emulate the practical situations, field data have more challenges. For example, the sampling frequency is generally lower, causing the data quality to be worse. The charging policies are not the same for field applications, making it difficult for feature extraction. Therefore, the implementation in field applications still requires investigations.

L3: The features are extracted from the directly measured parameters and the pure data-driven models are used, which lack physical meaning and model interpretability. Physical features are supposed to be more robust under different scenarios and help interpret the aging mechanisms, which are still needing further investigation.

The above three limitations are also seen as the subsequent works for the author to conduct in his postdoc career.

1.5. THESIS OUTLINE

The outcome of this Ph.D. project is summarized by the article-based thesis, including a Report and a collection of Selected Publications. The thesis structure and the relationship between the Report and Selection Publications are illustrated in Fig. 1-6. The specific contents of each chapter are summarized as follows.

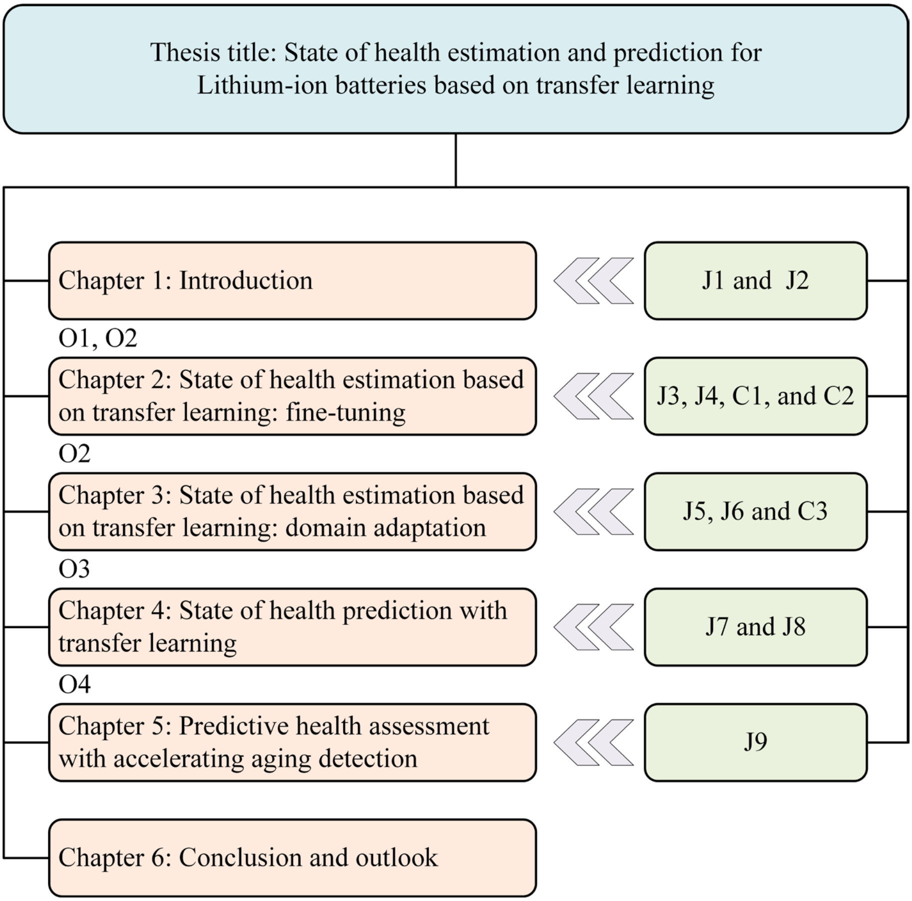

Figure 1-6 Chapter organizations and corresponding publications.

- Chapter 1: Introduction
  The research background and the state-of-the-art of battery health estimation and predictions are described first. Then, the main research gaps that motivate this Ph.D. project are analyzed. The objectives that contribute to solving the research

gaps are outlined thereafter and the limitations are also summarized. Finally, the thesis structure and the publications are outlined.

- Chapter 2: SOH estimation with model fine-tuning
  In this chapter, methods for TL-based battery SOH estimation with limited labeled data are investigated. Two scenarios with/without labeled data available from the source battery are considered. The data preprocessing strategy is proposed to ensure effective feature extraction from partial Q-V sequences under different loading profiles.

- Chapter 3: SOH estimation based on DA
  In the case of no labeled data available for model fine-tuning, this chapter investigates the role of DA in model improvement. Then, the combination of fine-tuning and DA as well as continual learning (CL) ability are studied.

- Chapter 4: SOH prediction with TL
  In this chapter, the extension of TL for battery SOH prediction for the whole degradation curve is presented. Both the fine-tuning with limited labeled data and DA without labeled data are explored. In addition, the problem with long-term prediction using recursive prediction is illustrated and solved by introducing long-term regularization, which ensures stable predictions for the whole degradation curve starting from the early aging stages.

- Chapter 5: Predictive health assessment with accelerating aging detection
  To improve the model integration, a MTL strategy is proposed to combine different prognostic tasks, and the framework is suitable for both point prediction and sequence predictions. With the collaboration of probabilistic point and sequence predictions, battery aging is divided into different stages according to the aging rates. Finally, accelerating aging is detected for the guidance of predictive health management.
- Chapter 6: Conclusion and outlook
  In the last chapter of this thesis, the main findings are summarized, and the future outlooks are presented.

1.6. LIST OF PUBLICATIONS

The research outcomes have been disseminated by publishing both journal and conference articles, which are listed below.

Journal articles

J1: Y. Che, X. Hu, X. Lin, J. Guo, and R. Teodorescu, “Health prognostics for lithium-ion batteries: mechanisms, methods, and prospects,” Energy and Environmental Science, vol. 16, pp. 338–371, 2023, doi: 10.1039/d2ee03019e.

J2: Y. Che, X. Hu, and R. Teodorescu, “Opportunities for battery aging mode diagnosis of renewable energy storage,” Joule, vol. 7, no. 7, pp. 1405–1407, 2023, doi: 10.1016/j.joule.2023.06.014.

J3: Y. Che, Y. Zheng, Y. Wu, X. Sui, P. Bharadwaj, D. Stroe, Y. Yang, X. Hu, and R. Teodorescu, “Data efficient health prognostic for batteries based on sequential information-driven probabilistic neural network,” Applied Energy, vol. 323, p. 119663, 2022, doi: 10.1016/j.apenergy.2022.119663.

J4: Y. Che, Y. Zheng, X. Sui, and R. Teodorescu, “Boosting battery state of health estimation based on self-supervised learning,” Journal of Energy Chemistry, vol. 84, pp. 335-346, 2023, doi: 10.1016/j.jechem.2023.05.034.

J5: Y. Che, S. B. Vilsen, J. Meng, X. Sui, and R. Teodorescu, “Battery health prognostic with sensor-free differential temperature voltammetry reconstruction and capacity estimation based on multi-domain adaptation,” eTransportation, vol. 17, p. 100245, 2023, doi: 10.1016/j.etran.2023.100245.

J6: Y. Che, Y. Zheng, X. Hu, S. Onori, R. Teodorescu, “Increasing generalization capability of battery health estimation using continual learning approach,” Cell Reports Physical Science. (accepted)

J7: Y. Che, D. I. Stroe, X. Hu, and R. Teodorescu, “Semi-supervised self-learning-based lifetime prediction for batteries,” IEEE Transactions on Industrial Informatics, vol. 19, no. 5, pp. 6471–6481, 2023, doi: 10.1109/TII.2022.3206776.

J8: Y. Che, F. Evariste, Y. Zheng, L. Xu, and R. Teodorescu, “Health prediction for lithium-ion batteries under unseen working conditions,” IEEE Transactions on Industrial Electronics. (major revision)

J9: Y. Che, Y. Zheng, F. Evariste, X. Sui, X. Hu, and R. Teodorescu, “Predictive health assessment for lithium-ion batteries with probabilistic degradation prediction and accelerating aging detection,” Reliability Engineering and System Safety, vol. 241, p. 109603, 2024, doi: 10.1016/j.ress.2023.109603.

Conference papers

C1: Y. Che, X. Sui, P. Bharadwaj, D. I. Stroe, and R. Teodorescu, “Battery Lifetime Prediction and Degradation Reconstruction based on Probabilistic Convolutional Neural Network,” 2022 IEEE 13th International Symposium on Power Electronics for Distributed Generation Systems, PEDG 2022, 2022, doi: 10.1109/PEDG54999.2022.9923247.

C2: Y. Che, D. I. Stroe, X. Sui, S. B. Vilsen, X. Hu, and R. Teodorescu, "Battery Aging Behavior Evaluation under Variable and Constant Temperatures with Real Loading Profiles," Conference Proceedings - IEEE Applied Power Electronics Conference and Exposition - APEC, vol. 2023-March, no. 2, pp. 2979–2983, 2023, doi: 10.1109/APEC43580.2023.10131534.

C3: Y. Che, X. Sui, R. Teodorescu, "State of Health Estimation for Smart Batteries using Transfer Learning with Data Cleaning" IFAC-PapersOnLine, 2023. vol. 56, pp. 3782-3787, 2023, doi: 10.1016/j.ifacol.2023.10.1306.

Other publications

O1: Y. Che, Y. Zheng, Y. Wu, X. Lin, J. Li, X. Hu, and R. Teodorescu, "Battery States Monitoring for Electric Vehicles Based on Transferred Multi-Task Learning," IEEE Transactions on Vehicular Technology, vol. 72, no. 8, pp. 10037–10047, 2023, doi: 10.1109/TVT.2023.3260466.

O2: Y. Zheng, Y. Che (corresponding author), X. Hu, X. Sui, and R. Teodorescu, "Sensorless Temperature Monitoring of Lithium-ion Batteries by Integrating Physics with Machine Learning," IEEE Transactions on Transportation Electrification, vol. PP, p. 1, 2023, doi: 10.1109/TTE.2023.3294417.

O3: Y. Zheng, Y. Che, X. Hu, X. Sui, D. Stroe, and R. Teodorescu, "Thermal state monitoring of lithium-ion batteries: Progress, challenges, and opportunities," Progress in Energy and Combustion Science, vol. 100 p. 101120, 2024, doi: 10.1016/j.pecs.2023.101120.

O4: J. Guo, Y. Che (corresponding author), K. Pedersen, and D.-I. Stroe, "Battery impedance spectrum prediction from partial charging voltage curve by machine learning," Journal of Energy Chemistry, vol. 79, pp. 211–221, 2023, doi: 10.1016/j.jechem.2023.01.004.

O5: K. Liu, Q. Peng, Y. Che (corresponding author), Y. Zheng, K. Li, R. Teodorescu, D. Widanage, and A. Barai, "Transfer learning for battery smarter state estimation and ageing prognostics : Recent progress , challenges , and prospects," Advances in Applied Energy, vol. 9, 2022, p. 100117, 2023, doi: 10.1016/j.adapen.2022.100117.

O6: Y. Wu, Z. Huang, Y. Zheng, Y. Liu, H. Li, Y. Che (corresponding author), J. Peng, and R. Teodorescu, "Spatial–temporal data-driven full driving cycle prediction for optimal energy management of battery/supercapacitor electric vehicles," Energy Conversion and Management, vol. 277, p. 116619, 2023, doi: 10.1016/j.enconman.2022.116619.

O7: Y. Zheng, N.A. Weinreich, A. Kulkarni, Y. Che, H. Sorouri, X. Sui, R, Teodorescu, “Sensorless State of Temperature Estimation for Smart Battery based on Electrochemical Impedance,” 2023 25th European Conference on Power Electronics and Applications (EPE'23 ECCE Europe), 2023, doi: 10.23919/EPE23ECCEEurope58414.2023.10264452.

O8: X. Sui, S. He, Y. Zheng, Y. Che, R. Teodorescu, “Early Prediction of Lithium-Ion Batteries Lifetime via Few-Shot Learning,” IECON 2023-49th Annual Conference of the IEEE Industrial Electronics Society, 2023.

CHAPTER 2. STATE OF HEALTH ESTIMATION BASED ON TRANSFER LEARNING: FINE-TUNING

SOH estimation is one main objective in battery health prognostics, which describes the current battery aging status. The main challenge is that only limited, or no labeled samples are available during practical applications and distinguished working conditions make it difficult to the accurate and reliable estimations. Therefore, TL strategies are proposed to deal with the SOH estimation under different scenarios to improve the accuracy and generalization.

In this chapter, it assumed only sparsely limited labeled data from the testing batteries are available. It emulates real-world conditions where labeled capacity is only available during maintenance testing. To demonstrate how limited labeled data help improve model accuracy and reliability, the fine-tuning-based TL is investigated. General feature extraction methods are proposed for effective feature extraction using a partial Q-V curve. The data clean method is proposed to extend the feature extraction framework to pulse current. Then, both the conditions that source batteries have labels or do not contain labels are considered. The model performance has been improved via learning from limited labeled data. Based on the investigations in this chapter, the role of sparsely labeled data is demonstrated with TL. The general framework is illustrated for reference in this field.

J3, J4, and C1 contribute to this chapter.

2.1. SOH ESTIMATION BASED ON SPARSELY LABELED DATA

2.1.1. EXPERIMENT AND DATA CLEANING

In the initial section, the data used in this thesis is briefly introduced. To demonstrate and verify the performance of the strategies derived in this project, both public and experimental data are collected for verification. The pubic datasets include those from [55], [72]–[74]. More importantly, comprehensive aging experiments have been conducted to collect aging data from different battery types working under different loading and temperature conditions. As shown in Fig. 2-1, both constant currents, dynamic loadings, and pulse currents are conducted under different constant temperature and variable temperatures. In addition, both fresh and second-life batteries are used for aging. More than 50 batteries with both NCA, LFP, NCM, and polymer materials in pouch, prismatic, and cylindrical formats are used for aging. Therefore, the aging datasets collected in this project contain various scenarios that make the verifications and evaluations of the advanced methodologies more comprehensive. The detailed use of the datasets for the verification is introduced in the following sections when applied for verifications. For more information, please also refer to the related published papers.

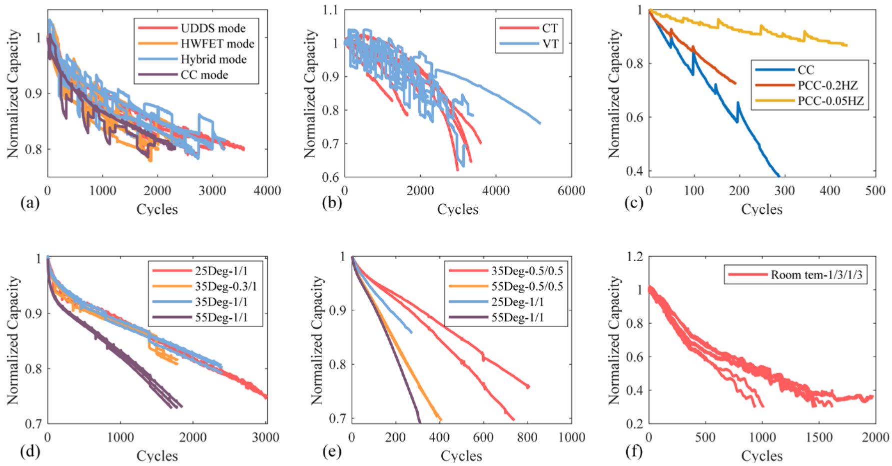

Figure 2-1 Experimental aging datasets with various battery types, loading profiles, and temperature conditions.

As discussed in Chapter 1, ample information from *Q-V* curve helps extract effective aging-related features for battery health estimation. The typical partial *Q-V* curve variations during aging are shown in Fig. 2-2(d), which show regular trends with battery aging, illustrating the characteristics of battery degradation that can be extracted. However, for the pulse charging or multi-stage constant current charging mode, voltage shows fluctuations during the transaction stages, which causes original *Q-V* to fluctuate. Hence, it's essential to initially apply a filtering process for curve smoothing. Rather than directly applying a filter to the original curve, which could potentially alter shapes and result in information loss, we opt to eliminate the rest periods, thus achieving a smoother charging curve.

The concept and effectiveness of this data-cleaning technique are exemplified in Fig. 2-2(a and b). As the capacity remains constant even as the voltage decreases during the rest periods, we can eliminate the data corresponding to these periods. This results in a steadily increasing capacity curve. When the current is reloaded after a rest period, the voltage increases, but it may not change rapidly enough to exceed the voltage value before the rest within the following few data points. Consequently, to ensure a monotonic change in the voltage curve, we also exclude the period during which the voltage remains lower than the pre-rest value. Finally, after cleaning the data, we obtain a monotonous *Q-V* curve, as depicted in Fig. 2-2 (d), which contrasts with the raw parameters showing significant fluctuations in Fig. 2-2 (c). Subsequently, we can apply interpolation to prepare inputs for the machine-learning model. The proposed data-cleaning method offers several advantages. Firstly, it effectively retains the primary aging information while providing smoothed data. Moreover, this approach is adaptable to a wide range of pulse current scenarios with varying duty cycles and frequencies. Furthermore, this cleaning method can also be applied for multi-step constant current charging processes for the data smoothing during current switch stages. Hence, the data preparation is universally applicable across different charging.

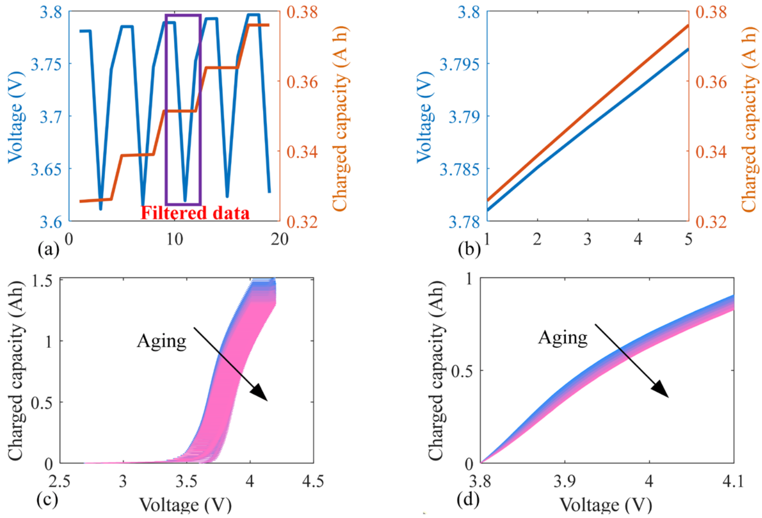

Figure 2-2 Effectiveness illustration of the data cleaning method. (a) Measured V, Q curves, and filtering period. (b) V and Q after cleaning. (c) Measured Q-V curves against aging. (d) Filtered Q-V curves against aging. Source: [J4]

2.1.2. FEATURE EXTRACTION BASED ON PARTIAL *Q-V* CURVES

The accuracy, reliability, and online applicability of battery health estimation and prediction algorithms are profoundly influenced by the derived HIs. We employ partial *Q-V* sequences for feature extraction, a strategy that aligns more closely with practical conditions where incomplete charge and discharge cycles are undergone by the batteries. The partial *Q-V* sequence can be mathematically expressed as follows with the lower limit m and upper limit n,

$$\begin{cases} \boldsymbol{V}s = [V_m, V_{m+1}, \dots, V_{n-1}, V_n] \\ \boldsymbol{Q}s = [Q_m, Q_{m+1}, \dots, Q_{n-1}, Q_n] \end{cases} \tag{2.1}$$

Note that the linear interpolation is applied to obtain uniform sequence lengths. To reveal the concealed insights regarding battery aging, we leverage the $\boldsymbol{Q}s$ sequences as well as the differential $\boldsymbol{DQ}s$ sequences. This study employs the standard deviation (std), Shannon entropy (ShanEn), and the first element of the principal components (fpc) derived from $\boldsymbol{Qs}$ and to $\boldsymbol{DQs}$ be HIs, as demonstrated below and the extraction process is summarized in Table 2-1,

$$\mathbf{HI} = \begin{bmatrix} \mathrm{std}(\boldsymbol{Qs}), \mathrm{ShanEn}(\boldsymbol{Qs}), \mathrm{fpc}(\boldsymbol{Qs}), \\ \mathrm{std}(\boldsymbol{DQs}), \mathrm{ShanEn}(\boldsymbol{DQs}^2), \mathrm{fpc}(\boldsymbol{DQs}) \end{bmatrix} \tag{2.2}$$

Table 2-1 Process for HIs extraction from partial Q-V curve

for i =1,2,3,…, cycle number:
  choose voltage range $\boldsymbol{V}_{seq} = [V_m, \dots, V_n]$ (2.3)
  calculate the charged capacity from a $\boldsymbol{V}$ range: $\boldsymbol{Q} = \int Idt$ (2.4)
  clean the voltage and capacity
    while j <len(V)
      if V_j<=$V_{j\text{-}1}$ or Q_j<=$Q_{j\text{-}1}$:
        remove V_j and Q_j
      else: j=j+1
  interpolate the Q-V curve: (2.5)
    $\boldsymbol{Q}_{seq} = \mathrm{Interp}(\boldsymbol{V}, \boldsymbol{Q}, \boldsymbol{V}_{seq})$
  calculate feature values:
    std_Q: std_$Q_i = \sqrt{\frac{\sum(Q_j-\mu)^2}{N}}$ (2.6)
    shen_Q: shen_$Q_i = -\sum p(x)\log_2 p(x)$ (2.7)
    fpc_Q: fpc_$Q_i = \mathrm{PCA}(Q)$ (2.8)
    other features: …

The normalization method by dividing the fresh capacity is used in this thesis. The described HIs extraction is implemented on the battery dataset introduced in [55] and the changes in HIs across cycles for the 124 batteries are depicted in Fig. 2-3(a), with every curve representing an individual cell. The variations in HIs exhibit comparable trends with the degradation curve of capacities, underscoring the effectiveness of the proposed HIs in accurately reflecting battery aging status. Additionally, correlation analysis between extracted HIs and battery SOH is conducted, with the heatmap visualized in Fig. 2-3(b). Pearson correlation coefficient (PCC) is popular for analyzing the effectiveness of the extracted HIs. The PCC between x and y can be expressed as follows [75],

$$\rho = \frac{\sum_{i=1}^{n}(x_i - \bar{x})(y_i - \bar{y})}{\sqrt{\sum_{i=1}^{n}(x_i - \bar{x})^2}\sqrt{\sum_{i=1}^{n}(y_i - \bar{y})^2}} \tag{2.9}$$

Remarkably, 99.9% of the PCC surpass 0.9, with a significant portion of them (80.24%) exceeding 0.95, indicating strong relationships between HIs and SOH. The correlations between life cycles and $\mathrm{std}(\boldsymbol{DQs})$, $\mathrm{ShanEn}(\boldsymbol{DQs}^2)$, and $\mathrm{fpc}(\boldsymbol{DQs})$ are demonstrated in Fig. 2-3(c), where every battery is represented by one point. The results of the analysis reveal strong linear correlations between three distinct HIs and the number of cycles. The PCC values are 0.918, 0.907, and 0.902, respectively. Furthermore, Fig. 2-3(c) underscores that the mapping relationship between HIs and lifetime for the 124 cells is contingent on the chosen HI. This HI-dependent characteristic presents an opportunity to enhance model performance by incorporating multiple HIs to help the recognition of aging patterns and identify related batteries for training. As a result, the proposition of employing multiple HIs in this context holds promise for enhancing the effectiveness of battery health prognostics due to the high correlations between both capacities and lifetime. The general HIs extraction framework is suitable for feature extraction for both SOH and EOL, indicating valuable practical significance.

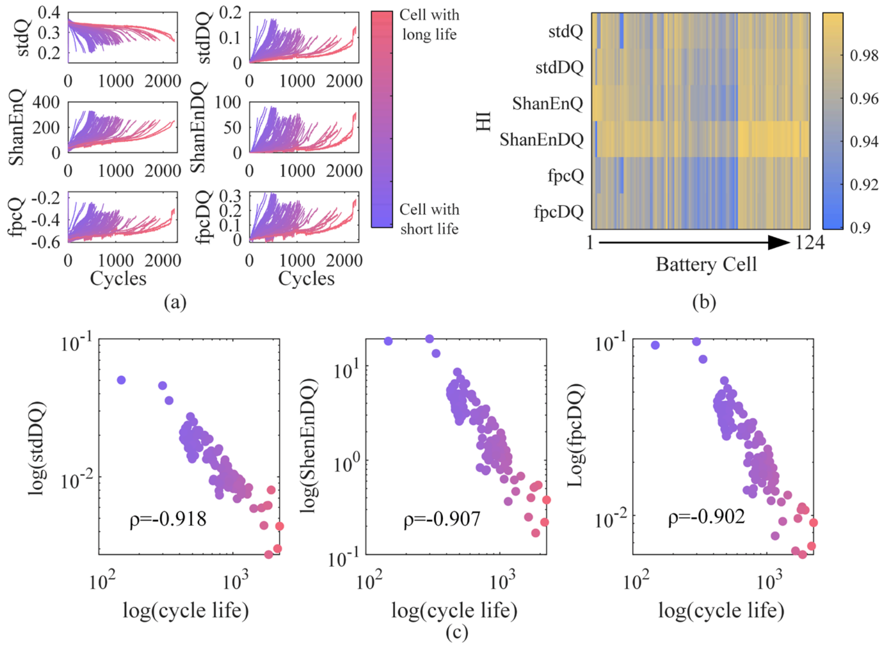

Figure 2-3 HIs evaluation, (a) HIs variations with running cycles, (b) PCC heatmaps between HIs and SOH, (c) PCC maps of the HIs against lifetime. Source: [J3]

2.1.3. SOH ESTIMATION FRAMEWORK WITH LIMITED LABELS

The overall framework for battery health estimation with fine-tuning using limited labeled data is shown in Fig. 2-4. The collected partial Q-V curves are firstly used for HIs extraction. Then the extracted HIs are employed across three key functions: degradation recognition, automatic reference battery selections, and base model training. Subsequently, the trained model serves as the foundational base model for the target battery, with an additional phase of fine-tuning aimed at adapting the degradation characteristics of target batteries. Finally, the adapted model is applied for target battery degradation reconstruction and health estimation through the obtained HIs. Under the proposed framework, upon reaching a checkpoint, the model undergoes a retraining process. Consequently, the model can be updated during usage.

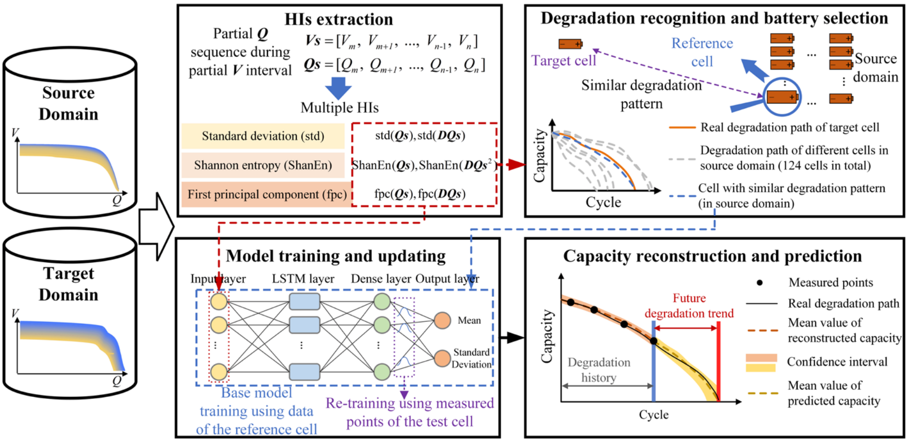

Figure 2-4 Framework for battery selection and probabilistic health estimation. Source: [J3]

The detailed steps for SOH estimation framework are introduced below. Firstly, a brief description of long-short-term-memory (LSTM) theory is provided, followed by a probabilistic regression. Thirdly, a method for automatic reference battery selection is proposed. Finally, the complete estimation framework is outlined.

2.1.3.1 Neural network with probabilistic regression

Battery SOH and RUL prediction have extensively adopted LSTM. The core concept of LSTM involves the integration of four gates to regulate information flow. This design effectively circumvents challenges related to gradient vanishing and exploding, facilitating the optimal utilization of historical data for enhanced prediction accuracy. A comprehensive exposition of the LSTM algorithm's intricacies can be found in [69], where the fundamental equations underpinning LSTM are as follows:

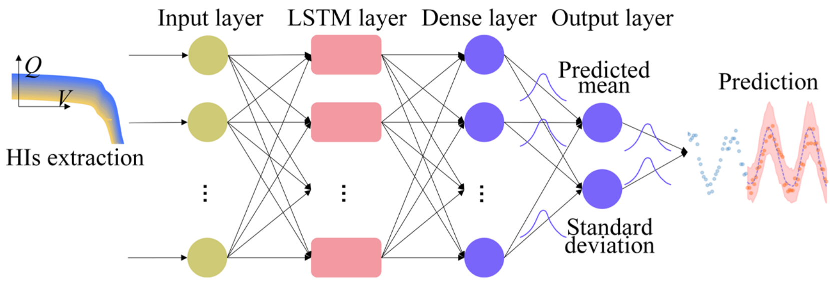

Figure 2-5 Proposed machine learning model. Source: [J3]

$$f(t) = \sigma(w_{f1}x(t) + w_{f2}h(t-1) + b_f) \tag{2.10}$$
$$i(t) = \sigma(w_{i1}x(t) + w_{i2}h(t-1) + b_i) \tag{2.11}$$
$$\tilde{S}(t) = tanh(w_{c1}x(t) + w_{c2}h(t-1) + b_c) \tag{2.12}$$
$$S(t) = f(t) \odot S(t-1) + i(t) \odot \tilde{S}(t) \tag{2.13}$$

$$o(t) = \sigma(w_{o1}x(t) + w_{o2}h(t-1) + b_o) \quad (2.14)$$
$$h(t) = o(t) \odot \tanh(S(t)) \quad (2.15)$$

where $x(t)$ and $h(t)$ represent the input and output, $f(t)$, $i(t)$, and $o(t)$ represent information updated by the forget, input, and output gate respectively, $S(t)$ refer to the state information, w and b represent the weights and biases, σ and tanh refer to the activation functions. Typically, following LSTM layer, fully connected layers are introduced to yield predictions. The computation procedure of neurons within these fully connected layers is elucidated as follows:

$$o = \sum_{i=1}^{N} w_i h_i + b_i \quad (2.16)$$

where *o* represents the output while *h* stands for the input, and *N* is the neuron numbers within the previous layer responsible for conveying information to the current layer. Once the model parameters have been trained, the specific value of the output will be obtained. Nonetheless, specific values often lack the capacity to adequately convey the algorithm's reliability. To surmount this constraint, probabilistic neural networks emerge as promising options [76], [77]. These networks can potentially offer probabilistic predictions by defining probability distributions for the weights and biases. The model's training process could involve manipulating the parameter distributions. Hence, the trained network has the capability to generate both the anticipated mean and the associated uncertainty, as described by the confidence interval (CI). In this context, the 95% CI is chosen to encapsulate the prediction's uncertainty. The negative log-likelihood loss function is used in training [78],

$$loss(z, y) = -y.\log\_prob(z) \quad (2.17)$$

where y and z represent predicted distribution and demanded practical output respectively, $y.\log\_prob(z)$ pertains to the logarithmic probability (logprob) of an individual sample (z) within a distribution of (y). The proposed neural network architecture is illustrated in Fig. 2-5. The detailed parameter setting could refer to J3. Specifically, HIs are fed into the network while the predicted mean and standard deviation are outputted. The last two layers are set trainable for fine-tuning with sparsely labeled data from the testing batteries. This strategic adjustment facilitates the adaptation of the model to accommodate the degradation patterns observed in testing batteries. Moreover, it leverages the insights gleaned from the reference batteries, optimizing the model's performance and adaptability.

2.1.3.2 Automatic training selection

Given the distinct relationships between HIs and battery lifecycles, the more effective approach is to consider all HIs when choosing batteries for model training. An automated method for selecting reference batteries through a weighting approach is proposed. Firstly, three potential candidates are identified by assessing the similarities, computed using the differences in HIs between the target battery and other source batteries. Then, three candidates per HI are assigned weights based on their order of similarity to the testing battery within the testing battery. The candidate ranked first receives a weight of 3, the second candidate is weighted 2, and the last one is given a weight of 1. Subsequently, all nine candidates (three candidates from each HI) are evaluated using this weighting scheme. Duplicate candidates selected by different HIs are consolidated by summing their weights. In the end, two source batteries with the highest combined weights are automatically chosen for model training. The proposed method amplifies the identification of relevant candidates by leveraging three HIs, thus enhancing the efficacy of the base model trained for SOH estimations.

2.1.4. RESULTS AND DISCUSSIONS

The representative results are presented. Both public and experimental datasets are applied for evaluations. The root-mean-square error (RMSE) and mean absolute error (MAE) are used for performance evaluations, expressed as,

$$RMSE = \sqrt{\frac{1}{N}\sum_{i=1}^{N}(\hat{z}_i - z_i)^2} \tag{2.18}$$

$$MAE = \frac{1}{N}\sum_{i=1}^{N}|\hat{z}_i - z_i| \tag{2.19}$$

where $\hat{z}_i$ and z_i are the estimated and real values for the i-th sample, and N is samples.

2.1.4.1 Results using MIT-Stanford dataset

This subsection showcases results with the MIT-Stanford dataset [55]. In addition to the 10th and 100th cycle, two additional checkpoints (50% and 90% of the lifetime) are incorporated for the purpose of model fine-tuning. Note that the selection of 50% and 90% in this study just serves as a representative choice, aimed at capturing aging stages at different points. In practical scenarios, checkpoints might only be accessible during maintenance, occurring at various life stages.

The evaluation process involves the sequential testing of all 124 batteries. For each iteration, one battery is designated as the testing battery. Simultaneously, the other batteries are collectively designated as source batteries, which serve as the reference pool for the automated selection of reference batteries. The red lines in Fig. 2-6(a) and 2-6(b), respectively, represent the RMSE and MAE of the proposed method. Two benchmarks only use the base model, and without any model retraining are compared. One employs every suggested HI, while the other only employs std-based HIs.

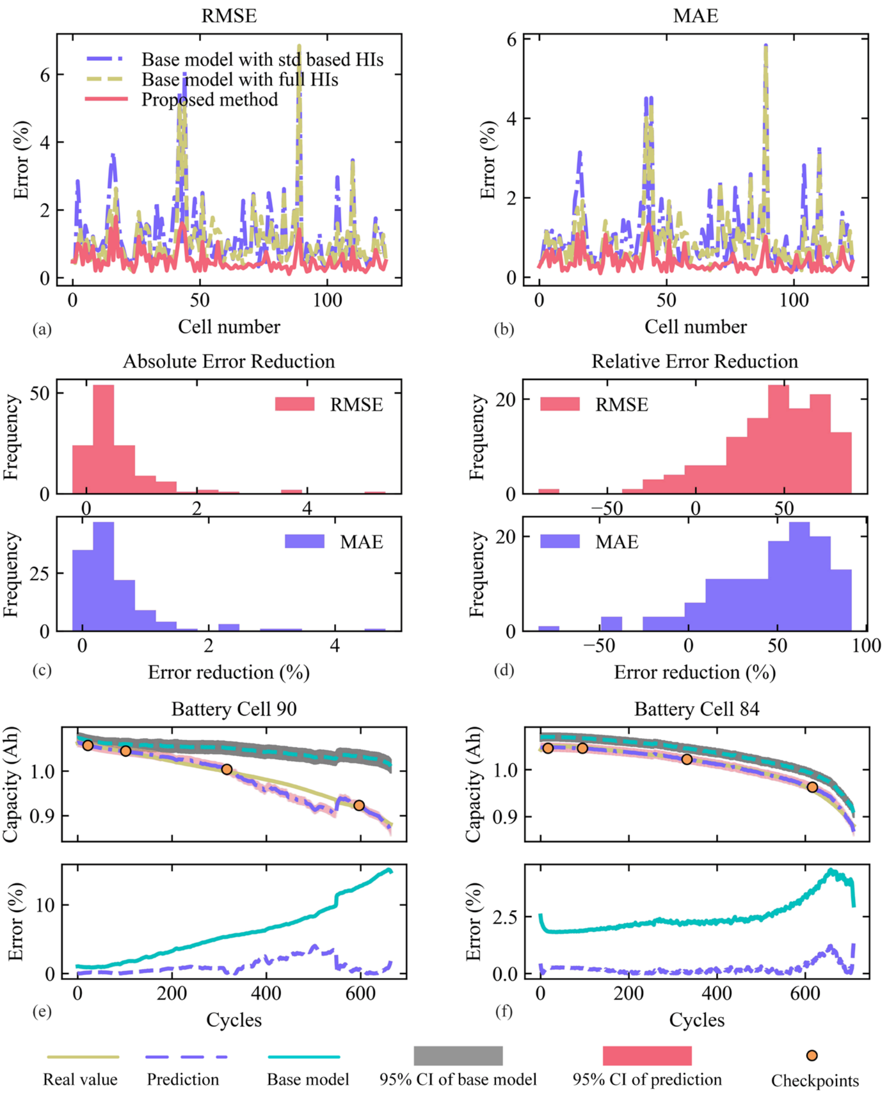

Figure 2-6 Estimation results with MIT-Stanford dataset. (a)/(b) RMSE/MAE of all batteries, (c) absolute error reduction histogram, (d) relative error reduction histogram, (e) results of cell 90, (f) results of cell 84. Source: [J3]

The mean, lowest, and highest RMSE and MAE values for all batteries using the suggested method as well as the two benchmarks are listed in Table 2-2. The results illustrate that using all HIs rather than just std-based HIs generally increases the accuracy. The model transfer and retraining process has the potential to significantly improve prognostic accuracy. The proposed method's mean values of RMSE and MAE are reduced by 0.60% and 0.53%, respectively, compared to the base model using full HIs. The maximum error can be significantly reduced in comparison to the two base models. Compared with the base model with only std-based HI, the full HIs help improve the accuracy, whose RMSE and MAE show reductions of 0.15% and 0.12% respectively.

The proposed method's enhancement in accuracy is depicted through absolute and relative error reductions. These reductions are illustrated in Fig. 2-6(c) and Fig. 2-6(d). Most cells exhibit improved accuracy. The most absolute error reduction exceeds 4%, while the majority falls within the 1% to 2% range. Notably, the proposed method achieves relative error reductions surpassing 50%, indicating a significant enhancement in accuracy. While there are situations, where adopting the TL leads to slightly worse results since errors are already quite small. This highlights that the automated selection method effectively identifies relevant batteries for initial modeling. Statistical outcomes showcasing accuracy improvement are listed in Table 2-3. The results reveal mean absolute reductions of 0.59% for RMSE and 0.53% for MAE (arRMSE and arMAE, respectively). Additionally, the mean relative error reductions for both RMSE and MAE (rrRMSE and rrMAE) are notable at 43.70% and 45.33%, respectively. Fig. 2-6(e) and 2-6(f) demonstrate two representative cells, providing clear evidence of the proposed method's enhancement over the base model that is based on only four labeled checkpoints. The results indicate that the base model successfully anticipates the degradation trends, albeit with considerable deviation from the accurate values. In contrast, the proposed method accurately estimates SOH with a small number of checkpoints utilized for fine-tuning.

Table 2-2 Errors of the proposed method and two benchmark methods. Source: [J3]

	Proposed model		Base model			
	RMSE	MAE	RMSE (full HIs)	MAE (full HIs)	RMSE (std HI)	MAE (std HI)
Mean	0.50%	0.38%	1.10%	0.91%	1.25%	1.03%
Minimum	0.11%	0.08%	0.18%	0.13%	0.28%	0.18%
Maximum	1.80%	1.33%	6.84%	5.82%	6.85%	5.83%

Table 2-3 Error reduction by the proposed method. Source: [J3]

	arRMSE	arMAE	rrRMSE	rrMAE
Mean	0.59%	0.53%	43.70%	45.33%
Minimum	-0.25%	-0.16%	-88.91%	-84.32%
Maximum	5.42%	4.80%	88.25%	91.74%

To illustrate the effectiveness of reference battery selection, a comparative analysis of estimated errors was conducted. Specifically, two batteries with medium lifetimes from the source dataset were chosen as references for comparison with the proposed strategy. In Fig. 2-7, boxplots depict the prediction errors of 124 battery cells under different testing. "Case A" represents the mean model, where two medium lifetime batteries serve as references, and "Case B" involves the "Case A" model, with fine-tuning using the same checkpoints. "Case C" corresponds to the base model, as previously discussed, while "Case D" reflects the results using the proposed method. Fig. 2-7 distinctly demonstrates that reference battery selection based on proposed HIs yields significant improvements in accuracy when compared with methods using medium lifetime batteries as references. This holds true for both scenarios with and without TL. Moreover, TL amplifies the enhancement by reducing the mean and variance of errors. For more evaluations, readers can refer to J3.

2.1.4.2 Extending applications with experimental datasets

In practical applications, the use of various battery types further exacerbates the limitations of the base model's performance. Therefore, the lab datasets serve as testing batteries to demonstrate the model's effectiveness, leveraging the MIT-Stanford dataset as the source domain, which has different battery types and working conditions. The specific parameters of the batteries can be found in J3. These batteries undergo aging across a spec trum of temperatures (ranging from 25 °C to 55 °C) and current rates (ranging from 0.3 C to 1 C), resulting in diverse aging patterns. The capacity curves of all 13 batteries are depicted in Fig. 2-8.

The estimations for three type-1 cells, aged at 55 °C, 35 °C with a current of 1 C, and 35 °C with a current of 0.3 C, are displayed in Fig. 2-9(a-c), respectively. Similarly, outcomes for three type-2 battery cells aged at 25 °C, 35 °C with a current of 0.5 C, and 55 °C with a current of 0.5 C, are presented in Fig. 2-9(d-f), respectively. Evidently, the estimations closely align with the actual values throughout the battery lifecycles. The relatively narrow 95% CIs indicate accurate and reliable predictions. Notably, even in Fig. 2-9(c), where the degradation curve experiences a sudden shift, the estimations still closely track the real values.

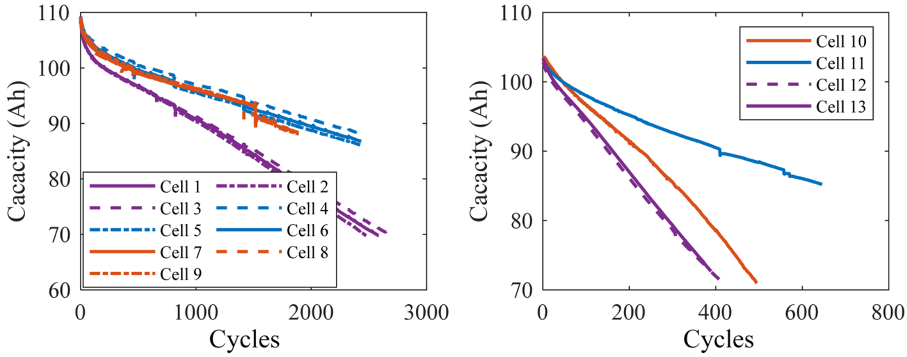

Figure 2-7 Capacities of experimental batteries. Source: [J3]

The statistical errors of estimations for all the batteries are summarized in Table 2-4, with comparisons with two benchmark approaches. The first solely employs the base model, while the second only employs the checkpoints for modeling, without transferring parameters from the initial base model (described as self-model). The-

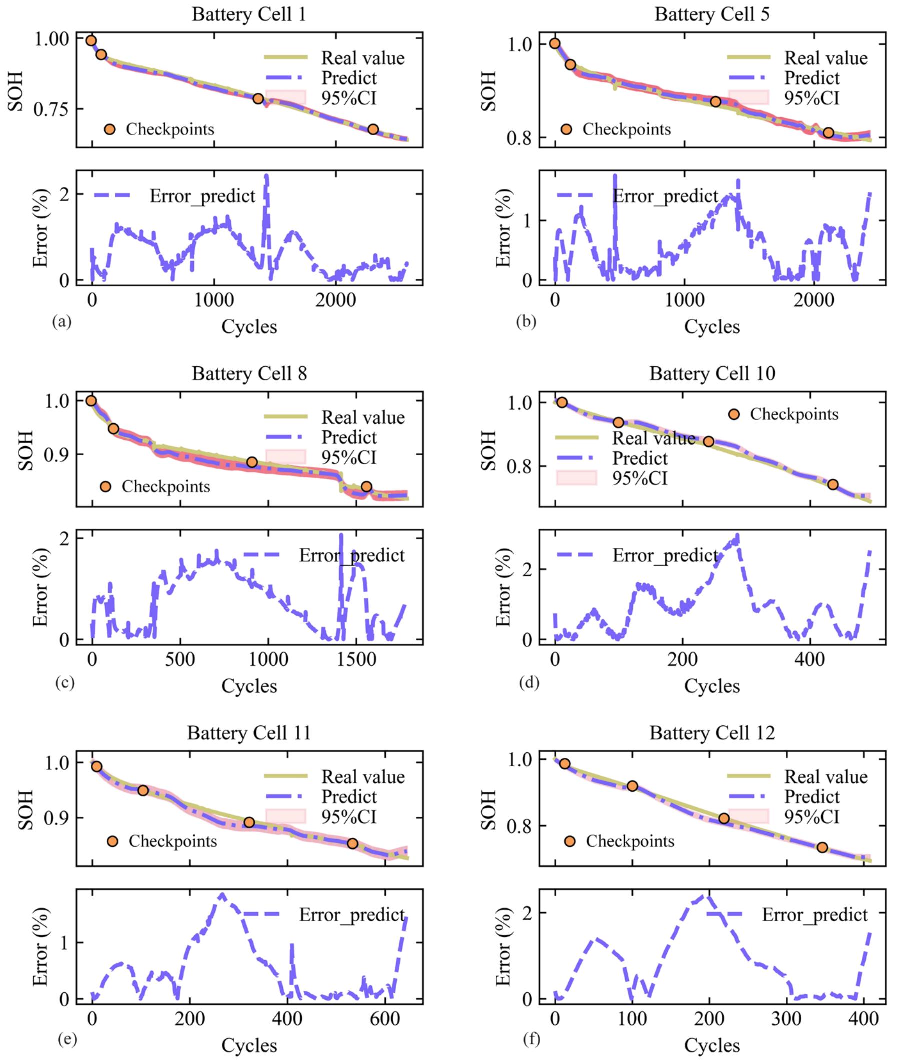

Figure 2-8 Results for lab datasets. Source: [J3]

mean errors of the proposed method remain below 0.8%, a stark contrast to the other two methods with errors exceeding 20%. Remarkably, the proposed method exhibits maximum RMSE and MAE values of merely 1.16% and 0.93, respectively. In contrast, these values reach 29.26% and 22.88% for the base model, and 29.09% and 19.94% for the self-model. These findings indicate that conventional ML methods falter in battery health estimation when datasets with limited known cycles are available. However, the proposed method still manages to yield satisfactory estimation results. Consequently, the significance of the proposed method becomes evident in battery health management. Its capability to extend knowledge from one battery aging dataset to effectively estimate other battery types holds great promise.

Table 2-4 Performance evaluations with lab datasets. Source: [J3]

	RMSE	MAE	RMSE (base model)	MAE (base model)	RMSE (self model)	MAE (self model)
Mean	0.78%	0.625%	24.64%	19.85%	22.19%	14.37%
Minimum	0.57%	0.43%	21.25%	16.21%	17.45%	9.82%
Maximum	1.16%	0.93%	29.26%	22.88%	29.09%	19.94%

2.1.5. SUMMARY

This section introduces a novel battery health estimation approach employing a probabilistic neural network with partial *Q-V* curve extracted HIs. Multiple HIs are extracted from partial *Q-V* sequences, demonstrating a strong connection with battery lifespan and capacity. The data cleaning strategy is proposed to ensure effective feature extraction under different loading profiles. Furthermore, an automatic relevant battery selection procedure is suggested to pinpoint appropriate batteries for initial modeling. Additionally, a new structure involving LSTM and probabilistic regression is introduced for battery health prognostics. This framework not only provides predicted mean values but also quantifies uncertainty. Further enhancement of prediction accuracy and reliability is achieved through a model transfer and fine-tuning process, utilizing only a small number of checkpoints. Validations using both public and experimental data indicate a significant improvement compared to conventional methods. The proposed method can be extended to estimations of batteries with different types and working conditions to the source batteries.

2.2. SELF-SUPERVISED STRATEGY FOR SOH ESTIMATION PERFORMANCE BOOSTING UNDER VARIOUS LOADINGS.

In the previous section, we assumed the presence of abundant labeled aging data from the source domain. However, practical scenarios often involve limited labeled samples for model training. As a result, incorporating unlabeled data into the modeling process becomes crucial to explore its efficacy in battery health prognostics. In this section, a novel self-supervised learning strategy that aims to enhance battery SOH estimation performance by leveraging learned characteristics from unlabeled data is proposed. Self-supervised learning is a contemporary learning strategy that has rapidly emerged. Its core objective is to enhance downstream tasks by capitalizing on the inherent supervision present within the input data itself [79]. This goal is achieved by typically employing a pretext task followed by a target task [80]. In the context of estimating battery SOH through self-supervised learning, the feature representation task and downstream SOH estimation task are supposed to be established.

2.2.1. BATTERY SOH ESTIMATION USING SELF-SUPERVISED LEARNING APPROACH

The overall structure of the self-supervised learning approach designed to boost battery SOH estimation is demonstrated in Fig. 2-9. This framework encompasses four primary stages: data preprocessing, initial training through a pretext task, further refinement through a target task, and comprehensive validations across various scenarios. In the data preprocessing phase, diverse data originating from batteries with varying types, subjected to different load profiles and environmental temperatures, is carefully filtered and aligned using the data cleaning method introduced in the previous section. The dataset consists of both unlabeled data, as well as sparsely labeled data, catering to the needs of pretext and downstream target learning respectively. The pretext learning stage focuses on capturing the underlying aging patterns embedded within the partial Q-V curve, utilizing an unsupervised approach that employs feature extraction with an auto-encoder and decoder. Subsequently, the encoding part learned during pretext training is migrated to the downstream target network. Here, an additional output regression layer is appended to facilitate the mapping of the relationship between partial Q-V curves and battery SOH. Through fine-tuning with the sparsely labeled data, this relationship is effectively delineated. The trained model is finally employed for SOH estimation, with accuracy evaluations under various scenarios. The detailed process is described in detail below.

2.2.1.1 Feature representative pretext learning

Most data gathered in the real world lacks labels, rendering it incompatible with traditional data-driven techniques reliant on supervised learning. Yet, the concealed insights regarding aging within operational data, like Q-V curves, exhibit a substantial correlation with battery aging. This correlation presents an avenue for enhancing SOH estimation models. Hence, within the feature-representative pretext learning process, only unlabeled data is harnessed to unveil the latent relationships between measured data and battery aging with the unsupervised framework. To elaborate, the charged Q-V curves are put into an encoder-decoder architecture. Post encoding, the decoding stage reconstructs the charged Q-V profiles. By juxtaposing these reconstructed profiles against their originals, mean square error (MSE) emerges as the loss metric to be diminished,

$$MSE = \frac{1}{N}\sum_{i=1}^{N}(\hat{\boldsymbol{y}}_i - \boldsymbol{y}_i)^2 \tag{2.20}$$

where $\boldsymbol{y}_i$ and $\hat{\boldsymbol{y}}_i$ represent measured and estimated curves respectively. Enhancing the interpretability of the ML approach aims at deciphering the factors underpinning its performance. Generally, model-based and post hoc methods have been widely used for unraveling the inner workings of ML models [81]. We employ the latter one to leverage the correlations among hidden states post auto-encoding and SOH.

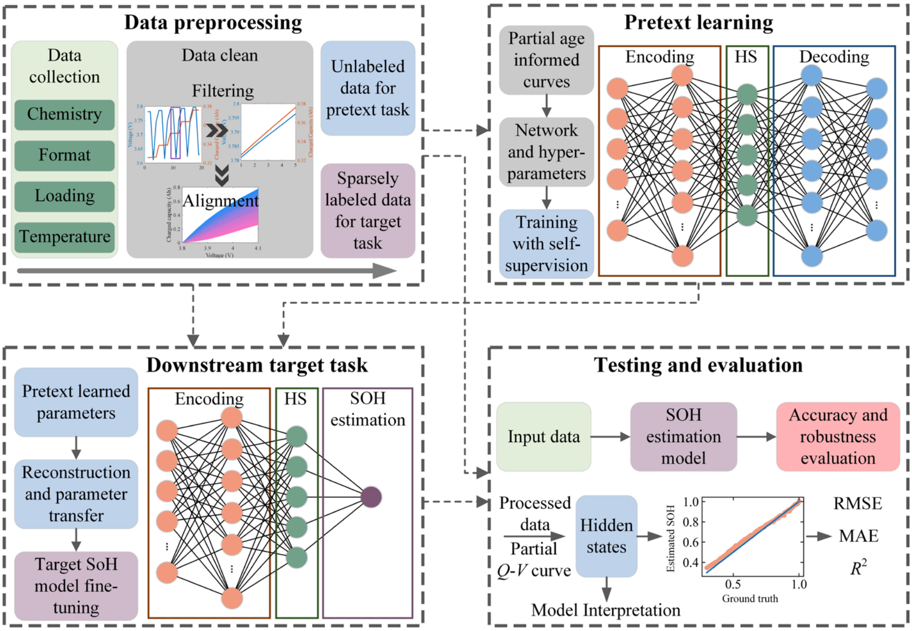

Figure 2-9 Framework of boosting battery SOH estimation based on self-supervised learning. Source: [J4]

2.2.1.2 Downstream SOH estimation learning

While obtaining a continuous stream of labeled data proves challenging, there is the possibility of acquiring sparsely labeled data during maintenance phases. Therefore, the encoding layers are adapted to incorporate a single output regression layer for SOH estimation, which is fine-tuned with sparsely labeled data. The input consists of partial Q-V curves from cycles with associated SOH labels, maintaining a constant as that used in pretext learning. The encoding layers retain the knowledge previously acquired from the unlabeled data, while the demanded mapping relationship between inputs and SOH is rapidly acquired through a slight retraining process. Consequently, the self-supervised learning approach facilitates the integration of learned aging-related information, simultaneously expediting the convergence process during subsequent target SOH estimation tasks. In comparison to previous TL-based SOH estimations, the proposed technique migrates knowledge gained from unlabeled data in the source domain. This renders the proposed method notably more efficient, as it effectively leverages a limited labeled sample. It is noteworthy that pretext learning can be conducted using unlabeled data sourced from either the battery being tested or from other batteries. However, only sparse labeled data from the tested battery are requisite for the fine-tuning stage.

2.2.2. ESTIMATION RESULTS WITH SELF-SUPERVISED FRAMEWORK

2.2.2.1 Pretext learning evaluation

13 batteries with different types and working conditions are used for effective demonstration. The detailed information is listed in our published paper J4. The primary objective of the encoding is to uncover the aging-related insights concealed within the unlabeled operating data. PCC between the acquired features and battery SOH are assessed to gauge the effectiveness of the pretext learning phase. Fig. 2-10 (a)-(e) illustrate the variations of the features (five neuron values) against SOH of B#1. The analysis delves into the correlations between every individual hidden feature (abbreviated as HS) and the respective SOH. The outcomes for all batteries are presented in Fig. 2-11(f). The results are quite compelling, revealing that all encoded hidden features display robust linear relationships with SOH. This finding signifies that the autoencoder successfully distills pivotal aging-related insights. Moreover, this observation lends credence to the explanation of the subsequent SOH estimation. It demonstrates that substantial correlations exist between these hidden features and the ultimate output (SOH).

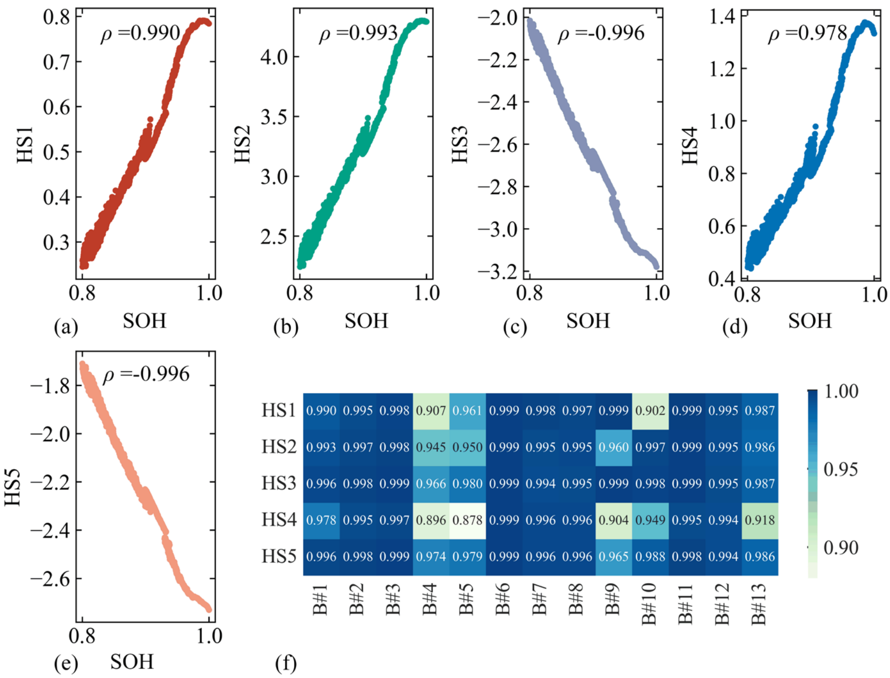

Figure 2-10 Correlations between the encoded features and battery SOH, (a-e) exemplary results for one battery, and (f) heatmaps for all batteries. Source: [J4]

The numeric outcomes across all 13 batteries demonstrate the applicability of pretext learning in extracting aging-related insights, effectively catering to batteries operating in diverse scenarios. A significant portion of the PCCs exceeds 0.99, underscoring the strong alignment between the learned features and actual aging traits. Interestingly, PCCs are slightly diminished under variable and high temperatures, relative to constant temperatures. This observation indicates temperature fluctuations indeed influence the pretext task's learning efficacy. Likewise, there is a marginal reduction in PCCs for pulse charging profiles. However, this reduction is not notably substantial, which substantiates that the data clean methodology proficiently retains core aging characteristics, aligning well with various application demands.

2.2.2.2 Downstream SOH estimation

The earlier demonstration of pretext learning underscores the acquisition of core aging characteristics through the utilization of unlabeled samples via auto-encoder. This section proceeds with the presentation and evaluation of downstream SOH estimation for batteries subjected to diverse aging conditions. For the target task, the parameters acquired through pretext learning in the neural network are employed and then fine-tuned for SOH estimation, which is conducted using a small subset of labeled data. Specifically, the initial 20% data is allocated for pretext learning, and downstream fine-tuning relies on just three labeled samples: the first cycle, the sample at 10% point, and the sample at 20% point. In addition to RMSE and MAE, the coefficient of determination (R^2) is also used for model evaluations.

The outcomes of the model are visually depicted in Fig. 2-11, encompassing the estimation for every individual battery, as well as estimations and error distributions for all 13 batteries. Detailed numeric results are documented in Table 2-5. These findings collectively reveal that the estimations align satisfactorily with the ground truths across all the testing batteries, irrespective of battery types, and operational or environmental temperature conditions. This substantiates the method's aptitude for generalization and robustness.

In the case of NCA battery estimations (i.e., B#1 to B#6 in the figure), the results exhibit a higher degree of accuracy, even when subjected to dynamic discharging current profiles. When considering the results for the two cells operating under variable temperature conditions, although the estimations show slightly larger deviations from actual SOH, they still converge satisfactorily. This indicates that estimations remain robust under variable temperature conditions and diverse aging profiles. Regarding second-life batteries, the estimations continue to exhibit accuracy although different aging patterns exist. Quantitatively, RMSE and MAE for these six batteries are both below 1.28% and 1.14%, respectively, and R^2 exceeds 0.95.

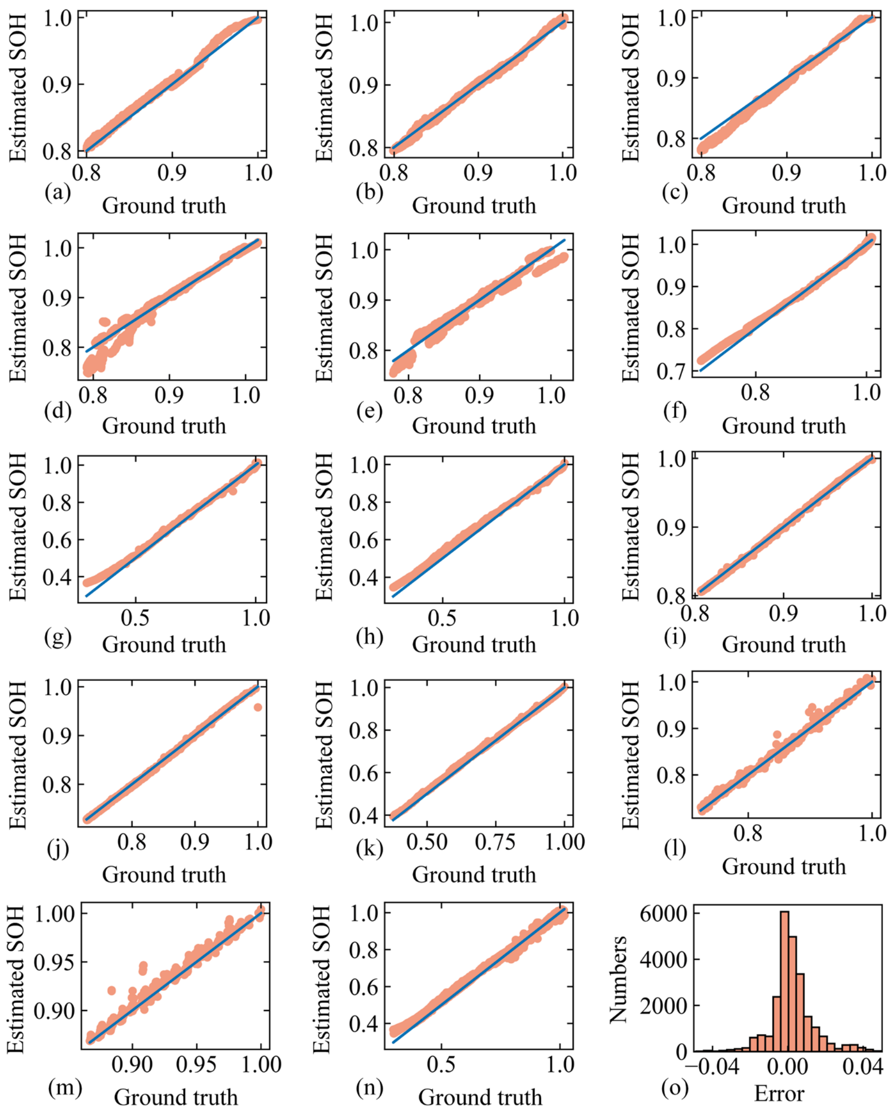

Figure 2-11 SOH estimation results based on self-supervised learning. (a-m) estimations for individual B#1-B#13, (n) estimations for all the batteries, and (o) error distribution of the estimations for all the batteries. Source: [J4]

Polymer batteries that operate at room temperature throughout their entire lifespan (until SOH drops below 0.4) exhibit promising outcomes, as indicated in Fig. 2-11(g and h). The depicted results also demonstrate favorable estimations with RMSE and MAE below 3% and 2.9% and R^2 exceeding 0.96. The final category of batteries, namely NCM batteries, undergoes aging through both CC and pulse current charging.

The employed data clean techniques and estimation methodology effectively accommodate SOH estimations even when subjected to pulse charging profiles, thereby expanding the potential scope of application. The outcome of the estimation process reveals the presence of a few outliers, but most of the estimations closely align with actual values. Specifically, for the battery subjected to a charging frequency of 0.2 Hz, RMSE, MAE, and R^2 stand at 0.873%, 0.615%, and 0.987 respectively. Similarly, for the battery undergoing a frequency of 0.05 Hz, these metrics are 0.645%, 0.425%, and 0.965 respectively.

Table 2-5 Results for the self-supervised SOH estimations. Source: [J4]

Battery	RMSE (%)	MAE (%)	R^2	Battery	RMSE (%)	MAE (%)	R^2
B#1	0.712	0.658	0.977	B#8	2.968	2.673	0.967
B#2	0.382	0.314	0.995	B#9	0.169	0.146	0.999
B#3	1.272	1.134	0.956	B#10	0.282	0.227	0.998
B#4	1.276	0.860	0.954	B#11	1.235	1.060	0.994
B#5	1.141	0.930	0.957	B#12	0.873	0.615	0.987
B#6	0.883	0.638	0.988	B#13	0.645	0.425	0.965
B#7	2.067	1.762	0.984	All	1.139	0.762	0.989

The estimation outcomes for all battery types are visually depicted in Fig. 2-12(n), while the error distribution is illustrated in Fig. 2-11(o). It is evident that the absolute errors remain within the range of 5%, with the majority falling below 2%. This observation underscores the robustness and precision of the SOH estimations across various application scenarios, encompassing distinct battery chemistries and configurations. This promising characteristic holds significance for real-world applications, given that the process only necessitates unlabeled data, along with a limited set of labeled data.

Subsequent mutual verification was undertaken to further assess the efficacy of the proposed framework. In this process, batteries B#1 through B#3 were employed for unsupervised pretext learning. This initial learning phase was followed by downstream fine-tuning, which was carried out using a small set of early sparsely labeled samples. The outcomes of this mutual verification approach were showcased through results concerning batteries B#4 to B#7, as illustrated in Fig. 2-12(a-d) respectively. The evaluation scenarios depicted in Fig. 2-13(a) and (b) were designed to assess the impact of incorporating information from constant temperature conditions to boost performance under varying temperatures. The outcomes in Fig. 2-12(c) aimed to validate the hypothesis that integrating aging insights garnered from new batteries contributes to the accuracy enhancement of second-life batteries. The concluding test scenario in Fig. 12(d) was devised to demonstrate that aging-related characteristics obtained from battery type prove valuable for accurately estimating the SOH of a different battery type. Importantly, these testing scenarios hold practical significance. Given the challenges associated with training models using an extensive volume of samples for onboard BMS, the approach of utilizing a pretext model trained on data from other batteries, followed by fine-tuning using sparsely labeled data, presents great value in boosting performance. Hence, the proposed framework effectively supports mutual utilization scenarios.

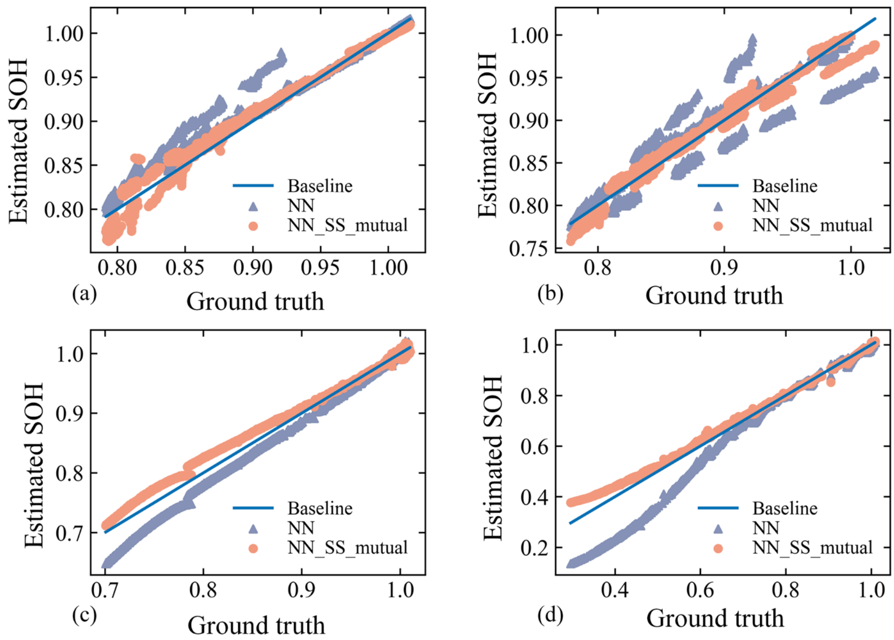

Figure 2-12 Verifications with unlabeled data from other batteries. (a)/(b)/(c)/(d) results for B#4/B#5/B#6/B#7. Source: [J4]

2.2.2.3 Comparative evaluations

For a further assessment, we present numerical comparisons with other ML models in Fig. 2-13, with detailed results provided in Table 2-6. In Fig. 2-13, each dot corresponds to the result achieved by one battery cell using the respective model, and the distribution signifies method's robustness and adaptability across diverse application scenarios. The outcomes listed in Table 2-6 are averaged indexes across all 13 batteries, offering insight into the overall performance of each model across various applications. Fig. 2-13 highlights that conventional models employing only supervised learning exhibit notable error spreads. Conversely, the proposed model showcases the smallest distribution, with all errors falling within lower ranges and R^2 attaining higher values. Referencing the indicators in Table 2-6, accuracy enhancement becomes more apparent. The average RMSE and MAE for the proposed NN_SS approach stand at only 1.07% and 0.88% respectively, whereas conventional methods surpass 2.27% and 1.73% respectively. This indicates that the proposed method mitigates errors by over 1 time on average. The average R^2, at 0.978 for NN_SS, also outperforms other methods, signaling closer convergence to actual values. Further, the average value of maximum absolute error stands merely 3.336%, reflecting a narrow error range and greater reliability in estimations compared to alternative techniques. Consequently, based on the comparative evaluations, the proposed self-supervised learning effectively boosts the accuracy and reliability of battery SOH estimation. More evaluations using public datasets are detailed in J4.

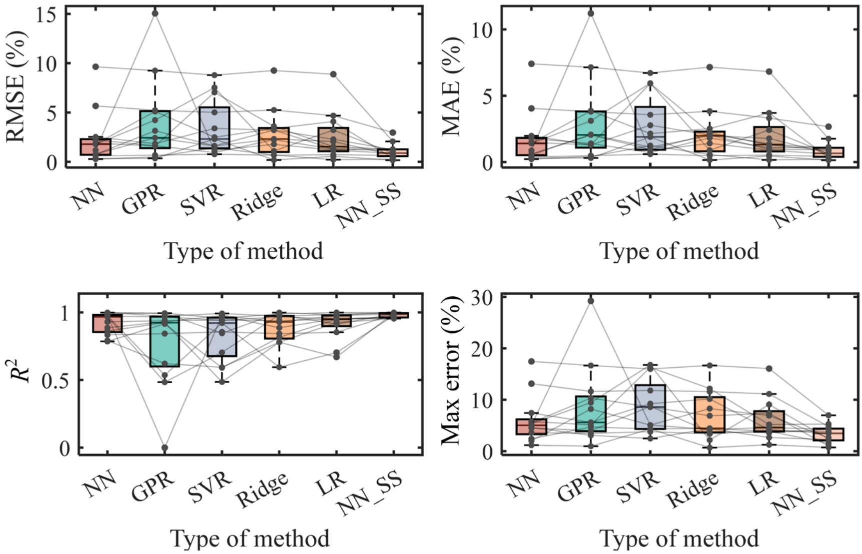

Figure 2-13 Comparative evaluations with different estimation models. Source: [J4]

Table 2-6 Mean values of each indicator with different models. Source: [J4]

Method	RMSE	MAE	R^2	Max error
NN	2.268	1.730	0.921	5.997
GPR	3.928	2.961	0.779	8.645
SVR	3.391	2.653	0.830	8.645
Ridge	2.840	2.094	0.883	6.828
LR	2.464	1.909	0.909	6.140
NN_SS	1.070	0.880	0.978	3.336

2.2.3. SUMMARY

This section presents an innovative self-supervised strategy designed to enhance battery SOH estimation. This is achieved by a pretext feature learning phase utilizing unlabeled data, followed by a downstream target learning phase involving a limited set of labeled samples for model fine-tuning. For pretext learning and the extraction of latent features, an auto-encoder-decoder architecture is employed. Through PCC analysis, the learned hidden features exhibit substantial coefficients exceeding 0.96 on average in relation to battery SOH. This attests to the effectiveness of the acquired aging characteristics. By utilizing only a small subset of labeled samples for learning the downstream SOH estimation, the proposed method's accuracy and reliability are substantiated to surpass conventional ML techniques. Using merely three labels, the proposed model yields RMSE and mean MAE of 1.07% and 0.88% respectively, alongside a mean maximum absolute error of 3.336%. Notably, the R^2 reaches 0.978. Furthermore, validations encompass diverse batteries, distinct loading profiles, and varying temperatures, underscoring method's robustness and potential for its continued enhancement throughout the aging process.

CHAPTER 3. STATE OF HEALTH ESTIMATION BASED ON TRANSFER LEARNING: DOMAIN ADAPTATION

Fine-tuning-based TL strategy is studied in the above chapter. Nevertheless, it still requires labels for model re-training. There are some cases where no labels are available. How to transfer knowledge without labels is also worth investigating. Therefore, unsupervised DA is proposed to deal with estimations under no labeled data available from the target batteries. The effectiveness of both SOH point estimation and differential temperature (dT) curve estimation is proved. Then, the combination use of both sparsely labeled data and unlabeled data is used for SOH estimation improvement based on a novel domain adaptative CL framework. The catastrophic forgetting problem for ML model is addressed with memory-based CL. The model can be initially built with only one battery, and continual updating during usage under different scenarios that increase the generalization ability. In addition, the unbiased feature distributions help interpret the model performance. Both two sections are verified using comprehensive experimental datasets obtained with different types of batteries working under different loadings and temperatures. With works in this chapter and the previous chapter, comprehensive TL-based battery SOH estimations are studied for the selected reference in intelligent battery management.

J5, J6, and C2 contribute to this chapter.

3.1. SOH ESTIMATION BASED ON DOMAIN ADAPTATION

The battery health prognostics framework for STS dT curve prediction and STP SOH estimation considering DA is depicted in Fig. 3-1. It begins with transforming Q-V sequence into a dQ-V sequence, which creates model inputs. The dT curve reconstruction model employs LSTM due to strong temporal relationships in time series data. Subsequently, a fully connected layer is appended to predict dT curve. To mitigate domain discrepancies existing between source and target batteries, maximum mean discrepancy (MMD) loss is applied after the second LSTM layer. The predicted dT and measured dQ sequences are consequently utilized to estimate battery SOH, where the MMD loss is again incorporated before the output layer to minimize domain discrepancies. Detailed frameworks for end-to-end battery health prognostics are described in next subsections, where the dT prediction and SOH estimation are presented in detail.

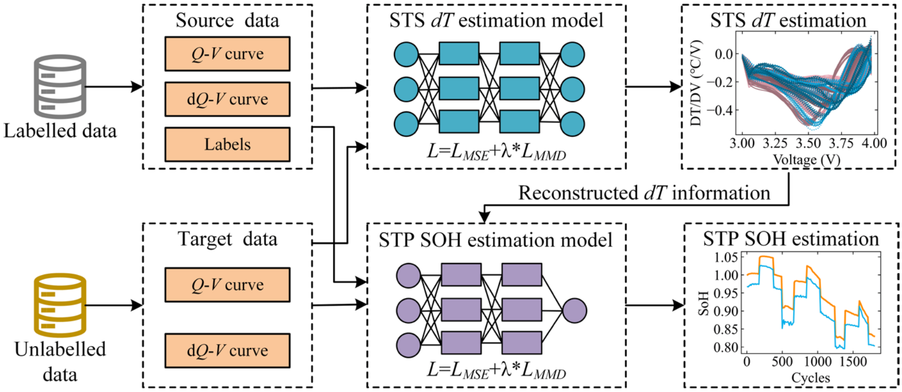

Figure 3-1 Flowchart for DA-based battery health prognostics containing dT prediction and SOH estimation. Source: [J5]

3.1.1. END-TO-END ESTIMATION

3.1.1.1 d*T* curve reconstruction

Temperature variations are important indicators to be monitored especially during charging to ensure safe operation [82]. The dT curve is also important information for battery health estimation [83], [84]. Obtaining temperature variations for each cell in a battery pack is impractical due to the limited thermal sensors. Therefore, estimation of temperature variations is also a crucial task. The dT prediction is achieved by the STS structure in this section. STS prediction framework facilitates the reconstruction of dT curve with input of dQ sequence. The process to generate these sequences involves the following steps. Constructing the dQ sequence necessitates ensuring voltage passes through a specific voltage range. STS dT prediction based on the NN depicted in Fig. 3-2. Within this architecture, the LSTM layer is employed to extract time-series properties. An output layer is introduced after the second LSTM to generate the predicted dT sequence. These sequences are derived by segmenting corresponding curves using identical voltage sequences, resulting in an output length matching the input. Specific settings for the network structure can refer to J5.

3.1.1.2 SOH estimation

Following dT reconstruction, temperature information is integrated with the electric information (dQ) to estimate SOH with STP framework. To be specific, dQ is utilized as the first input dimension. Furthermore, incorporating temperature variation details is crucial, as it encompasses significant aging-related information and significantly enhances SOH estimation accuracy, which has been demonstrated in prior research [83]. Consequently, the predicted dT is incorporated as an additional input feature into the SOH estimation model. The model to estimate SOH with STP architecture is also illustrated in Fig. 3-2, which adheres to a similar overall design as the NN employed in predicting dT curve. Initially, time-series dQ and dT are learned by two LSTM layers, followed by the output layer containing a single neuron to yield the ultimate SOH estimation. The hyperparameters remain consistent with those of the dT curve reconstruction model, except for the output neuron, which is set as 1 to output SOH.

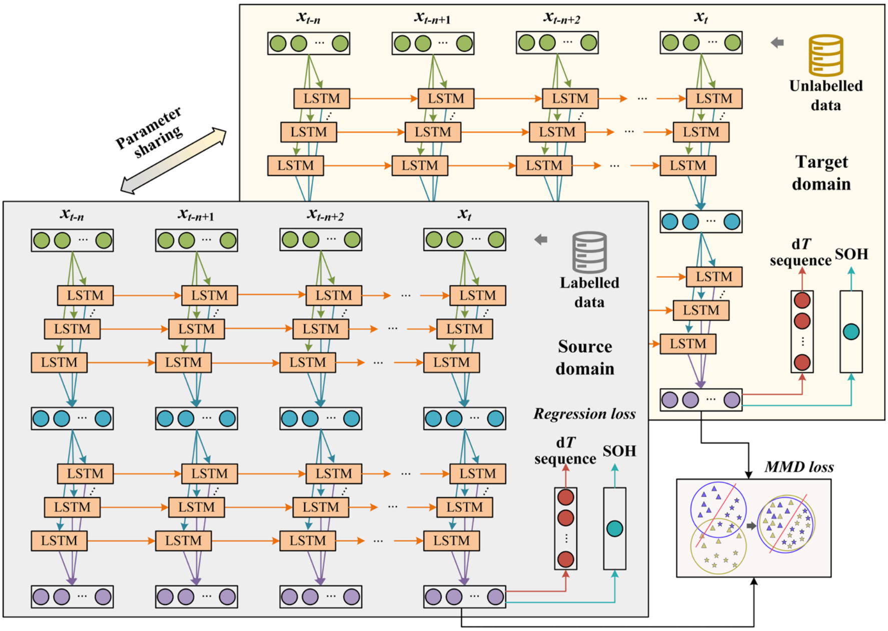

Figure 3-2 Model for domain adaptative dT prediction and SOH estimation. Source: [J5]

3.1.2. TRANSFER LEARNING WITH DOMAIN ADAPTATION

Conventional data-driven techniques often encounter difficulties in generalization. Models trained on a source battery might not perform well on testing batteries, especially when distinct dissimilarities exist in the application scenarios. These differences give rise to significant discrepancies between domains of source and testing batteries. In many existing techniques, a limited set of labeled data from the testing battery is utilized for model fine-tuning. However, obtaining labeled data is often impractical in real-world scenarios. As a result, leveraging unlabeled data becomes more valuable to enhance prognostic accuracy. In pursuit of this objective, this study employs MMD to alleviate domain incongruities present in the hidden features. The integration of MMD into the original model is illustrated in Fig. 3-2. This involves diminishing the domain discrepancies between the source and target battery in the outputs from the last time step of LSTM to enhance the model accuracy.

The disparity between two probability distributions can be quantified by MMD by evaluating the difference in their mean embeddings of features [85]. The MMD between datasets $X = \{x_i\}_{i=1}^{n_1}$ and $Y = \{y_i\}_{i=1}^{n_2}$ is expressed as [86],

$$MMD_{\mathcal{H}}(X,Y) = sup_{\Phi\in\mathcal{H}}(E_p[\Phi(x)] - E_q[\Phi(y)]) \tag{3.1}$$

where $\mathcal{H}$ is a reproducing kernel Hilbert space (RKHS), $\Phi(\cdot)$ represents a nonlinear mapping function that transforms data from the original space to the RKHS space, and p and q are probability distributions that generate the two sets of data. MMD can be empirically approximated as [87], [88],

$$MMD_{\mathcal{H}}^2(X,Y) = \left\| \frac{1}{n_1}\sum_{i=1}^{n_1}\Phi(x_i) - \frac{1}{n_2}\sum_{j=1}^{n_2}\Phi(y_j) \right\|_{\mathcal{H}}^2 \tag{3.2}$$

The expression can be obtained by kernel trick [88],

$$\begin{aligned} MMD_{\mathcal{H}}^2(X,Y) = {} & \frac{1}{n_1^2}\sum_{i=1}^{n_1}\sum_{j=1}^{n_2} k(x_i, x_j) - \frac{2}{n_1 n_2}\sum_{i=1}^{n_1}\sum_{j=1}^{n_2} k(x_i, y_j) \\ & + \frac{1}{n_2^2}\sum_{i=1}^{n_1}\sum_{j=1}^{n_2} k(y_i, y_j) \end{aligned} \tag{3.3}$$

where k(·,·) represents kernel function of RKHS, with specific usage of the Gaussian radial basis function (RBF) kernel [88],

$$k(x_i, y_j) = \exp\left((-||x_i - y_j||^2)/2\gamma^2\right) \tag{3.4}$$

During the training phases for both dT prediction and SOH estimation, the MSE is employed to assess the regression quality. Simultaneously, MMD loss aims to gauge the divergence between the produced hidden features in different domains. As a result, the ultimate loss function encompasses both regression and transfer losses, forming a composite evaluation criterion denoted as,

$$\mathcal{L} = \mathcal{L}_{MSE} + \lambda\mathcal{L}_{MMD} \tag{3.5}$$

where λ serves as a weight, signifying the penalty coefficient that quantifies the extent to which DA should be taken into account.

3.1.3. HEALTH PROGNOSTIC RESULTS AND DISCUSSION

3.1.3.1 Results for dT prediction

The outcomes include dT predictions for fresh and second-life batteries in this section. The detailed information on the used batteries can refer to J5. The results for fresh batteries (lab dataset#1) undergoing dynamic discharging are shown in Fig. 3-3. Fig. 3-3 (a) - (c) showcase outcomes when utilizing cell 1 (UDDS) as source battery to predict the dT curve of and target cell 2 (HWFET). Conversely, Fig. 3-3 (d) - (f) depicts results in the inverse situation. The results obtained by basic LSTM model are depicted in Fig. 3-3(a) and 3-3(d), while Fig. 3-3(b) and 3-3(e) demonstrate outcomes derived from the proposed model. Moreover, Fig. 3-3(c) and Fig. 3-3 (f) display peak values extracted from predicted dT curves as well as actual dT curves. Within the figures, "Real," "Base," and "DA" correspond to the actual curve, outcomes from conventional model, and proposed approach, respectively. The results highlight the LSTM-based STS model's ability for dT curve predictions using dQ as input even without relying on temperature sensors. However, the basic LSTM model's reconstructed curve occasionally exhibits noticeable anomalies, attributed to domain discrepancies between the training and testing batteries. The DA-based model, on the other hand, exhibits enhanced performance. The dT curve's peak value, a crucial indicator for battery health prognostics, holds a strong correlation with battery capacity [83], [89]. Furthermore, peaks derived from the predicted dT curves become closer to real values.

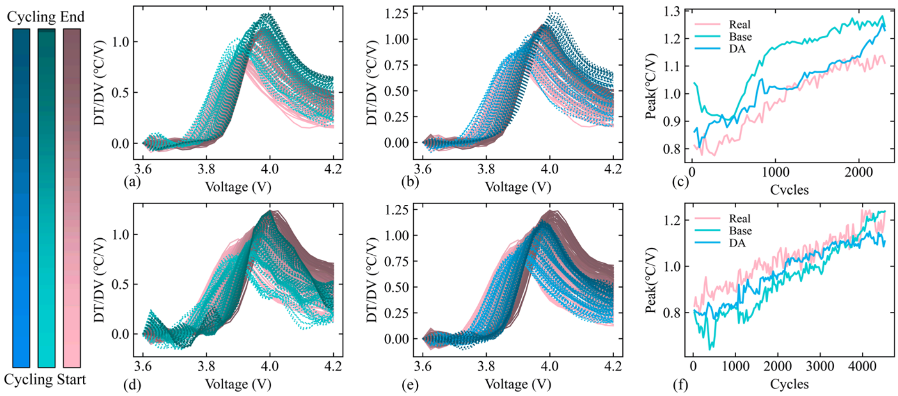

Figure 3-3 The dT curve and peak value predictions for batteries aged under dynamic discharging loading profiles. Source: [J5]

The performance for dT predictions of second-life batteries (lab dataset#2) under varying temperatures is also assessed. The outcome of these estimations is depicted in Fig. 3-4, with each subfigure's interpretation mirroring that of Fig. 3-3. In the context of fluctuating temperatures, dT curves also exhibit unstable variations from beginning to the end of cycling due to the influence of the relationship between capacity and environmental temperature on degradation curve shape. Within this testing condition, the predicted dT curves through the proposed model exhibit substantial enhancement compared to the conventional approach. While basic LSTM can estimate the dT curve trends, significant disparities persist between the reconstructed and actual curves. Furthermore, estimated peak values significantly deviate from actual values, potentially adversely affecting SOH estimation. In contrast, the dT curves and corresponding peak values predicted by the proposed model closely align with actual values. This underscores the potential of extracting temperature information to enhance health prognostics.

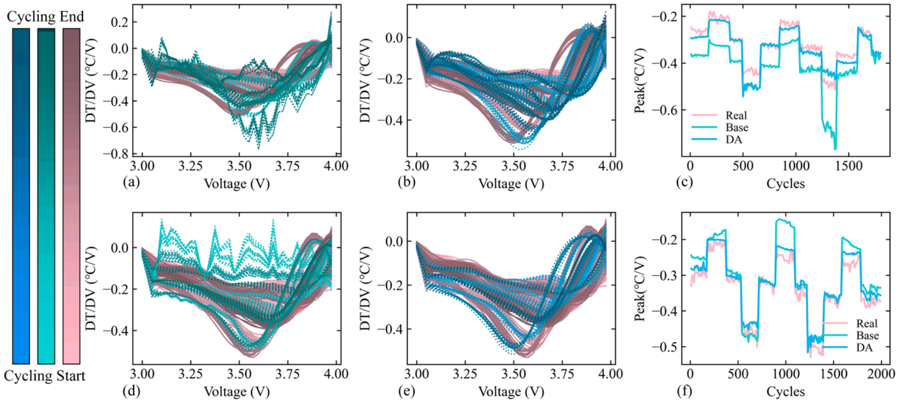

Figure 3-4 The dT curve and peak value predictions for second-life batteries aged under variable environmental temperature. Source: [J5]

Numerical results are presented in Table 3-1 and Table 3-2, outlining the errors of predicted dT curves and peak values, respectively. Significant improvements are demonstrated in the proposed method compared to the conventional LSTM-based model. For conventional model predicted dT curves, mean RMSE and MAE across are 0.085 °C/V and 0.063 °C/V, respectively. In contrast, the proposed model yielded these two values of 0.066 °C/V and 0.049 °C/V, translating to a 22.6% error reduction. Additionally, the proposed method demonstrated error reductions of 51.5% and 54.4% in predicted peak values, as compared to the basic LSTM.

Furthermore, the evaluation incorporates three commonly used ML algorithms – feedforward NN (ANN), GPR, and RF – for STS dT estimation comparison. Results indicate that conventional LSTM, RF, and GPR exhibit close accuracy, surpassing the ANN. While one method may outperform others in specific battery cases, it may lag in different scenarios, highlighting the limited robustness of conventional data-driven techniques. However, the proposed model with DA enhances LSTM accuracy by addressing domain discrepancies and maintaining high accuracy across various working conditions. Table 3-3 provides the maximum absolute error (MaxAE) for the predicted dT, comparing basic LSTM and proposed domain adaptive LSTM. The mean MaxAE for using basic LSTM across four scenarios is 0.156 °C/V, while the proposed method yields 0.100 °C/V. For peak values, the MaxAE is 0.218 °C/V with conventional LSTM and 0.117 °C/V with the proposed DA-based LSTM. Both sets of results underline the improved accuracy brought about by the proposed model. The comparative outcomes underscore that the proposed approach outperforms conventional data-driven methods in terms of accuracy and robustness.

Table 3-1 Errors (℃/V) comparisons for the dT curve reconstruction. Source: [J5]

	Error	L#1_C1_to_C2	L#1_C2_to_C1	L#2_C1_to_C2	L#2_C2_to_C1	Mean
LSTM	RMSE	0.109	0.106	0.083	0.044	0.085
	MAE	0.083	0.081	0.056	0.033	0.063
LSTM_DA	RMSE	0.084	0.088	0.050	0.042	0.066
	MAE	0.063	0.066	0.036	0.032	0.049
ANN	RMSE	0.113	0.172	0.086	0.064	0.109
	MAE	0.084	0.141	0.061	0.052	0.085
RF	RMSE	0.113	0.107	0.078	0.063	0.090
	MAE	0.094	0.080	0.050	0.048	0.068
GPR	RMSE	0.098	0.123	0.079	0.058	0.089
	MAE	0.075	0.094	0.058	0.043	0.067

Table 3-2 Errors (℃/V) comparisons for the estimated peak values. Source: [J5]

	Error	L#1_C1_to_C2	L#1_C2_to_C1	L#2_C1_to_C2	L#2_C2_to_C1	Mean
LSTM	RMSE	0.139	0.107	0.09	0.039	0.094
	MAE	0.127	0.092	0.077	0.03	0.082
LSTM_DA	RMSE	0.063	0.066	0.031	0.022	0.045
	MAE	0.051	0.055	0.024	0.018	0.037
ANN	RMSE	0.159	0.208	0.072	0.051	0.123
	MAE	0.157	0.198	0.059	0.033	0.112
RF	RMSE	0.126	0.116	0.062	0.069	0.093
	MAE	0.113	0.109	0.041	0.059	0.08
GPR	RMSE	0.08	0.167	0.062	0.067	0.094
	MAE	0.068	0.162	0.042	0.057	0.082

Table 3-3 Maximum absolute errors (℃/V) for dT curve reconstruction. Source: [J5]

Test	LSTM		LSTM_DA	
	Curve	Peak value	Curve	Peak value
L#1_C1_to_C2	0.125	0.279	0.111	0.157
L#1_C2_to_C1	0.155	0.230	0.136	0.169
L#2_C1_to_C2	0.233	0.261	0.090	0.090
L#2_C2_to_C1	0.111	0.101	0.064	0.054
Mean	0.156	0.218	0.100	0.117

3.1.3.2 SOH estimation

The outcomes of SOH estimations for fresh batteries undergoing dynamic discharging are displayed in Fig. 3-5(a)-(b) and Fig. 3-5 (c)-(d), respectively. These estimations are compared against results obtained using the conventional LSTM-predicted dT curve and the DA-based LSTM-predicted dT curve, while without DA applied to SOH estimation model. These two benchmark methods are respectively labeled as "Benchmark 1" and "Benchmark 2". Additionally, estimations obtained by the proposed approach are referred to as "Multi DA," which employs a two-stage DA.

Observations reveal that employing a DA-based model to predict dT curve leads to more precise thermal characteristics. This, in turn, translates to a noticeable improvement in results from "Benchmark 1" to "Benchmark 2." The improved correlation between estimated and real SOH values is evident in Fig. 3-5, reflecting a more linear relationship. Numeric results for SOH estimation errors are outlined in Table 3-4. Results indicate that RMSE and MAE values respectively decrease from 2.241% and 1.828% to 1.756% and 1.573% for cell 1 when transitioning from "Benchmark 1" to "Benchmark 2", which are from 3.317% and 3.123% to 1.687% and 1.524% for cell 2. Incorporating DA in SOH estimation model results in further enhancements, reducing RMSE and MAE values respectively to 1.671% and 1.519% for cell 1, and 1.364% and 1.257% for cell 2. This evaluation underscores that employing multi-stage DA processes solely using unlabeled data significantly improves battery health prognostics when compared to conventional models.

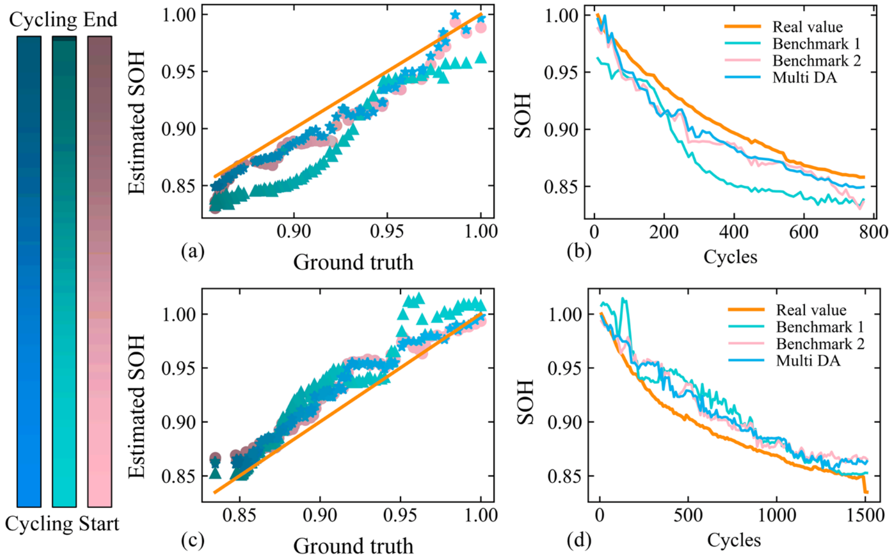

Figure 3-5 SOH estimations for batteries aged under dynamic discharging profiles. (a)/(b) results of L#1_C1_to_C2 situation, (c)/(d) results of L#1_C2_to_C1 situation. Source: [J5]

SOH estimation results for second-life batteries undergoing varying environmental temperatures are also assessed, where the outcomes for cell 2 and cell 1 are depicted respectively in Fig. 3-6 (a)-(b) and Fig. 3-6 (c)-(d). The intermittent shifts in SOH curves result from temperature changes, given the different charged/discharged capacities associated with varying temperatures. Two benchmarks are employed for comparison, in a manner analogous to the previous discussions. Results in Fig. 3-6 (b) and Fig. 3-6 (d) clearly depict a convergence of real values from benchmarks towards the proposed "Multi-DA" approach. Conversely, estimation results reveal that while a linear correlation exists between estimated and real SOH for benchmarks, deviations from the perfect fitting line suggest disparities. On the contrary, estimated SOH values from the proposed model demonstrate less divergences from the real values. The colors of the dots do not show monotonic variations in Fig. 3-6 (a) and Fig. 3-6 (c), and gaps in the dots result from varying temperatures. Numerical outcomes presented in Table 3-4 distinctly highlight the improved accuracy of the proposed model. "Benchmark 1" demonstrates larger estimation errors than "Benchmark 2", which suggests that DA-based dT curve prediction offers thermal characteristics for improving SOH estimation accuracy. The mean values of RMSE and MAE for "Benchmark 1" surpass 3.3%, which is larger than 2.7% for “Benchmark 2” and is substantially reduced to below 1.8% with the proposed model. The RMSE and MAE are respectively reduced by 17.763% and 18.302% by incorporating thermal characteristics in “Benchmark 2” with comparisons to “Benchmark 1”. The two indexes show significant reductions of 47.010% and 49.572% respectively with the proposed model, where MaxAE also drops from 7.340% remarkably to 4.689%.

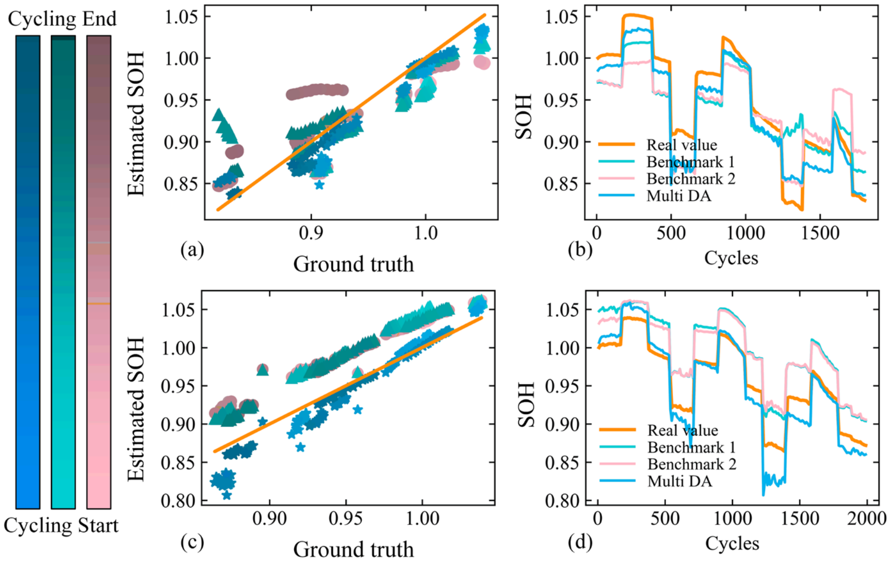

Figure 3-6 SOH estimations for second-life batteries aged under variable environmental temperatures. (a)/(b) results of L#1_C1_to_C2 situation, (c)/(d) results of L#1_C2_to_C1 situation. Source: [J5]

While existing publications have validated that dT curve information can improve SOH estimation performances, we further substantiate this assertion under varying temperature conditions. In order to showcase the role of thermal characteristics on SOH estimation, numerical results of the proposed model and approaches lacking predicted dT as input are demonstrated in Table 3-5. In the table, " without dT" refers to a model solely trained using dQ curves for SOH estimations. Outcomes indicate the inclusion of predicted dT curve result in improved accuracy, while DA benefit for future performance improvements. These findings underscore that dT curve-derived thermal characteristics contribute to improved SOH estimation. This improvement stems from temperature effects on battery capacity, which is essential as environmental temperatures fluctuate with changing seasons. Consequently, the additional thermal depiction provided by the predicted dT curves through the proposed prognostic model serves a dual purpose: enabling thermal behavior monitoring and enhancing SOH estimation accuracy. More analysis and evaluations using public datasets can refer to J5.

Table 3-4 Errors of SOH estimation results (%). Source: [J5]

	Error	L#1_C1 to_C2	L#1_C2 to_C1	L#2_C1 to_C2	L#2_C2 to_C1	Mean
Benchmark 1	RMSE	3.317	2.241	3.717	4.102	3.344
	MAE	3.123	1.828	3.18	4.021	3.038
	MaxAE	4.807	5.687	11.33	7.534	7.340
Benchmark 2	RMSE	1.687	1.756	3.649	3.907	2.750
	MAE	1.524	1.573	3.011	3.819	2.482
	MaxAE	3.218	3.649	7.344	7.621	5.458
Multi DA	RMSE	1.364	1.671	2.091	1.961	1.772
	MAE	1.257	1.519	1.842	1.511	1.532
	MaxAE	2.816	3.525	5.896	6.519	4.689

Table 3-5 SOH estimations with/without predicted dT as features. Source: [J5]

Method	L#2_C1_to_C2		L#2_C2_to_C1	
	RMSE (%)	MAE (%)	RMSE (%)	MAE (%)
Benchmark without *dT*	3.738	3.478	3.984	3.919
DA without *dT*	2.647	1.999	3.262	2.901
Benchmark with *dT*	3.649	3.011	3.907	3.819
Multi DA	2.091	1.842	1.961	1.511

3.1.4. SUMMARY

This section introduces an innovative end-to-end methodology, featuring multi-stage multi-DA, aimed at sensor-free dT prediction and SOH estimation utilizing partial Q-V data. DA is integrated for accuracy and generalization improvement, which effectively mitigates domain discrepancies. The predicted *d*T curve is introduced as an additional feature, supplying thermal characteristics for SOH estimation improvement. An additional stage of DA is employed, further minimizing domain discrepancy in hidden features used for SOH estimation. This comprehensive approach effectively addresses the challenges of temperature-influenced battery behavior monitoring and accurate SOH estimation.

The outcomes for dT curve predictions clearly demonstrate that the proposed model yields error reductions of over 20% in comparison to conventional methods lacking DA. Moreover, the accuracy of SOH estimation benefits from the predicted dT curve, leading to RMSE and MAE reductions of 17.763% and 18.302% respectively, as compared to a benchmark model utilizing only Q-V curve information. By incorporating DA into SOH estimation, these values can be further reduced by 47.010% and 49.572%, respectively. Furthermore, the study's scope extends to verification using two public datasets, affirming the method's generalization capabilities. Remarkably, the proposed strategy utilizes only unlabeled data from testing batteries, thereby expanding the repertoire of TL strategies to enhance prognostic performance. This promising strategy is adaptable to various applications, as proven by the satisfactory results across different scenarios.

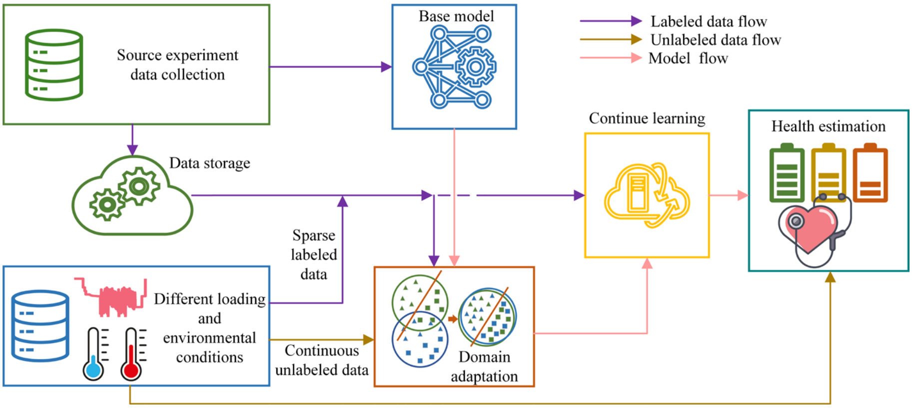

Figure 3-7 Framework to integrate both labeled and unlabeled data for TL-based battery SOH estimation. Source: [J6]

3.2. DOMAIN ADAPTATIVE CONTINUAL LEARNING STRATEGY

3.2.1. FRAMEWORK

In this section, based on both the fine-tuning and DA strategies invested above, the primary objective is to explore a method that maximizes the utility of both unlabeled and labeled data derived from batteries operating under diverse conditions. The aim is to enhance the accuracy, reliability, and generalization of data-driven battery health estimation models while avoiding catastrophic forgetting. The approach veers away from employing extensive source data for model training. Instead, the model is initialized using data from only a battery that has aged under CC conditions. This initial model is then refined across various applications, fostering continuous learning of aging information across a spectrum of scenarios. This allows the model to effectively cater to estimations in diverse scenarios. Memory-based CL updates are facilitated using only unlabeled data and sparsely labeled data. The model can be interpreted based on unbiased hidden state distributions across various scenarios. The overall framework is illustrated in Fig. 3-7, encapsulating the entire methodology. Specifically, the base model is initially trained on one source battery. The DA is then used to reduce the hidden feature domain discrepancies using the historical unlabeled data. The model is retrained using sparsely labeled data from the testing battery and sparsely stored data from the source battery. The final model is then employed to forecast target batteries' health under various scenarios. The detailed information can be referred to J6.

3.2.2. CONTINUAL LEARNING ABILITY

A significant challenge in the application of data-driven models is "catastrophic forgetting.", which means the model forgets the previously learned characteristics after retraining. In contrast, our model has the ability to continuously learn new aging information while retaining the capability to accurately estimate SOH for batteries with similar aging conditions encountered previously. To illustrate and evaluate this capability, we utilize the batteries aging with different C-rates and temperatures described in Chapter 2 for demonstrations.

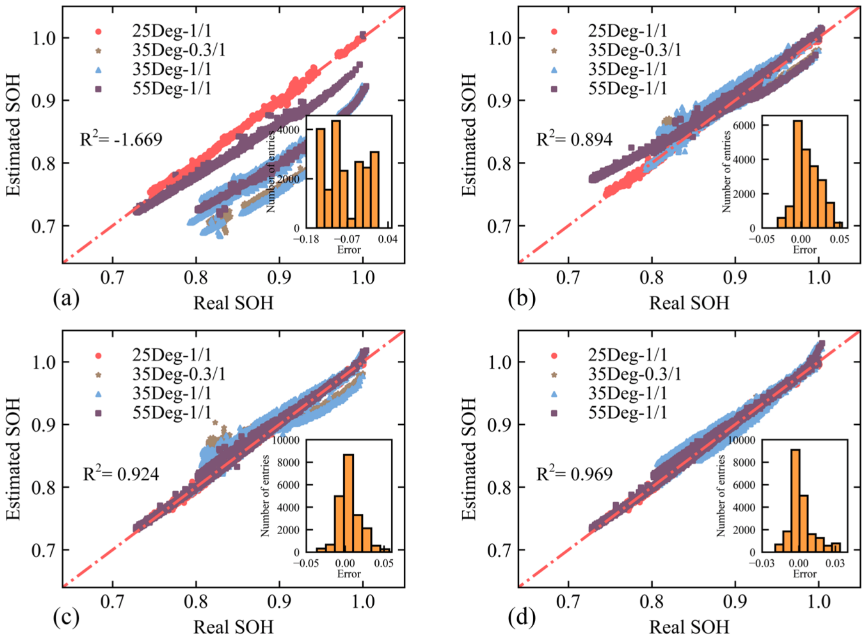

Figure 3-8 CL abilities. (a) estimated SOH and errors with initial model trained using data from 1C/25 ℃ (b) updated results with data from 1C/35 ℃ (c) updated results with data from 1C/55 ℃ (d) updated results with data from 0.3C/35 ℃. Source: [J6]

Our demonstration involves several steps, showcased in Fig. 3-8. Firstly, an initial base model trained using one cell aged at 1C under 25°C for training is used to estimate SOH for all batteries aged at 1C under 35°C and 55°C, and 0.3C under 35°C, as shown in Fig. 3-8(a). Subsequently, sparse data from batteries aging at 35°C with 1C are used for model updating, incorporating DA with sparsely labeled and unlabeled data collected from an early stage. The updated model is then employed for SOH estimation of all batteries, as displayed in Fig. 3-8(b). Further, sparse data from a battery aged at 1C/55°C and 0.3C/35°C are used to continually update the model sequentially. The estimation performance on all batteries is shown in Fig. 3-8(c) and Fig. 3-8(d), respectively. This process demonstrates that our model continuously acquires new aging information across diverse scenarios while retaining previously learned information. Comparative analysis reveals remarkable improvement from the initial base model to the final model. R^2 increases from -1.669 to 0.969, and the primary error distribution narrows from [-0.152, 0.014] to [-0.019, 0.034]. RMSE and MAE progressively decrease across cases a to d (Fig. 3-8(a) to Fig. 3-8(d)), as indicated in Table 3-6. For instance, RMSE and MAE for the final model in estimating all batteries decrease to 0.959% and 0.629% from initial values of 8.957% and 7.399%, respectively.

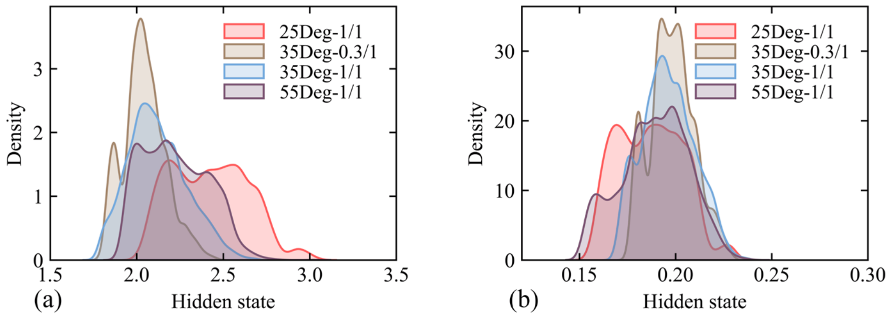

Figure 3-9 Hidden state distributions of batteries under different scenarios using (a) initial model and (b) final updated model. Source: [J9]

The model can be interpreted by the comparative results demonstrated in Fig. 3-9 (a) and Fig. 3-9 (b), where the hidden state distributions of batteries with different scenarios outputted by the initial model and the final updated model are presented. It clarifies the failure reason of the initial model for health estimations under different conditions and the reason for the generalization of our model is increased during usage. The feature distributions are almost overlapped, which enables the estimation model to have better accuracy and generalization under various working conditions.

Table 3-6 Numerical evaluation of CL ability. Source: [J6]

Case	RMSE	MAE	R^2	Error range
Case a	8.957%	7.399%	-1.669	[-0.152, 0.014]
Case b	1.782%	1.318%	0.894	[-0.030, 0.053]
Case c	1.513%	1.003%	0.924	[-0.036, 0.080]
Case d	0.959%	0.629%	0.969	[-0.019, 0.034]

To underscore the advantages of our approach over previously introduced fine-tuning methods, results obtained by the fine-tuning-based approach are illustrated in Fig. 3-10 (a-c). It becomes evident that while the fine-tuned model performs better for the target battery after updates, it suffers from catastrophic forgetting, leading to deteriorated performance in prior estimation scenarios. The distribution of hidden states, depicted in Fig. 3-10 (d), offers insight into this phenomenon post fine-tuning. It underscores that domain discrepancies persist between diverse scenarios, leading to poor model performance for previous tasks.

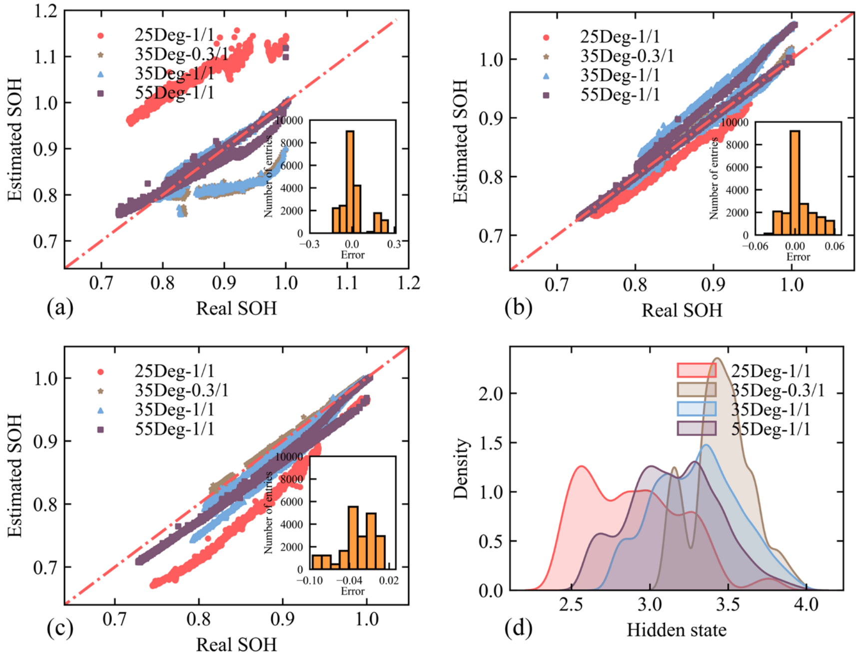

Figure 3-10 Model performance with fine-tuning strategy. (a) estimated SOH and errors with the initial model trained using data from 1C/25 ℃ (b) fine-tuned with data from 1C/35 ℃ (c) fine-tuned with data from 1C/55 ℃ (d) hidden state distributions. Source: [J6]

3.2.3. COMPARISONS WITH OTHER MACHINE LEARNINGS.

One of the major strengths of our model is its ability to sidestep catastrophic forgetting while absorbing new aging information. To assess accuracy and robustness across all estimation scenarios, we conduct a comparative analysis with other TL strategies, encompassing fine-tuning and basic DA. The RMSE for target and source batteries under different CC and temperature conditions (one battery serving as the source domain and others as testing batteries) is presented in Fig. 3-11(a) and Fig. 3-11(b), respectively. Notably, our model excels in scenarios involving diverse dynamic discharging profiles and variable temperatures, exhibiting a slender error distribution. This indicates superior accuracy and reliability compared to other models. For batteries in dynamic working currents and variable temperatures in their first and second-life states, RMSE and MAE outcomes are showcased in Fig. 3-11(c) and Fig. 3-11(d). Here, target batteries exhibit differing current rates and temperatures from the source battery, resulting in the base model displaying poor accuracy on the target domain. However, the introduction of information from batteries through TL or CL substantially reduces errors. While pure unlabeled data-enabled DA enhances accuracy for the target domain, sparse limited data further bolsters target domain accuracy. In contrast, pure fine-tuning grapples with catastrophic forgetting. Notably, our model consistently sustains strong performance across both target and source domains, with errors confined to a minimal range.

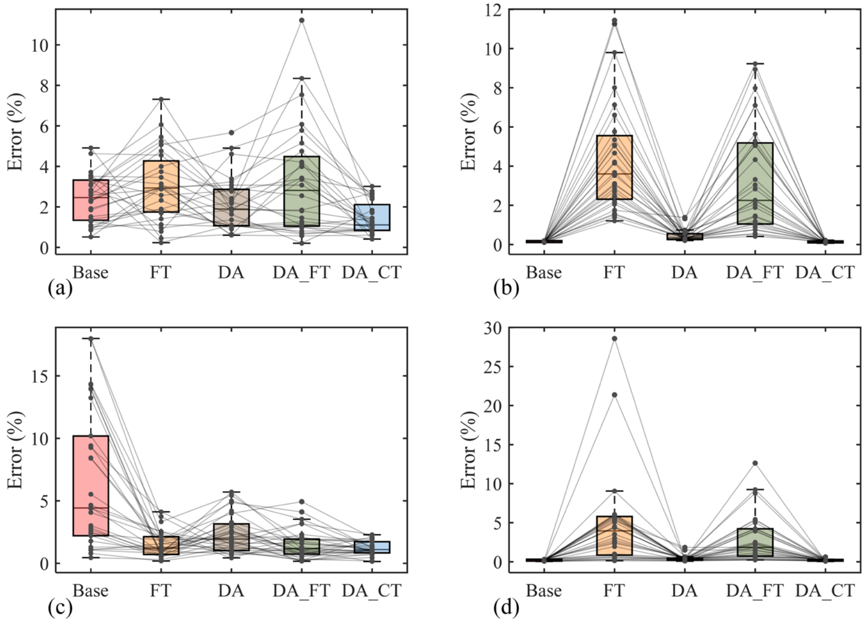

Figure 3-11 Comparisons with other transfer learnings. RMSE for (a) target and (b) source batteries with different C rates and temperatures. RMSE for (c) target and (d) source batteries with dynamic currents and variable temperatures. Source: [J6]

The comprehensive numerical statistical results for all batteries are presented in Table 3-7 and Table 3-8, illustrating the performance on the target domains and previously seen conditions respectively. The proposed model exhibits minimal mean and maximum errors, as well as reduced standard deviation (std) of error distributions. These characteristics collectively indicate precise and reliable estimations across diverse domains encompassing varied aging profiles and temperature conditions. Specifically, the mean and maximum RMSE for the target domain are 1.312% and 3.015% respectively, signifying an over threefold reduction from the initial base model. Notably, the std experiences a substantial decrease from 4.562 to a mere 0.682. Furthermore, the evaluation encompasses four widely employed ML methods for battery SOH estimation: LR, SVR, GPR, and RF. The outcomes, as demonstrated in Table 3-7 and Table 3-8, underscore that while these four methods perform well within their trained source domains, they fall short of delivering satisfactory estimations for target domains featuring diverse application conditions. It's also important to anticipate that these models would likely face challenges with catastrophic forgetting if solely updated using newly acquired data, similar to the fine-tuning strategy. In contrast, the proposed framework demonstrates superiority in terms of performance across both source and target domains when compared to conventional ML and TL methods.

Table 3-7 Numerical evaluation for the target conditions. Source: [J6]

Method	RMSE (%)			MAE (%)		
	Mean	Max	Std	Mean	Max	Std
BASE	4.573	17.987	4.562	4.193	17.965	4.475
FT	2.361	11.213	2.218	1.838	8.129	1.700
DA	2.259	5.704	1.412	1.949	5.484	1.274
DA_FT	2.361	11.213	2.218	1.838	8.129	1.700
DA_CT	1.312	3.015	0.682	1.085	2.662	0.628
GPR	3.952	17.959	3.999	3.497	17.938	3.719
RF	3.930	17.834	3.462	3.549	17.722	3.372
LR	14.758	185.806	35.519	10.784	147.825	27.389
SVR	4.137	23.651	5.170	3.893	23.633	5.121

Table 3-8 Numerical evaluation for the previously seen conditions. Source: [J6]

Method	RMSE (%)			MAE (%)		
	Mean	Max	Std	Mean	Max	Std
BASE	0.172	0.324	0.087	0.126	0.242	0.067
FT	3.108	12.633	2.869	2.826	12.076	2.679
DA	0.420	1.838	0.339	0.328	1.797	0.321
DA_FT	3.108	12.633	2.869	2.826	12.076	2.679
DA_CT	0.159	0.623	0.102	0.128	0.666	0.107
GPR	0.077	0.199	0.056	0.056	0.147	0.042
RF	0.039	0.074	0.021	0.026	0.046	0.013
LR	0.129	0.297	0.089	0.095	0.221	0.067
SVR	0.225	0.604	0.181	0.179	0.523	0.163

3.2.4. SUMMARY

In this section a data-driven battery health estimation model grounded in domain-adaptive CL is proposed, addressing a spectrum of challenges including limited generalization and robustness, extensive labeled data requirements, catastrophic forgetting, and limited interpretability. The proposed model begins with data from a common aging test and extends to estimations under unknown conditions, harnessing solely unlabeled data and sparsely limited labeled data from early stages. Crucially, our model is interpretable. By effectively reducing domain discrepancies between source and target batteries, our model interprets the notable estimation performances achieved. Furthermore, our model evolves continually, leveraging both unlabeled and labeled data from unknown conditions to enhance performance while retaining prior task proficiency, thereby mitigating catastrophic forgetting. In comparison to other TL approaches, our model excels in utilizing both unlabeled and labeled target battery data for model refinement. It outperforms in accuracy and robustness across diverse testing scenarios, yielding an average RMSE of merely 1.312% and even reaching an RMSE of just 3.015% in the most challenging testing scenario. Additionally, the proposed model showcases heightened resilience to variations in data learning ratios when compared to other TL methods.

CHAPTER 4. STATE OF HEALTH PREDICTION WITH TRANSFER LEARNING

Prognostics of the battery health are significant to get an insight into the degradation in the future, which can help users know the health conditions in the future and guide the predictive maintenance for optimal use and lifetime extension. However, predicting the SOH in future cycles is more challenging than estimating SOH at current time. The domain discrepancy makes the degradation curves different from each other which deteriorates the prediction performance. Therefore, in this chapter, TL strategies are explored for the SOH prediction.

The work in the previous chapter indicates only limited labeled samples could help reconstruct the historical degradation curve satisfactorily. Therefore, the investigation of using pseudo-labeled data for model updating with semi-supervised learning is conducted in this chapter. The feature extrapolation with DA is also investigated for the SOH prediction model without the necessary requirement of labeled data from the testing batteries. One key factor that causes the unstable future curve prediction is solved by introducing a long-term regularization strategy. Therefore, TL methods for SOH prediction introduced in this chapter can be adopted considering different application situations of the obtained data.

J7 and J8 contribute to this chapter.

4.1. SOH TRAJECTORY PREDICTION BASED ON SEMI-SUPERVISED TRANSFER LEARNING

As investigated in the previous chapters, only limited labeled capacity can ensure a very accurate reconstruction of the historical capacities. Therefore, future SOH prediction model is fine-tuned with the pseudo values from the reproduced historical capacities. The overall semi-supervised self-learning (SSSL) framework based future trajectory and lifetime predictions is illustrated in Fig. 4-1. The dataset is divided into two parts: the source domain (SD), and target domain (TD) with limited labels. Within SD, two models are trained: one for SOH estimation and the other for future SOH prediction. The two models undergo initial offline training using source-labeled data to ensure their effectiveness. Moving to TD, the SOH estimation model is first retrained by only using limited labels to reconstruct historical curves. The proposed HIs introduced in Chapter 2 are employed for the reconstruction of historical SOH using SOH estimation model. Subsequently, SOH prediction model is self-trained using the reproduced SOH as pseudo labels. Both retraining and self-training occur online using available checkpoints, allowing for quick training due to the use of limited data and the acceleration by the base model. Consequently, both offline training and online fine-tuning are conducted, which aims at improving accuracy and generalization. Finally, future SOH is sequentially predicted until the battery reaches its EOL.

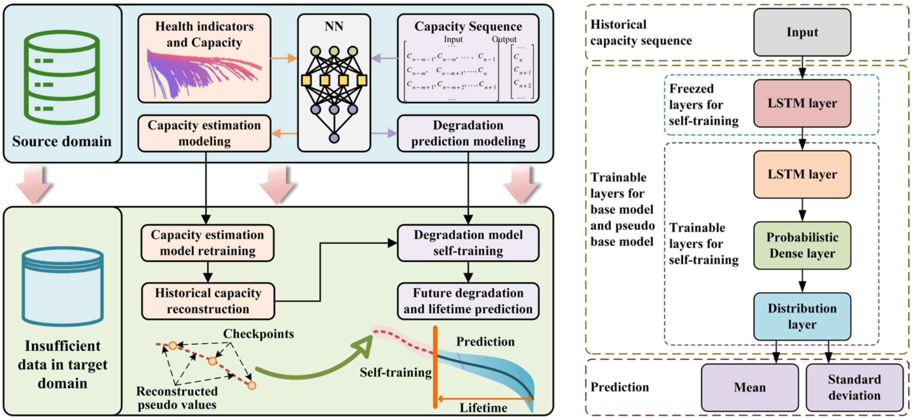

Figure 4-1 Framework and network construction of semi-supervised battery trajectory prediction method. Source: [J7]

4.1.1. HISTORICAL SOH RECONSTRUCTION

Effective HIs extracted from partial *Q*-*V* curves (introduced in Chapter 2) enable the reconstruction of pseudo-historical SOH, using limited labels for model retraining. To begin, the SOH estimation model is pre-trained with labeled data from SD. In this pre-training phase, the inputs consist of the extracted HIs, and the model's output is the battery SOH corresponding to each cycle.

Subsequently, for reconstructing testing battery historical SOH, a limited number of checkpoints containing labels are necessary to fine-tune the last fully connected layer. These checkpoints can be collected in practical scenarios when undergoing maintenance activities. Afterward, the historical SOH between these checkpoints can be reconstructed with the updated model, which has been demonstrated in Chapter 2. These reconstructed SOH serve as pseudo labels for downstream SOH prediction model self-training, which will be detailed in the subsequent subsection.

4.1.2. SEMI-SUPERVISED TRAJECTORY AND LIFETIME PREDICTION

The extrapolation method, i.e., the SOH prediction model, employed for forecasting future SOH along with uncertainty, is introduced. The schematic representation of the proposed model is presented in Fig. 4-2, whose detailed construction and fine-tuning processes are described below.

4.1.2.1 Lifetime modeling

When it comes to sequence-based capacity prediction, the initial step involves reconstructing the capacities to establish the inputs and outputs as described by Equation (4-1) and Equation (4-2), respectively.

$$[C_{i-m}, C_{i-m+1}, \dots, C_{i-1}, C_i] \tag{4.1}$$

$$[C_{i+1}, C_{i+2}, \dots, C_{i+n}] \tag{4.2}$$

where C_i represents SOH of ith cycle, m and n respectively denote the input and predicted length.

The model architecture depicted in Fig. 4-1 is employed for model training. It begins with the inclusion of two LSTM layers. Subsequently, a probabilistic dense layer is incorporated. The fundamental role of the probabilistic dense layer mirrors that of a conventional dense layer but with a distinction—the weights and biases are defined as distributions rather than specific values, as described in the previous chapter. The procedure for training the lifetime model involves initially training it using data from three batteries in the SD. Subsequently, SSSL is employed for model fine-tuning to predict SOH of the testing batteries.

4.1.2.2 Self-training for SOH prediction

Degradation patterns exhibited by batteries in SD may differ from those observed in TDs. Using SOH prediction model trained solely with SD data for predicting the future SOH of testing batteries in TDs could lead to predictions deviating from the expected curves. The concept of SSSL is proposed to enhance the model's adaptability in making predictions under varied application scenarios.

The first scenario involves predicting the battery SOH and lifetime, which belong to the same type but operate under different conditions compared to those in t SD. In this case, the first LSTM layer is kept frozen after initial training. This is done to preserve general characteristics specific to this battery type. The following LSTM, probabilistic fully connected, and distribution layers are made trainable, enabling them to acquire new information subscribed to the testing battery. The reconstructed pseudo-SOH labels are utilized for SSSL to enhance the SOH prediction model. Ultimately, SOH curve is predicted to obtain the future degradation curve and battery lifetime.

The second scenario involves predicting battery SOH and lifetime with different battery types compared to those in SD. In this situation, one battery from TD is randomly selected, and its entire degradation curve is reconstructed using seven checkpoints: the first cycle, 10% cycle, 30% cycle, 50% cycle, 70% cycle, 90% cycle, and the last cycle. Subsequently, SOH prediction model is retrained to adapt degradation patterns specific to the new battery type. The initial parameter values for training are provided by the corresponding model trained in SD. After retraining, the same SSSL approach mentioned above is employed for the SOH and lifetime predictions of other batteries within the TD. Consequently, two self-training processes are utilized to enhance the SOH prediction model in this scenario.

4.1.3. RESULTS AND DISCUSSION

Predictions under the two scenarios mentioned earlier are presented and evaluated. The assessment involves analyzing both SOH and lifetime prediction errors in comparison to expected real values.

4.1.3.1 Predictions for batteries undergoing different loading profiles

In this section, we present and evaluate predictions for batteries that belong to the same type while undergoing different working conditions. While batteries of the same type exhibit similar degradation patterns, variations of aging rates and curve shapes can still occur. To evaluate the proposed prediction approach, we first train the base model using data from three source batteries [55]. Subsequently, we implement the SSSL process in TD1 [72]. Fig. 4-2 illustrates RMSE and MAE values calculated for the complete capacity curves, encompassing both historically reconstructed segments and future predicted segments. The mean errors across all 45 cells are tabulated in Table 4-1. The term "checkpoints" refers to specific known points, such as those occurring at 10%, 30%, 50%, and 90% of the entire cycle life, which are representative of sparsely labeled data, often obtained during maintenance.

Fig. 4-2 demonstrates a substantial reduction in prediction errors as the number of available checkpoints increases. With three checkpoints, absolute errors in lifetime prediction fluctuate within a range of 50 cycles. All RMSE values are below 3.15%, and all MAE values are below 1.4%. As the early stages of battery capacity degradation occur very slowly, the predictions exhibit low errors and strong generalization for all cells, even with only three checkpoints. Furthermore, the presence of an additional checkpoint during the later stages of battery usage, characterized by more rapid capacity degradation, leads to a rapid decline in predicted errors. All predicted lifetime absolute errors remain below 15 cycles, while SOH RMSE and MAE stay below 0.68% and 0.38%, respectively.

Table 4-1 presents the average errors for lifetime predictions and future capacity predictions. It is evident that with just two early-stage checkpoints, the mean error of predicted lifetime stands at 96.4 cycles. However, this error quickly decreases to 22.68 cycles upon inclusion of a third checkpoint. Meanwhile, the mean RMSE and MAE values have been reduced to 1.19% and 0.67%, respectively, indicating a close alignment between predicted and actual SOH. Furthermore, with the acquisition of another additional checkpoint in the fast-degrading phase, the mean error of the predicted lifetime drops significantly to 7.27 cycles. The mean predicted RMSE and MAE values further decrease to 0.27% and 0.18%, respectively. These outcomes indicate that the proposed model effectively predicts future SOH and exhibits strong generalization capabilities across diverse loading profiles and ranges of lifetime for all batteries within TD1.

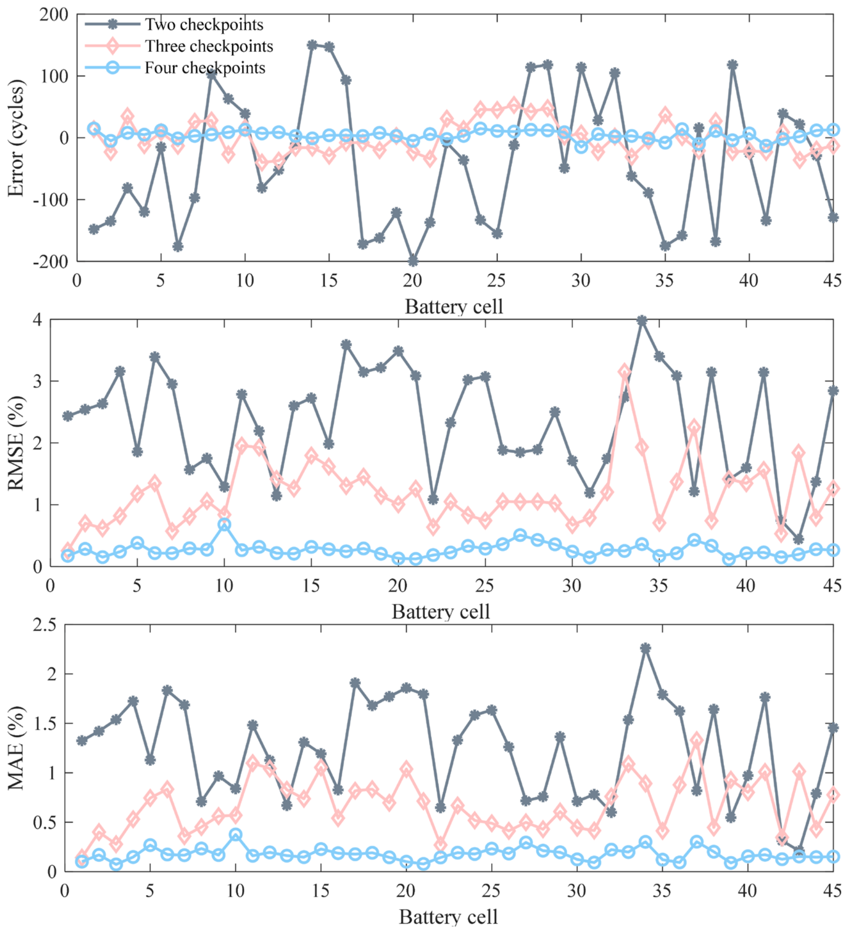

Figure 4-2 Errors of the predicted lifetime, SOH RMSE and MAE. Source: [J7]

Table 4-1 Predicted mean errors for TD1. Source: [J7]

Checkpoints	Mean absolute error of predicted lifetime	Mean RMSE of predicted SOH curves	Mean MAE of predicted SOH curves
2	96.40 cycles	2.33%	1.24%
3	22.68 cycles	1.19%	0.67%
4	7.27 cycles	0.27%	0.18%

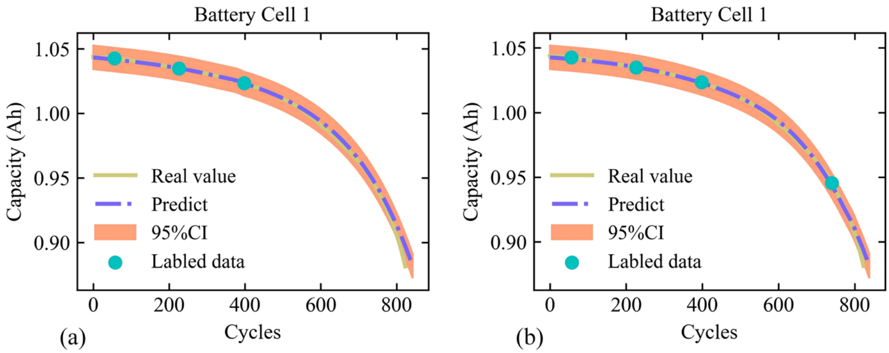

Figure 4-3 Predictions for cell 1 using (a)/(b) 3/4 checkpoints. Source [J7]

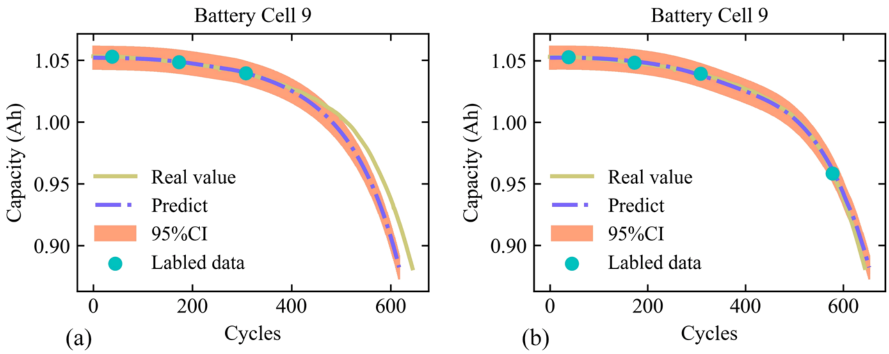

Figure 4-4 Predictions for cell 9 using (a)/(b) 3/4 checkpoints. Source [J7]

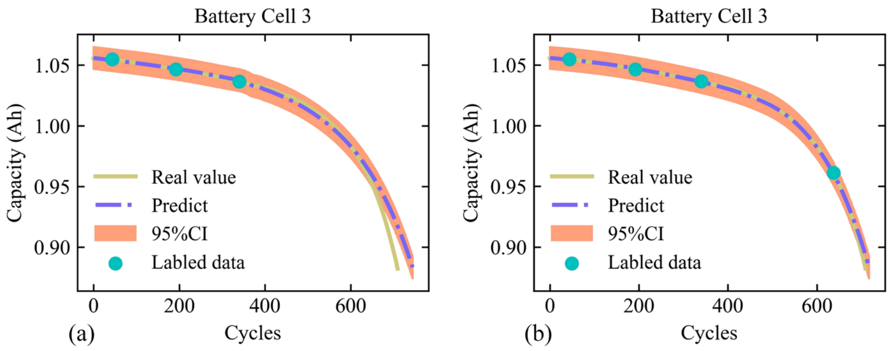

Figure 4-5 Predictions for cell 3 using (a)/(b) 3/4 checkpoints. Source [J7]

The predictions for three batteries within TD1 are illustrated in Fig. 4-3 to Fig. 4-5, specifically showcasing the outcomes for cell 1, cell 9, and cell 3, detailed in J7. In each figure, (a) portrays predictions utilizing three labeled checkpoints, while (b) demonstrates predictions with four labeled checkpoints. Fig. 4-3 exemplifies a case where the predicted lifetime closely aligns with the actual lifetime considering three checkpoints. As shown in Fig. 4-3(a), despite accurate lifetime prediction, additional accuracy is achieved in predicting future SOH upon including one label, as depicted in Fig. 4-3(b). This leads to a reduction in RMSE and MAE of predicted SOH from 0.26% and 0.14% to 0.17% and 0.10%, respectively. In Fig. 4-4(a), a scenario unfolds where the predicted lifetime falls short of the actual lifetime, resulting in a 27-cycle error. Nonetheless, predicted future SOH still mirrors the pattern observed in real degradations. The predicted SOH RMSE and MAE stand at 1.06% and 0.56%, respectively. Furthermore, with the acquisition of an additional checkpoint situated in fast aging phase, the predicted SOH curve converges more closely to the expected real curve, as demonstrated in Fig. 4-4(b) Lifetime prediction error reduces to 9 cycles, and RMSE and MAE of the predicted SOH curve decrease to 0.27% and 0.17%, respectively. For cell 3, depicted in Fig. 4-5(a), predicted lifetime surpasses the actual value, resulting in a 35-cycle difference. Nevertheless, the predicted future SOH curve continues to align well with real values, yielding RMSE and MAE of merely 0.62% and 0.15%, respectively. With the introduction of a fourth label, as seen in Fig. 4-5(b), the prediction accuracy improves even further, with an error of merely 8 cycles, SOH RMSE and MAE stand at just 0.15% and 0.07%, respectively. The 95% CI encompasses real SOH, underscoring the reliability of predicted outcomes.

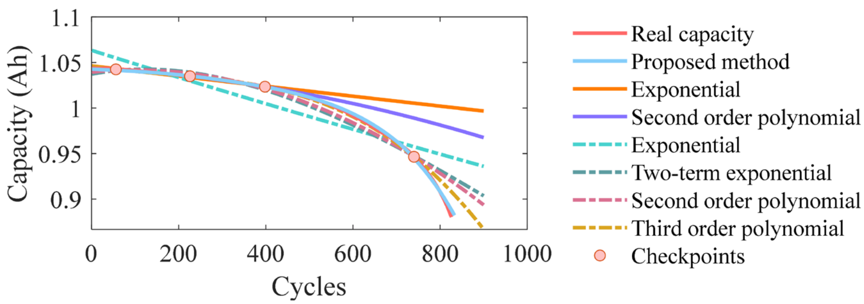

Figure 4-6 Comparison with curve fitting methods. Source: [J7]

Experimental results above underscore satisfactory performance of the proposed method in reconstructing historical degradation curves and predicting future trajectories using limited labels. To provide further evaluation, comparisons with curve-fitting methods are depicted in Fig. 4-6, which are the results derived from cell 1. The solid lines represent actual values and predictions achieved with three checkpoints. Given that empirical models are supposed to have fewer unknown parameters than available labels, exponential and second-order polynomial functions are employed. The outcomes reveal that curve-fitting methods struggle to accurately predict SOH curves with too limited labels. Even with four labels available, curve-fitting models (depicted by dot-dash lines) still exhibit huge errors. Among these models, the third-order polynomial function yields the most accurate prediction, yet its error of 52 cycles significantly surpasses the prediction achieved by the proposed model utilizing only three labeled checkpoints. Therefore, these comparative evaluations strongly suggest the proposed model outperforms curve-fitting techniques in predicting future SOH curves and lifetime with very limited labels.

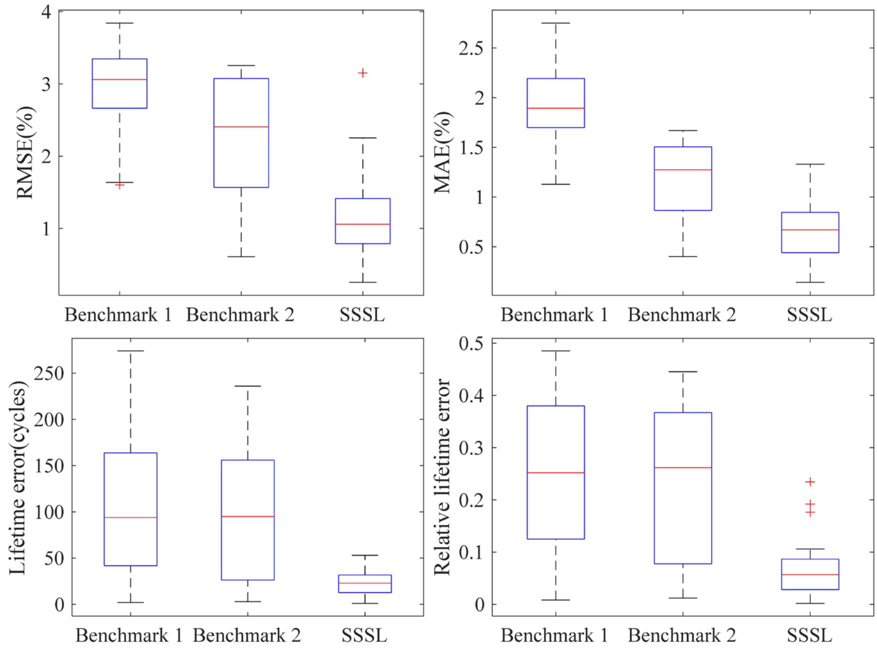

Figure 4-7 Prediction performances of proposed model with comparisons to two benchmark methods. Source: [J7]

To assess the prediction enhancement provided by the proposed SSSL approach, two benchmark methods are employed for comparative evaluations, as shown in Fig. 4-7. The model structure for SOH estimation and predictions of the benchmarks remains the same as the model used in our method. The distinction lies in whether SOH estimation model is retrained using sparse labels and whether SOH prediction model undergoes self-training utilizing reconstructed pseudo-historical SOH. Specifically, detailed conditions of the two benchmark methods are listed as follows. Benchmark 1: In this scenario, SOH estimation model is utilized to estimate historical SOH, and SOH prediction model is employed to predict future degradation using the estimated SOH. Benchmark 2: In this case, SOH estimation model is retrained using sparse labels, and reconstructed SOH from this retrained model is used to predict the further SOH degradation curve without self-training SOH prediction model. Proposed SSSL method involves both retraining SOH estimation model using sparse labels and self-training SOH prediction model using reconstructed pseudo-historical SOH. This approach aims to improve both SOH estimation and prediction. The results indicate the narrowest error distribution of the proposed model compared to these two benchmarks, representing more accurate and reliable health predictions.

Table 4-2 presents the absolute mean RMSE and MAE values for SOH predictions, as well as average error and relative error of lifetime predictions, along with the computational burden of the entire prediction procedure concerning all 45 batteries TD1. The outcomes illustrate the progression pattern from Benchmark 1 to Benchmark 2, and further to the newly introduced model. The suggested approach demonstrates a reduction of 59.39% and 65.10% in the mean RMSE and MAE, respectively with comparisons to conventional model (Benchmark 1). Similarly, errors and relative errors of lifetime prediction are respectively curtailed by 78.69% and 74.61%.

The computation time encompasses the duration needed for the complete retraining of SOH estimation model, self-training of SOH prediction model, historical SOH reconstruction, and future SOH degradation predictions. The average time taken for computation across all 45 cells culminates in the ultimate computational time shown in Table 4-2. The findings indicate additional processes of retraining and self-training do not entail a substantial increase in computation, only extending by approximately 17 seconds (less than 81%). Taking into account the commendable enhancement in accuracy and the manageable rise in computational load, the proposed method evidently presents significant progress in predicting future SOH degradation and lifetime, even with limited sparse labels.

Table 4-2 Numerical comparisons with two benchmark methods. Source: [J7]

Index	Benchmark 1	Benchmark 2	SSSL
RMSE (%)	2.93%	2.27%	1.19%
MAE (%)	1.92%	1.18%	0.67%
Lifetime error (cycles)	106.42	81.93	22.68
Relative lifetime error (%)	25.09%	20.54%	6.37%
Computational time (s)	21.28	28.06	38.49

4.1.3.2 Predictions for different battery types

Real-world applications frequently necessitate predictions for distinct battery types that exhibit varied degradation behaviors. Consequently, this section assesses the viability of the proposed method in predicting under such applicable scenarios. In this application, due to the notably distinct degradation patterns exhibited by batteries in the SD dataset, an initial step involves employing a single battery with seven reference points. This battery is used to reconstruct the SOH trajectory for self-training SOH prediction model. Subsequently, the updated model undergoes refinements following the procedures outlined in the prior section. These enhancements facilitate the prediction of future SOH and final lifetime for new-type batteries characterized by distinctive aging patterns.

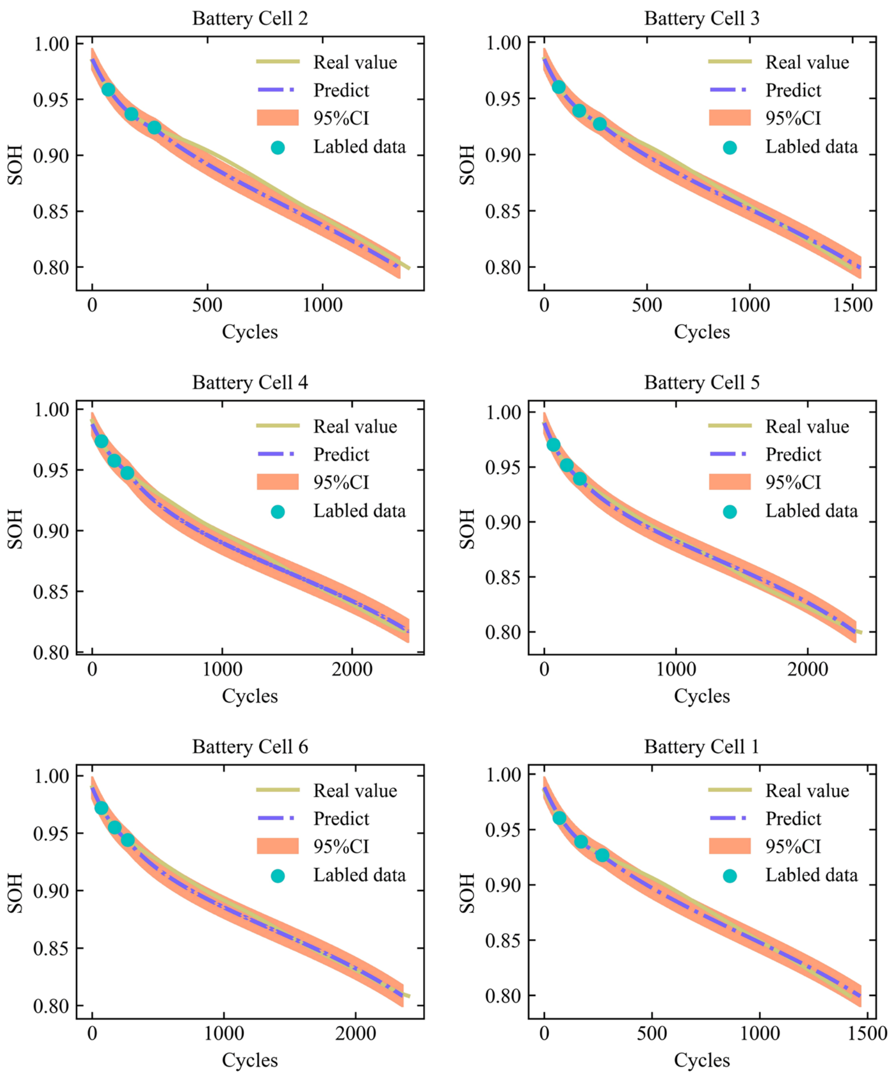

Figure 4-8 Lifetime prediction results for batteries in TD2. Source: [J7]

This section focuses on the predictions and evaluation pertaining to batteries in TD2 (batteries aged under different current rates and environmental temperatures). The prediction results for battery cell 2 through cell 6 are depicted in Fig. 4-8. In this instance, three labels from early stages (100, 200, and 300 cycle) are employed. Notably, outcomes indicate accurate and reliable predictions for these testing batteries, despite variations in their lifetime ranges. The predicted future SOH trajectory aligns closely with actual values, while 95% CIs effectively converge with real degradation curves. These findings underscore the efficacy of the proposed model in predicting battery SOH trajectories and lifetimes of diverse types with disparate aging patterns. To assess the impact of selecting the initial retrained battery, cell 6 serves as the starting point for the complete neural network retraining. Subsequently, this retrained model is employed for predictions of cell 1, as shown in Fig. 4-8. Remarkably, the outcomes demonstrate accurate and reliable predictions. This underscores the strong generalization capability of the proposed method, wherein it can effectively adapt to different battery types and aging characteristics.

Numerical outcomes of future SOH and lifetime predictions of batteries in TD2 are listed in Table 4-3. Notably, the lifespan of batteries subjected to 55 ℃ aging conditions is approximately 1000 cycles, whereas batteries exposed to 35 ℃ aging conditions exhibit remaining lifespans exceeding 2000 cycles. Results signify that predicted lifetime errors remain under 50 cycles. As a result, relative errors are confined to less than 4.1% for batteries undergoing 55 ℃ aging with approximately 1000 cycles left, and less than 2.1% for conditions under 35 ℃ with over 2000 remaining cycles. The early lifetime prognosticated errors are sufficiently modest. The errors for future SOH curves are uniformly minimal across all batteries. Specifically, RMSEs and MAEs are respectively under 0.81% and 0.70%.

Table 4-3 Future SOH and lifetime prediction results for TD2 batteries. Source: [J7]

Battery cell	Real lifetime	Predicted lifetime	Absolute error	Relative error	RMSE of capacities	MAE of capacities
Cell 1	982	1029	47 cycles	4.08%	0.51%	0.41%
Cell 2	931	893	-38 cycles	-3.44%	0.81%	0.70%
Cell 3	1034	1082	48 cycles	3.93%	0.53%	0.41%
Cell 4	2131	2164	33 cycles	1.55%	0.54%	0.45%
Cell 5	2013	1975	-38 cycles	1.78%	0.36%	0.30%
Cell 6	2131	2088	-43 cycles	2.02%	0.44%	0.34%

4.1.4. SUMMARY

Predicting future degradation curves and corresponding lifetimes stands as crucial yet intricate endeavors in the realm of intelligent battery management. This section introduces an innovative SSSL prediction framework to address these challenges. The framework's foundation involves the initial training of base models for historical SOH reconstruction, future SOH and lifetime predictions. This is executed using three randomly selected source batteries. To facilitate SOH reconstruction, three HIs are extracted considering practical partial curve requirements. Subsequently, a self-training strategy is introduced, harnessing the potential of pseudo values to enhance the prediction model's accuracy. An intriguing aspect is the minimal requirement for labeled checkpoints, aligning with real-world scenarios wherein an abundance of unlabeled data exists alongside limited labeled data. The efficacy of the proposed model is assessed across various scenarios. This evaluation encompasses instances where differing battery types and/or distinct degrading patterns are considered.

The findings through experimental validations underscore the efficacy of the proposed approach across diverse prediction scenarios. For predictions on batteries with same type but distinct current profiles, even utilizing just three labels, the mean prediction errors of the lifetimes remain below 23 cycles. Incorporating an additional checkpoint located in fast aging phases further reduces errors to under 8 cycles. When extending the framework for predictions of different battery types, which boasts a lifespan exceeding 2000 cycles, results reveal predicted errors below 50 cycles and relative errors below 4.1% using merely three labels within the first 300 cycles. Consequently, the proposed SSSL-based method aptly achieves early degradation curve prediction with commendable precision and reliability.

4.2. LONG-TERM DEGRADATION TRAJECTORY PREDICTION WITH DOMAIN ADAPTATION AND LONG-TERM REGULARIZATION

4.2.1. MULTI-TASK LEARNING-BASED FUTURE DEGRADATION TRAJECTORY PREDICTION WITH FEATURE EXTRAPOLATION

Capacity is not readily accessible in real-world applications, making it impractical to use capacity extrapolation methods for predicting battery health. On the other hand, the features mentioned earlier can be obtained from operational data after simple preprocessing steps. As a result, extrapolating these features becomes a viable approach for practical applications. Moreover, battery SOH can also be predicted using these features through established relationships. Therefore, in this study, we employ MTL to predict future SOH by extrapolating the extracted features with DA and a long-term regularization, eliminating the need for labeled data from the target batteries. The model framework is shown in Fig. 4-9.

More specifically, the model takes various historical features, as introduced in the previous section, as inputs, and it predicts the future values of these features as well as SOH. To meet practical needs, it is possible to define different prediction horizons within a single prediction step. Therefore, the general representations of the input matrix **X** and the output matrix **Y** for each sample can be formulated as follows,

$$\mathbf{X}\big|\mathbf{Y} = \begin{bmatrix} f_{1,i-m}, & f_{2,i-m}, & f_{3,i-m} \\ f_{1,i+1-m}, & f_{2,i+1-m}, & f_{3,i+1-m} \\ \dots, & \dots, & \dots \\ f_{1,i}, & f_{2,i}, & f_{3,i} \end{bmatrix} \left\| \begin{bmatrix} f_{1,i+1}, & f_{2,i+1}, & f_{3,i+1}, & s_{i+1} \\ f_{1,i+2}, & f_{2,i+2}, & f_{3,i+2}, & s_{i+2} \\ \dots, & \dots, & \dots, & \dots \\ f_{1,i+n}, & f_{2,i+n}, & f_{3,i+n}, & s_{i+n} \end{bmatrix} \right. \tag{4.3}$$

The model is composed of two components: a base section for learning shared information, and task-specific segments connected afterward for making individual predictions. Various types of networks can be employed for the base part, while, in the task-specific sections, a multilayer perceptron (MLP) is utilized. In this study, we have opted for a base network based on a gated recurrent unit (GRU)-based recurrent neural network, augmented with a fully connected layer [69]. Many prior research papers have already conducted comparisons among various deep neural networks. Given the primary focus of this paper on enhancing performance through DA and achieving long-term prediction results, we have restricted our experiments to using the GRU network in this paper. However, it's worth noting that this methodology can be readily extended to incorporate other deep neural networks in future studies. In our chosen architecture, the base network part employs 128 neurons for the GRU layer and 64 neurons for the fully connected layer. In the task-specific sections, the MLPs are configured with 64, 32, and 1 neuron, respectively. It's important to note that this work utilizes three features that were previously introduced in our research as illustrative examples for future trajectory prediction. However, it's flexible and straightforward to incorporate or replace these features with more advanced ones tailored to specific applications. During the training process, the model minimizes the regression losses for all the features, as well as the SOH. To learn the mapping relationships effectively, we calculate the weighted mean value of the three losses for feature regression, which serves as the feature regression loss. Additionally, the loss associated with SOH prediction is regarded as the SOH regression loss for the source battery. To quantify these regression losses, we compute the mean square errors (MSE) between the model predictions and the actual ground truth values.

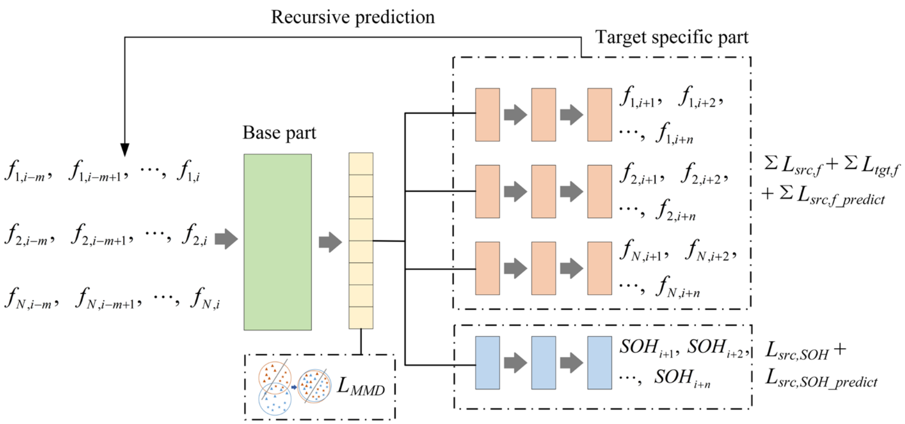

Figure 4-9 MTL-based SOH prediction framework. Source: [J8]

4.2.2. LONG-TERM REGULARIZATION AND DOMAIN ADAPTATION

There is a notable domain discrepancy among various batteries due to differences in applications and inherent properties. To improve model's performance on testing batteries, fine-tuning can be carried out using freshly acquired labeled samples from the target domain, as presented and evaluated in the above section. However, in many practical scenarios, obtaining labeled SOH is challenging, and only operational measurements are accessible. Consequently, it is imperative to explore unsupervised DA. The MMD loss, as introduced in the previous chapter, is included to describe hidden feature domain discrepancy between source and target batteries produced by the base network part.

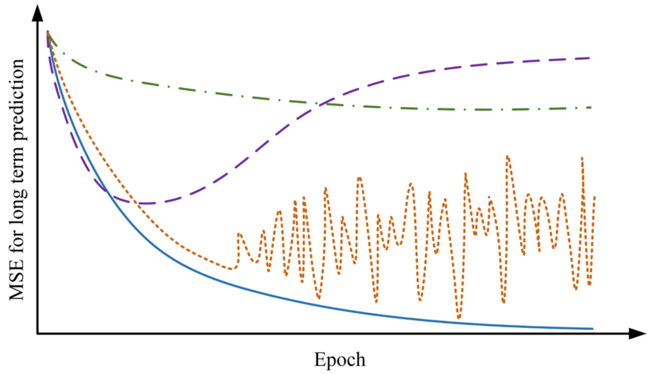

Figure 4-10 Commonly seen MSE variations with epochs for long-term prediction when training the STP model. Source: [J8]

In the context of degradation trajectory prediction, especially in the case of long-term predictions using a recursive framework, a significant challenge arises from the fact that cumulative errors can lead to predictions deteriorating or flattening rapidly. Fig. 4-10 illustrates four commonly observed MSEs associated with long-term trajectory prediction during the training of the STP model. In an ideal scenario, the MSE for long-term trajectory prediction, based on extrapolations made by the STP model, should exhibit a consistent decrease, as indicated by the solid blue lines. However, under various conditions, represented by the dashed lines, other scenarios are also likely to occur. These scenarios might involve the MSEs for long-term trajectory prediction becoming significantly large or exhibiting instability. Hence, ensuring reliable long-term prediction performance through the extrapolation of the STP model poses a considerable challenge. To address this issue, this section introduces a long-term dependency regularization approach, which involves incorporating an additional recursive prediction loss for the source battery. In this approach, we perform recursive predictions on the source battery, aiming to forecast the entire degradation trajectory from its initial state. Subsequently, we calculate the loss between the predicted trajectory and the actual values to assess and constrain long-term prediction performance during training. Consequently, the final model becomes well-suited for both short-term and more challenging tasks of long-term recursive predictions.

In summary, the comprehensive loss function includes several components: regression losses for the features of both the source and target batteries, regression loss for the SOH of the source battery, MMD loss to mitigate domain discrepancy, and long-term prediction losses for both the features and SOH of the source battery. The complete expression of the loss function is as follows,

$$
\begin{aligned}
L = \alpha\left(\sum L_{src,f} + \sum L_{src,f\_predict}\right) + \sum \beta L_{tgt,f} + \\
\mu\left(L_{src,SOH} + L_{src,SOH\_predict}\right) + \lambda L_{MMD}
\end{aligned}
\tag{4.4}
$$

where *α, β, μ, λ* are weighting coefficients.

To mitigate the uncertainty arising from manual weight allocation, streamline the weight-tuning process, and enhance the model's adaptability across various applications, we employ an automatic weight allocation scheme. Specifically, we employ the homoscedastic uncertainty method introduced in [90] for task-specific weight allocation. This is achieved by maximizing the Gaussian likelihood. The model output can be defined as the following likelihood with weights W on input x, and an observation noise scalar σ ,

$$
p\left(y \middle| f^{W}\left(x\right)\right) = N(f^{W}\left(x\right), \sigma^{2})
\tag{4.5}
$$

In negative minimum likelihood inference, the objective is to maximize the log-likelihood of the model. This can be expressed as,

$$
\log p(y \mid f^{W}(x)) \propto -\frac{1}{2\sigma^{2}}\left\| y - f^{W}(x) \right\|^{2} - \log\sigma
\tag{4.6}
$$

In the case of multi-task-based outputs, the likelihood can be expressed as,

$$
p(y_1, y_2, ..., y_k \left| f^{W}(x)\right.) = p(y_1 \left| f^{W}(x)\right.) p(y_2 \left| f^{W}(x)\right.) ... p(y_k \left| f^{W}(x)\right.)
\tag{4.7}
$$

Therefore, the negative log-likelihood of the multi-tasks model outputs is,

$$
\begin{aligned}
-\log p(y_1, y_2, ..., y_k \mid f^{W}(x)) \propto \frac{1}{2\sigma^{2}}\left\| y_1 - f^{W}(x) \right\|^{2} + \frac{1}{2\sigma^{2}}\left\| y_2 - f^{W}(x) \right\|^{2} + \\
... + \frac{1}{2\sigma^{2}}\left\| y_k - f^{W}(x) \right\|^{2} + \log\sigma_1\sigma_2...\sigma_k
\end{aligned}
\tag{4.8}
$$

where the former k items represent the loss of the multiple outputs while the last objective learns the relative weight of these losses adaptively. Indeed, as the noise parameter σ_k increases, the weight assigned to the kth loss decreases, and conversely, as σ decreases, the weight increases. Moreover, the final objective can serve as a regularization mechanism, preventing the noise parameter from growing excessively, which could lead to disregarding the data itself. In this way, the weight for each task is allocated adaptively based on the data characteristics encountered during training. Additionally, the learning rate is initialized at 0.01 for the first 200 epochs. Afterward, it is adjusted dynamically by multiplying it by 0.98 every 5 epochs until reaching 300 epochs to enhance training in later stages and help fine-tune the model effectively.

4.2.3. PREDICTION RESULTS

To assess performance and compare it with several benchmark methods, we utilize the following metrics: RMSE, MAE, and MaxAE. Additionally, we include the R^2 and PCC to evaluate the prediction performance. We examine and discuss three distinct cases to illustrate the model's performance under various application scenarios. In these cases, long-term predictions commence from an early stage, typically at 100 cycles, and extend to forecast the entire trajectory.

4.2.3.1 Predictions for different dynamic loadings

In this case, we employ a battery aged under CC to predict the health of batteries subjected to dynamic loading profiles. This setup mimics a real-world scenario where an experimental battery is trained for predictions under real-world usage patterns.

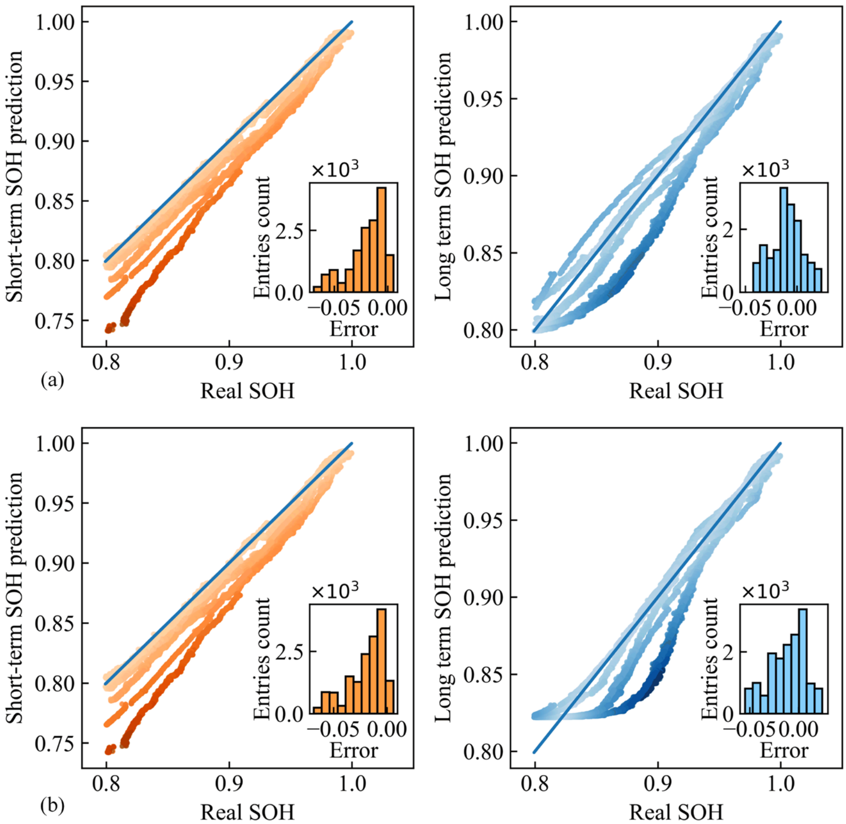

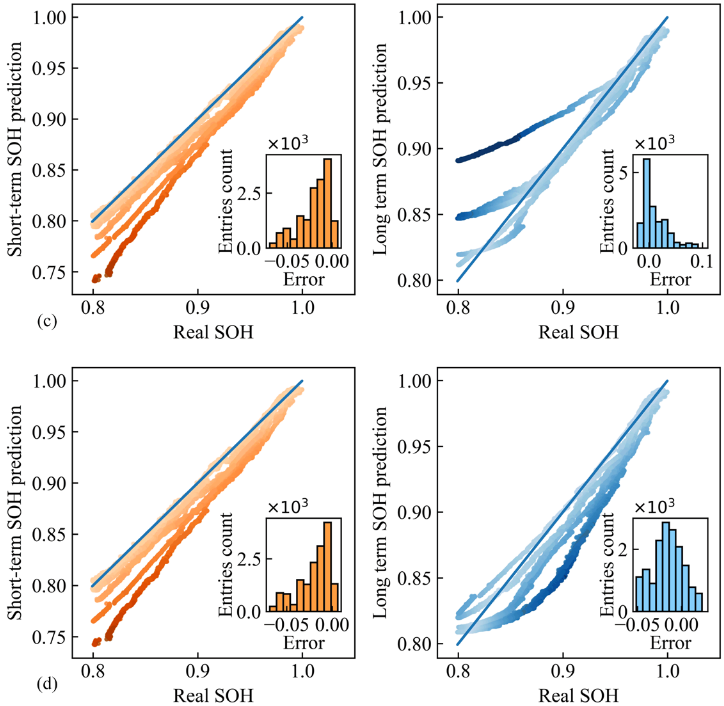

Figure 4-11 Prediction results for dynamic loadings. (a) proposed model, (b) Benchmark 1, (c) Benchmark 2, (d) Benchmark 3. Source: [J8]

The short-term and long-term predictions for all six batteries (B#2 to B#7) generated using our proposed method are displayed in Fig. 4.11(a). The predictions of three benchmarks are also presented in Fig. 4.11(b)-4.11(d) for comparative evaluations. These benchmarks are the MTL without DA or long-term regularization (Benchmark 1), the model only with DA (Benchmark 2), and the model only with long-term regularization (Benchmark 3). The results suggest that there are no substantial differences in short-term predictions among the various methods, which is consistent with the findings presented in Table 4-4. These methods exhibit similar accuracy and fitting effectiveness, although our method demonstrates superior overall performance.

Indeed, when it comes to long-term prediction, the differences between the proposed method and the benchmarks become more pronounced. In scenarios where no long-term regularization is applied, as demonstrated in Fig. 4-11(b) and Fig. 4-11(c), predictions tend to flatten out over time, leading to a loss of predictive capability during extrapolation. For instance, when looking at the conventional method represented by Benchmark 1, the prediction errors are not excessively large, with RMSE and MAE at 2.171% and 1.654% respectively. However, as depicted in Fig. 4-11(b), the predictions start to flatten out in the lower SOH range. This indicates that the predictions struggle to predict battery lifetimes, and the model fails to effectively predict the entire trajectories. The predictions produced by Benchmark 2 also exhibit a decline in long-term prediction performance, characterized by substantial errors and low fitting coefficients. It's apparent that while some predictions may yield satisfactory results, others perform poorly under Benchmark 2. This inconsistency underscores the importance of incorporating long-term regularization to stabilize the model's long-term prediction ability. In contrast, when considering the results with long-term regularization, as depicted in Fig. 4-11(a) and Fig. 4-11(d), the predictions improve, particularly in the lower SOH range. This enhancement ensures that the predictions remain effective throughout the entire lifetime of the batteries. When DA is employed, the predictions generated by the proposed method exhibit improved accuracy and fitting effectiveness compared to the benchmarks that do not utilize DA. As summarized in Table 4-4, all indicators have significant improvements when using the proposed method in contrast to the benchmarks. Specifically, both RMSE and MAE are less than 1.83% for the entire predicted trajectory. Moreover, the R^2 exceeds 0.86, and the PCC between the predicted curve and the real curve is greater than 0.95.

Table 4-4 Long/short-term prediction results. Source: [J8]

Predictions		Bench-mark 1	Bench-mark 2	Bench-mark 3	Proposed
Short-term prediction	RMSE	2.586	2.569	2.593	2.554
	MAE	1.964	1.967	1.968	1.957
	MaxAE	6.855	6.946	6.852	6.934
	R2	0.781	0.781	0.780	0.784
	PCC	0.954	0.955	0.954	0.956
Long-term prediction	RMSE	2.171	2.501	2.303	1.822
	MAE	1.654	1.732	1.884	1.464
	MaxAE	5.490	9.157	5.120	4.225
	R2	0.791	0.614	0.750	0.862
	PCC	0.926	0.884	0.936	0.951

Interestingly, the results reveal that long-term predictions exhibit fewer errors compared to short-term predictions. This phenomenon can be attributed to the fact that short-term predictions rely on features that are extracted at the current time, while long-term predictions are derived from extrapolated features. The features obtained under different operational conditions display noticeable discrepancies. These differences in features introduce variations in the regression relationship between the features and SOH, leading to larger errors in short-term predictions. On the other hand, in long-term predictions, the features themselves are predicted, and the future features may deviate from the actual extracted ones but align better with the SOH-feature relationship. Consequently, long-term predictions tend to have better accuracy. In summary, these results suggest that the proposed model is capable of effectively predicting the entire degradation trajectory even under unforeseen conditions, starting from the early stages of data acquisition.

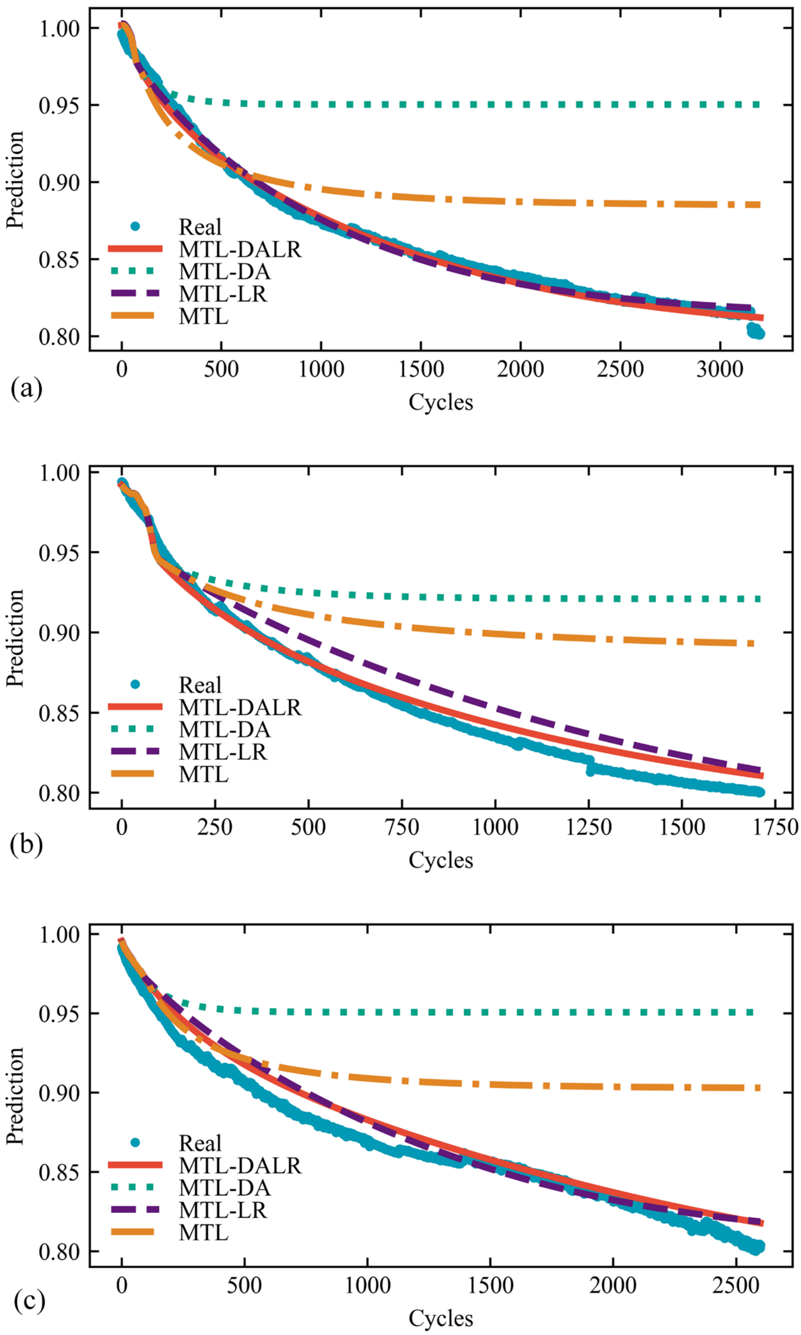

Figure 4-12 Fig. 6 Long-term trajectory prediction for batteries aging under (a) UDDS profile, (b) HWFET profile, and (c) Hybrid profile. Source: [J8]

4.2.3.2 Predictions for similar loadings with different SOC ranges

In the next set of experiments, a more moderate condition is examined. An additional cell that operates under similar loading conditions is introduced alongside the CC cell to serve as a source battery. This setup is designed to assess the prediction performance for another cell subjected to dynamic loadings at different SOC ranges. Similar to the previous experiments, the predictions begin from the same starting point, which is at 100 cycles. These experiments encompass three distinct loading profiles, each resulting in different lifetime ranges and degradation patterns. By evaluating performance across these diverse scenarios, we can gain a more comprehensive understanding of the model's predictive capabilities. The results for these three working profiles are presented in Fig. 4-12, and the corresponding numerical outcomes are detailed in Table 4-5.

Table 4-5 Predictions of different dynamic loadings. Source: [J8]

Working condition	Index	Bench-mark 1	Bench-mark 2	Bench-mark 3	Proposed
UDDS	RMSE	4.416	9.779	0.407	0.375
	MAE	3.785	8.881	0.328	0.314
	MaxAE	8.437	14.930	1.721	1.196
	R2	-2.677	-174.482	0.992	0.994
	PCC	0.914	0.674	0.996	0.997
HWFET	RMSE	5.943	7.905	1.513	0.764
	MAE	5.135	6.904	1.433	0.645
	MaxAE	9.308	12.091	2.353	1.595
	R2	-7.065	-32.915	0.884	0.974
	PCC	0.937	0.808	0.997	0.998
Hybrid	RMSE	5.437	9.352	1.087	0.992
	MAE	4.708	8.521	0.923	0.879
	MaxAE	10.290	15.050	2.059	1.818
	R2	-7.150	-199/316	0.947	0.950
	PCC	0.896	0.708	0.989	0.995

The results indicate that long-term trajectory predictions are unsuccessful when long-term regularization is not included. Both the two benchmarks, MTL (Benchmark 1) and MTL+DA (Benchmark 2), tend to flatten out several steps after the recursive process. Interestingly, the DA-based method experiences this flattening phenomenon even sooner than the basic MTL method. This observation may be attributed to the model's efforts to minimize MMD loss, potentially at the expense of its long-term prediction capabilities. Additionally, it's worth noting that when incorporating an additional battery for training, long-term predictions tend to exhibit this flattening behavior more readily compared to the results observed in the above prediction scenarios. Upon incorporating long-term regularization, the predictions become stable throughout the entire lifetime. With DA included during training, the proposed method (MTL+DALR) produces predictions that are closer to actual degradation curve when compared to MTL+LR (Benchmark 3), even though Benchmark 3 addresses the primary issue of long-term trajectory prediction. Numerical results listed in Table 4-5 support these findings, demonstrating that the proposed model achieves the highest accuracy and fitting effectiveness. Specifically, RMSE and MAE are less than 1% for all three dynamic loading profiles, accompanied by fitting coefficients exceeding 0.95. These results collectively indicate that the proposed method delivers satisfactory predictions throughout the entire trajectory, starting from the early stages of data acquisition.

4.2.3.3 Predictions with variable temperature conditions

In the third case, the objective is to use batteries that have aged under constant temperature conditions as source batteries to predict the degradation of batteries operating under variable temperature conditions. This scenario simulates real-world conditions where weather fluctuations can lead to varying degradation patterns that differ from those observed under constant temperature conditions.

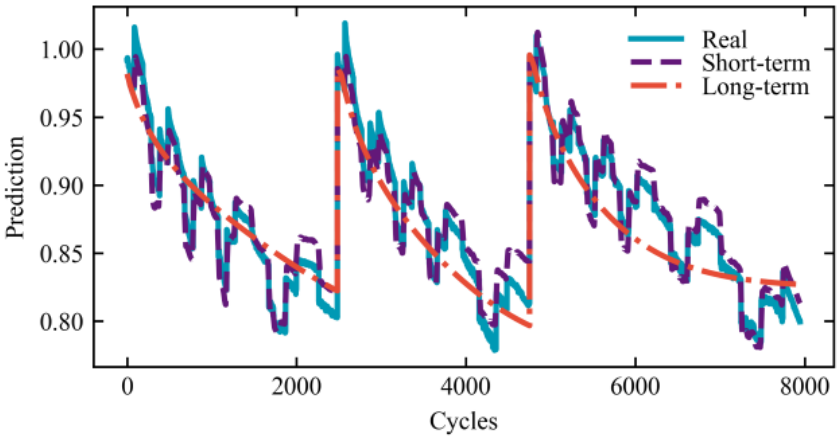

Figure 4-13 Short and long-term predictions for the three testing batteries aging under dynamic currents and variable temperatures. Source: [J8]

Results presented in Fig. 4-13 demonstrate the real values alongside short-term and long-term predictions for three batteries undergoing degradation under dynamic loadings and variable environmental temperatures. The short-term predictions successfully capture the fluctuations in SOH caused by temperature variations, with RMSE and MAE of 1.190% and 0.999%, respectively. In terms of long-term predictive performance, the predictions starting from the early stages also align well with the overall degradation patterns, yielding RMSE and MAE values of 2.447% and 2.051%, respectively. This suggests that the degradation trajectories can be effectively modeled and predicted. However, it's important to note that practical applications typically involve batteries operating under variable temperature conditions. Therefore, considering seasonal temperature variations as additional input information may further improve the accuracy of predicting overall degradation trajectories. Given the primary focus of this work on DA and long-term regularization, the study of trajectory distribution predictions will be explored in future research, as proposed in J1.

4.2.4. SUMMARY

This paper introduces an innovative framework for degradation trajectory predictions of batteries operating under previously unobserved working conditions. MTL is designed to predict future SOH values through the recursive predictions of highly effective features, without requirements of prior SOH values. Furthermore, a DA strategy and long-term regularization techniques are proposed to enhance the model's ability to make stable predictions during the recursive process. To assist in the training process, automatic weight allocation and learning rate adjustment mechanisms are introduced. The effectiveness of this approach is evaluated through a series of experiments where batteries are aged under various loading profiles that closely resemble practical operating conditions. The results demonstrate the advancements achieved by the proposed method, which excels in delivering accurate predictions for both short-term and long-term trajectories compared to three benchmark models. The predicted RMSE and MAE are respectively within 1.822% and 1.464% for predictions that commence from the early stages. These predictions rely solely on one battery that has aged under constant current profiles, serving as the source battery, without utilizing any labels from the testing batteries operating under both urban and highway loadings. The RMSE and MAE are respectively less than 0.992% and 0.879% and the fitting coefficient is larger than 0.95. Furthermore, the model's predictive performance can be further enhanced by incorporating an additional source battery operating under the same loading conditions but at different SOC ranges. Under variable temperature conditions, the model's predictions effectively capture the overall degradation trends.

CHAPTER 5. PREDICTIVE HEALTH ASSESSMENT WITH ACCELERATING AGING DETECTION

The SOH prediction methods introduced in the previous chapter provide future degradation information. In order to take advantage of the predictions for the guidance of predictive maintenance. The degradation regions of different aging stages are generally divided by the onset of knee point, where the aging rate is accelerated thereafter. Therefore, the detection of battery knee is critical in battery health prognostics and management. In addition, probabilistic detection is more valuable than point detection for management strategies design since one-point prediction is generally not so accurate and the time for management within one point is limited.

To deal with this practical application requirement, this chapter proposed a general framework that makes use of the probabilistic predictions for both the point and sequence predictions for the accelerating aging region detection that help better guide the predictive maintenance. The same DL structure for the multi-task sequence predictions of battery SOH and aging rate is employed for the knee point prediction to provide the baseline for onboard detection. Based on the two predictions, a probabilistic aging rate deviation method is proposed for the different aging regions detection. Moreover, cloud-edge framework is adopted considering practical applications where TL can be implemented. With investigations in this chapter, the general framework for accelerating aging detection with integral use of both point prediction and sequence prediction is demonstrated. The maintenance, replacement, or optimal control can be conducted by the guidance of the detection to extend the lifetime of the battery packs during practical applications.

J9 contributes to this chapter.

5.1. KNEE POINT PREDICTION

5.1.1. BATTERY KNEE DEFINITION AND BASIC MECHANISMS

The presence of a knee point can be attributed to aging-related mechanisms, including but not limited to processes such as resistance growth, lithium plating, and electrode saturation, as visually illustrated in Fig. 5-1. For an in-depth exploration of these intricate mechanisms, please refer to the source provided in [91]. To provide a concise overview, lithium plating stands out as a major contributor to battery degradation and the emergence of a knee point. This phenomenon is particularly pronounced under high-charge currents and/or low-temperature situations. Metallic lithium in this scenario is formed on the electrode surface with lithium ions, which generally are supposed to intercalate into the electrode [91], [92]. This process can result in the depletion of the electrolyte due to side reactions or gas generation, leading to active material loss and lithium plating, ultimately culminating in the appearance of a knee [93]. Moreover, the depletion of additives can exert an influence on knee onset through mechanisms like resistance growth and lithium plating. Mechanical deformation, driven by microscopic and macroscopic pressures, can hasten aging and contribute to the knee phenomenon [68], [94]. In cases where side reactions predominantly occur at the cathode, electrode saturation emerges as a significant factor. This saturation occurs when the loss rate of active material outpaces reduction in lithium inventory [91]. As batteries age, their internal resistance increases primarily due to SEI growth and byproducts of side reactions. Lastly, the percolation-limited connectivity driving knee stems from percolation theory and explains electrolyte dry-out mechanisms [95] [91].

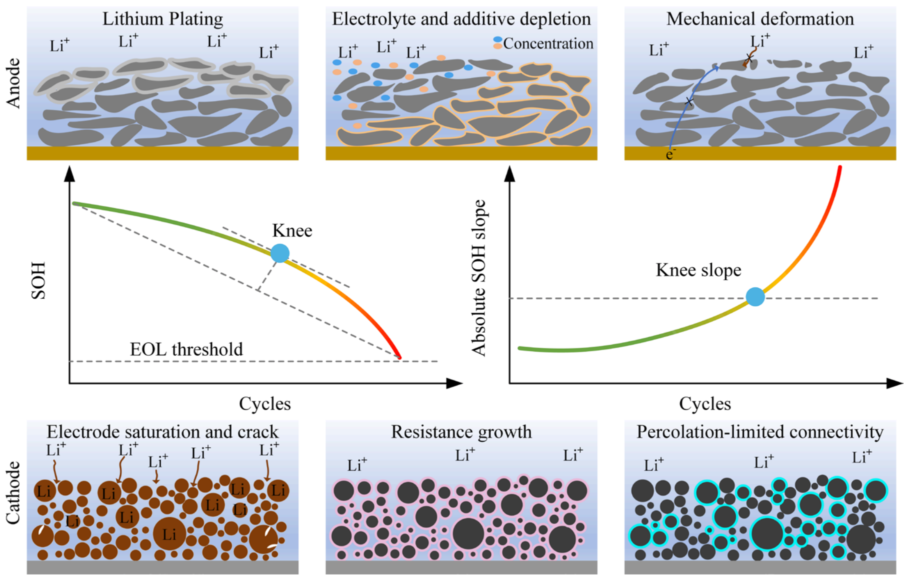

Figure 5-1 Battery knee and main related mechanisms. Source: [J9]

Methods for identifying knee points are diverse and extensively summarized in [91]. A majority of these methods necessitate the complete degradation curve for computation that is typically employed for offline identifications. The aging rate is described by curve slope, which can be determined by taking the difference between the predicted SOH, or directly predicted, thereby enabling online applications. To evaluate accelerated aging in real-time, Kneedle method is adopted. This method posits that slope value of knee is consistent with a line drawn from beginning to the EOL, as illustrated in Fig. 5-1. This approach provides a means to assess accelerating aging dynamics while being executed onboard [96]. In particular, our approach involves calculating the knee slope by drawing a line from the 10th cycle (as adapted from [55]) to EOL point, which is symbolically represented as,

$$k_{knee} = \frac{SoH_{\mathrm{EoL}} - SoH_{10}}{\mathrm{EoL} - 10} \tag{5.1}$$

5.1.2. EARLY STAGE MTL-STP PROGNOSTICS

Battery design and optimization significantly benefit from early predictions of lifetime and knee onset, particularly in endeavors like optimizing fast charging strategies [72], [97]. Recent studies have concentrated on single objectives within prediction realm or have employed multiple models for diverse prediction tasks. This approach escalates complexity and hinders algorithmic integration into BMS. To address this, MTL is introduced, aiming to consolidate different prediction tasks by facilitating shared information learning for related prognostics, whose general structure is illustrated in Fig. 5-2.

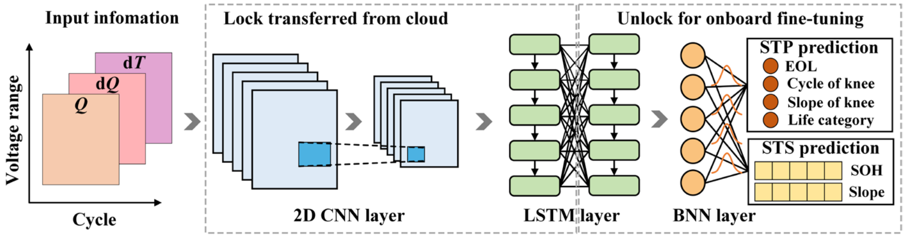

Figure 5-2 General MTL structure for battery health prognostics. Source: [J9]

In this architecture, input information comprises measured voltage, capacity, and temperature data. This data is processed into three sequences: a Q sequence, a dQ sequence, and a dT sequence. The model adopts a CNN-LSTM-BNN structure. The 2D CNN layer serves for spatial information extraction from partial measurement sequences, capturing the correlation between voltage ranges and various features. Subsequently, LSTM layer captures sequential relationships through different running cycles, while BNN facilitates probabilistic predictions. This amalgamation culminates in a neural network output, expressed as follows,

$$\hat{y} = \mathrm{BNN}(\mathrm{LSTM}(\mathrm{CNN}(Q, \mathrm{d}Q, \mathrm{d}T))), \tag{5.2}$$

where the output is one point for STP prognostics and sequences in STS prognostics. During training, the overall loss is a combination of individual task losses, each weighted by a factor of λ,

$$L = \sum_{N} \lambda_i L_i \ . \tag{5.3}$$

The negative log-likelihood loss function is employed, as described in Chapter 2 [78]. Specifically, STP model employs 4 loss functions, while the STS model employs 2 loss functions.

5.2. SEQUENTIAL SOH AND AGING RATE PREDICTIONS

Capability of onboard prediction holds crucial importance in health prognostics for guiding proactive predictive management. Beyond merely predicting the future SOH, it's equally vital to assess the rates of degradation in the upcoming SOH curve, which is effectively described by slopes of the forecasted SOH curve. As previously introduced, STS framework offers distinct advantages for accurate future SOH prediction, eliminating the need for an iterative process that could lead to gradient vanishing or acceleration issues during prediction. To simultaneously predict degradation variations in forthcoming cycles, the MTL approach is also harnessed. To maintain consistency, the same model framework utilized for STP-based early prognostics is employed, except for output numbers. For point prediction, output length is set to 1, while for *n* of STS model-based future curve predictions. Input data selection involves employing a *m* cycle-based sliding window. Consequently, a comprehensive *m*-to-*n* STS model is established. For the STS prediction, default values for *m* and *n* are set to 30 and 50, respectively. Similar to STP model, input information comprises *Q* sequences, d*Q* sequences, and d*T* sequences. The output of this framework includes both SOH and aging rates.

Slopes of SOH curve experience variations at each data point and can be overly responsive to local fluctuations, potentially leading to inaccurate alerts. Furthermore, as battery aging unfolds over an extended duration, the assessment of accelerating aging necessitates accounting for the overall degradation rate. Consequently, preprocessing the SOH curve data is essential before computing slopes during data preparation for training. Common techniques like filtering and empirical mode decomposition (EMD) are often utilized to produce SOH curve smoothing. However, despite these efforts, processed curves can still be affected by abrupt local variations. To address this challenge, empirical exponential model (EEM) is introduced to fit SOH curve, subsequently serving for slope calculation. The empirical model can be represented as,

$$y = a * e^{bx} + c * e^{dx} \tag{5.4}$$

where a, b, c, d are four fitting coefficients, and the cycle number and SOH are represented by x and y respectively. Upon this fitted curve, slope (k) at current cycle (i) is calculated by determining two adjacent SOH differences,

$$k_i = y_i - y_{i-1} \tag{5.5}$$

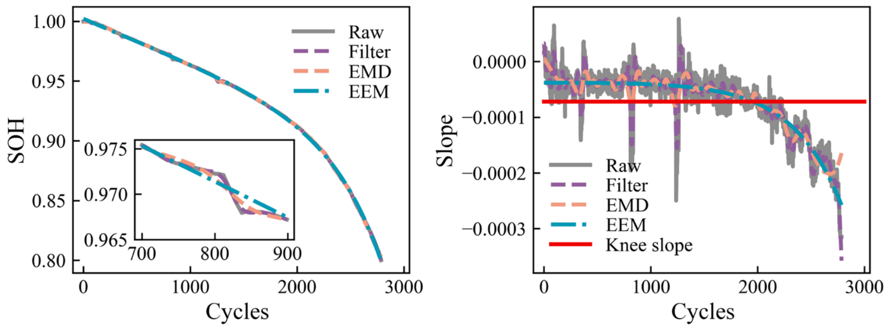

Figure 5-3 Effectiveness of different slope acquisition methods. Source: [J9]

Fig. 5-3 presents a comparison of the slope variations obtained through different methods using data from an experimental battery. The filter-based approach utilizes a Savitzky-Golay filter using a cubic polynomial fitting function with a window length of 55. While the filter and EMD methods contribute to a smoother degradation curve, the resulting slope variations remain notably sharp. In contrast, EEM method preserves overall degradation characteristics and exhibits smoother slope variations. By leveraging EEM-derived slopes, MTL framework can more effectively capture degradation variation properties in conjunction with SOH predictions. The intricate architecture of the network is detailed in J9.

5.3. PREDICTIVE HEALTH ASSESSMENT WITH PROBABILISTIC PREDICTIONS AND ACCELERATING AGING DETECTION

Predictive health management, particularly for the identification of accelerating aging, is crucial in devising effective strategies to prolong battery life. By detecting the onset of the knee point, interventions can be implemented to delay this occurrence and extend the battery lifetime. Drawing inspiration from battery internal short circuit stages delineated in [82], our approach categorizes aging into three distinct regions. In the "green" region, the slope of degradation changes slowly. Subsequently, it transitions to the "yellow" region, where acceleration becomes apparent around the knee point. Finally, aging enters the "red" region characterized by rapid degradation. Predictive actions should be initiated before entering the "red" region, striking a balance between cost-saving and efficient battery management. As a result, accurately and timely identifying the "yellow" region is of paramount significance. Leveraging probabilistic predictions for both future degradations and knee slopes, our approach facilitates accelerating aging assessment. This enables stakeholders to take proactive measures before the battery's health declines rapidly, ensuring optimized battery performance and lifetime.

In a more detailed breakdown, as depicted in Fig. 5-4, three aging regions are distinctly demarcated by two CIs: one for knee slope point predictions and the other for future degradation prognostics. Here, the inverse value of slope is deployed to effectively represent acceleration. The lower boundary of the "yellow" region is established through the intersection of the upper CI limit for sequence prognostics and the lower CI limit for the knee slope prediction. Conversely, the upper boundary is determined by the CI intersection in the opposite scenario. As a result, when signaling the impending onset of accelerating aging, it's imperative to initiate predictive health management measures to extend battery lifetime. This approach ensures timely and effective interventions for optimizing battery health.

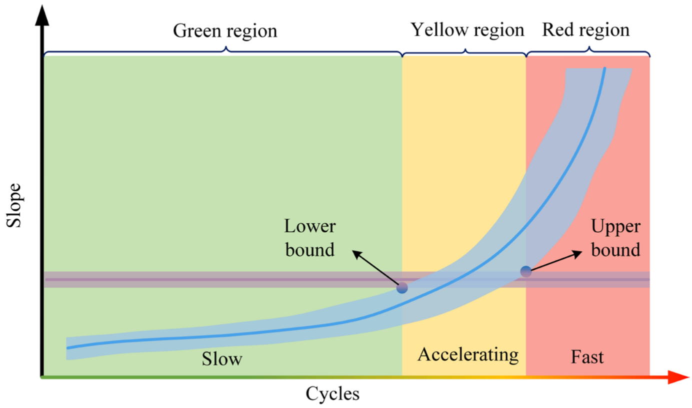

Figure 5-4 Probabilistic prognostics driven accelerating aging detection. Source: [J9]

In this study, our model is trained initially on cloud and then transmitted to the edge device. The edge device facilitates onboard prognostics by utilizing input information through a sliding window approach. Furthermore, TL emerges as a potent strategy to enhance accuracy and broaden applicability across diverse scenarios. To this end, a FT approach can be employed on edge. Specifically, this involves retraining the second LSTM and probabilistic layer, as depicted in Fig. 5-2. This design minimizes computational load while capitalizing on pre-learned mapping relationships. The outcome is an approach that effectively balances computational feasibility with accurate predictive capabilities for onboard applications.

The overall framework is illustrated in Fig. 5-5. To begin, early aging prognostics are considered. This entails predicting key characteristics like knee slope and other lifetime-related parameters through the utilization of a probabilistic STP-MTL model. The prognosticated knee slope subsequently serves as a pivotal reference for downstream health assessment. Then, a probabilistic STS model for forecasting future SOH and degradation slopes acted. This prediction process leverages sliding windows to take information from partial *Q*-*V* and *T*-*V* curves. The model is trained offline on cloud and subsequently deployed on an edge device for real-time prognostics. The resulting online predictions are harnessed for health assessment, wherein historical information can be incorporated via TL. These outcomes hold significant implications for guiding health management strategies to extend battery lifetime.

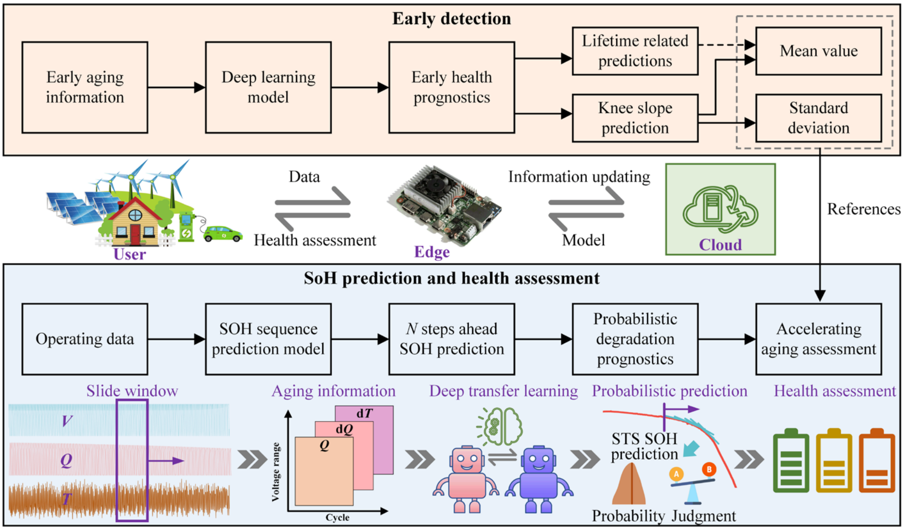

Figure 5-5 Overall framework for predictive battery health assessment. Source: [J9]

5.4. RESULTS AND DISCUSSION

5.4.1. EARLY AGING DETECTION

STP framework extends beyond conventional single-point prediction or classification approaches, offering predictions for a broader range of life-related parameters. Notably, it enables forecasts about the cycle and slope of battery knee, battery EOL, and lifetime classifications. Unlike conventional models that focus on one singular prognostic, STP-MTL model embraces a more holistic perspective, allowing for comprehensive prognostics. We maintain consistency with works in previous chapters utilizing partial Q, dQ, and dT curves as model inputs, ensuring alignment with previous methodologies and enhancing the overall coherence of the project.

Fig. 5-6(a) presents early prognostics of knee slopes. For a more detailed analysis, numerical results are tabulated in Table 5-1. This comparison includes the utilization of a single model for various tasks, following the approach outlined in Severson et al. [55]. The results indicate a strong alignment with the ideal fitting line within the CIs, illustrating the reliability of most prognostics. Significantly, MTL model enhances accuracy while demanding fewer cycles for input. The mean absolute percentage error (MAPE) for slope prediction stands at 9.97%, which effectively meets the requirements for probabilistic warning boundary establishment, as demonstrated in Fig. 5-6(a). Furthermore, MTL model not only excels in single knee slope prognostics but also opens the door for other valuable lifetime-related predictions. Demonstrating this versatility, our model highlights knee cycle, EOL cycle predictions, and lifetime classification, as showcased in Fig. 5-6(b) to Fig. 5-6(d), respectively.

The introduction of two additional prognostic tasks, namely EOL and knee cycle prediction, also showcases improvements with MAPE of less than 10.25% and 10.81% respectively. Furthermore, the incorporation of a classification task enhances the model's integration. Notably, our methodology employs partial *Q* and *T* curves instead of the entire discharge process employed in [55], also eliminating the need for manual feature engineering, rendering it more suitable and feasible for real applications. An advantage lies in the ease with which the regression and classification tasks can be combined via MTL. This streamlines the modeling process while enhancing algorithm integration within BMSs. Additionally, MTL model is adaptable for expansion with additional tasks of interest to researchers, thereby bolstering its versatility and potential applicability.

Table 5-1 Model performance evaluations. Source: [J9]

Prediction task	MAE	MAE [55]	MAPE	MAPE [55]
Slope of knee	2.37*10-5	3.11*10-5	9.97%	11.81%
EoL cycle	90 (cycles)	94 (cycles)	10.25%	11.70%
Cycle of knee	71 (cycles)	74 (cycles)	10.81%	12.71%
Lifetime classification	3 items	4 items	6%	8%

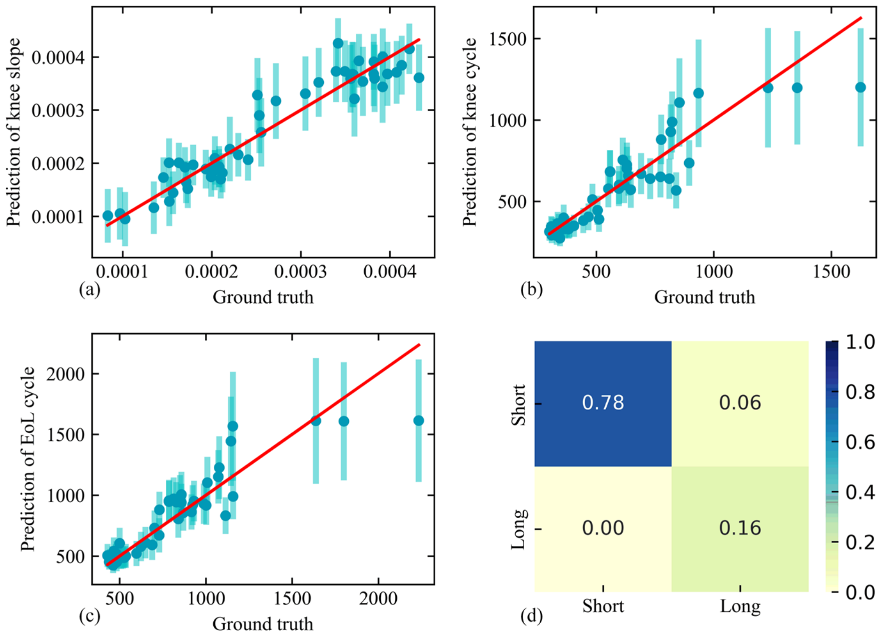

Figure 5-6 Early state prognostics with STP MTL model. Source: [J9]

5.4.2. MULTI-STEP AHEAD SOH PREDICTION

Both the SOH and the degradation slopes of 50 steps ahead are predicted, which roughly translates to an early warning of around two months. This prediction horizon is highly practical, considering scenarios where batteries are recharged every one to two days. Fig. 5-7 illustrates the predictions for three batteries. The outcomes demonstrate that future degradation characteristics are accurately prognosticated. The STS model is flexibly adapted to accommodate various prediction horizons. As an illustration, SOH predictions with different horizons are presented in Table 5-2. These errors are computed across all testing batteries. This evaluation showcases the general performance across batteries undergoing distinct current profiles, each characterized by its unique aging pattern. The results reveal that the prediction accuracy remains remarkably consistent across different horizons, with only a marginal increase of approximately 0.2% in RMSE when transitioning from 25 cycles to 100 cycles. There is also a slight increase observed in CI. This demonstrates the robustness of the STS model, which yields highly accurate and reliable future degradation curve predictions across various demanded horizons.

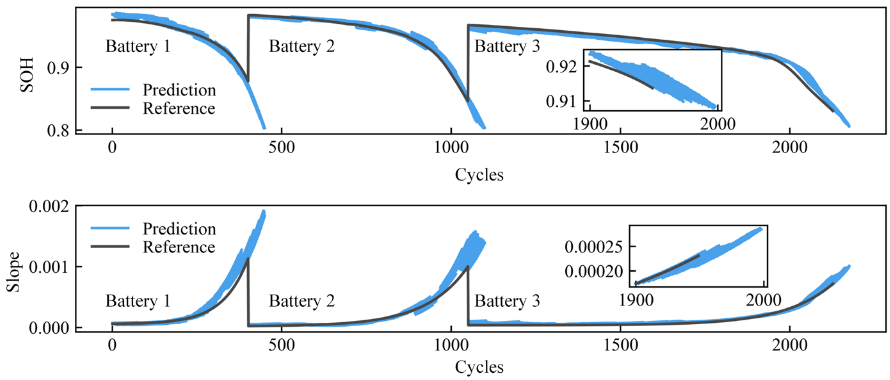

Figure 5-7 SOH and slope predictions for 50 steps of three batteries. Source: [J9]

Table 5-2 Evaluations for SOH prediction with different horizons. Source: [J9]

Prediction horizon	25 cycles	50 cycles	75 cycles	100 cycles
RMSE (%)	1.202	1.334	1.351	1.405
MAE (%)	0.856	0.912	0.949	0.951
Mean CI range (%)	1.960	1.967	2.180	2.191

The prediction offers insights into future degradation in the prediction horizons. In addition to assessing the accuracy of the predicted sequence as a whole, it's essential to evaluate predictions and errors at specific points within the predicted sequence. Specifically, evaluations for two distinct points on the predicted curve – the 1st point and the 50th point – are presented in Fig. 5-8(a). The results highlight that a significant portion of SOH predictions closely converge to actual values, whether considering the 1st or 50th point. Notably, when comparing the predictions of the two points, the predicted slope variations exhibit relatively larger deviations from the actual values for the 50th point. To further quantify the accuracy, the absolute error and relative error distributions are depicted in Fig. 5-8(b). These distributions underscore that the errors are predominantly below 5%, with a substantial concentration of errors around 0. This reinforces the reliability of STS model for predicting all 50 batteries, each undergoing different aging trajectories.

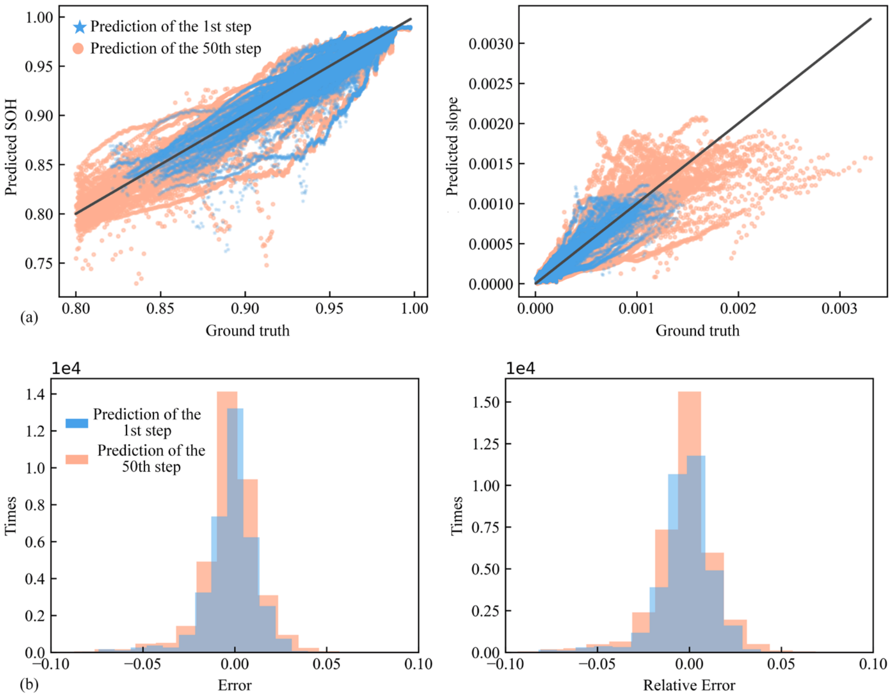

Figure 5-8 Evaluations of future predicted 1st point and 50th point. (a) prediction results, (b) errors and relative errors. Source: [J9]

5.4.3. ONBOARD HEALTH ASSESSMENT

Onboard health assessment plays a pivotal role in facilitating timely predictive maintenance strategies, ensuring that batteries vulnerable to accelerating aging are optimally managed to extend their operational lifetimes. By leveraging the probabilistic STP and STS predictions, it becomes possible to detect distinct working condition stages: the "green" health region, the "yellow" accelerating aging region, and the "red" fast aging region.

To illustrate effectiveness of these assessments, health evaluations for three batteries, each possessing varying lifespans, are depicted in Fig. 5-9. In each figure, the left segment illustrates the predicted future 50th SOH point, while the right segment showcases slope trajectories for the same point. The outcomes underscore the capability of the proposed model and strategy to effectively track actual values and accurately identify accelerating aging region onsets. CI associated with predictions o-

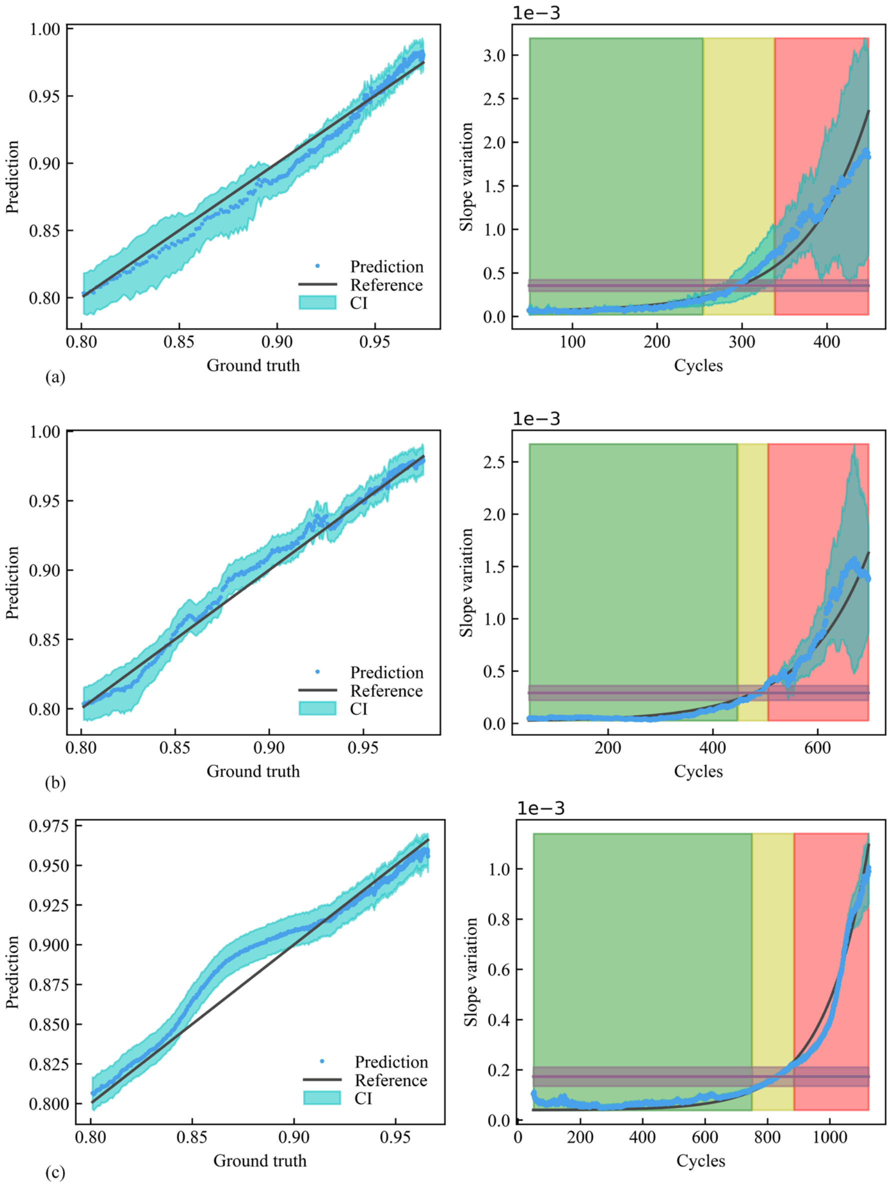

Figure 5-9 Health assessments for three batteries with diverse life ranges. Source: [J9]

-ffer valuable probabilistic boundaries. Notably, fluctuations in SOH predictions can lead to substantial fluctuations if utilized for slope calculations. As a result, relying solely on the calculated slopes of predicted SOH for assessment can yield wrong warnings about accelerating aging. Conversely, leveraging predicted slopes from MTL approach mitigates the potential for drastic changes across orders of magnitude, even in the presence of fluctuations. As a consequence, the accelerating aging warning becomes more reliable, facilitating more precise and timely predictive health management strategies. This approach not only aids in avoiding premature maintenance but also optimizes resource utilization by targeting interventions where they are most needed.

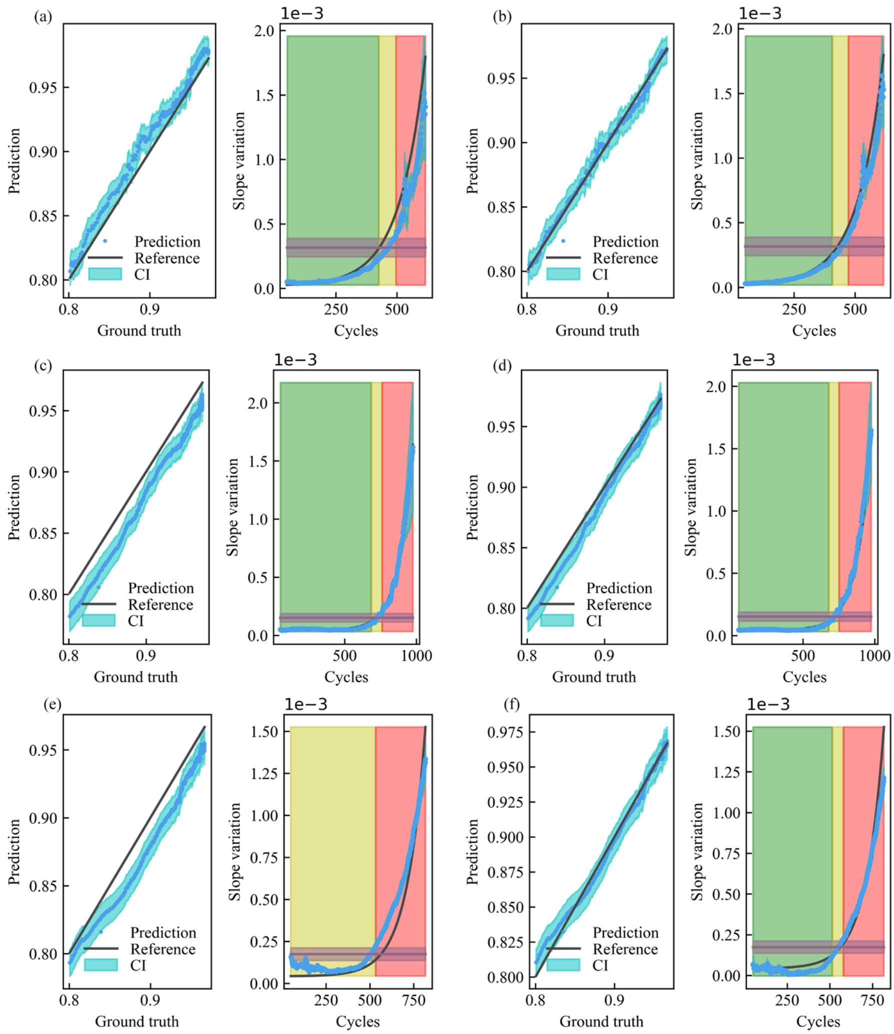

Figure 5-10 Figure 5-10 Model improvement through fine-tuning. (a), (c), and (e), predicted future 50th SOH point and the assessment based on base model. (b), (d), and (f) the corresponding results with fine-tuning using the first 10% of data. Source: [J9]

Updating the model during cycling is a convenient approach to enhance the model's performance, particularly in scenarios where the initial model does not perfectly align with testing battery. This process allows the model to adapt to specific battery behaviors that may not have been well captured by the initial model. In Fig. 5-10, two representative batteries demonstrate this concept. The initial predictions for these batteries are either larger-shifted or smaller-shifted relative to the true values, as depicted in Fig. 5-10(a) and Fig. 5-10(c), respectively. By performing fine-tuning with initial 10% data, significant improvements can be observed in both the accuracy of SOH predictions and the detection of accelerating aging, as shown in Fig. 5-10(b) and Fig. 5-10(d). Furthermore, Fig. 5-10(e) presents a scenario where the predicted SOH values are consistently underestimated, resulting in an early "yellow" region detection due to the predicted slope falling below the lower bound from the start. In such cases, the assessment loses its practical significance and effectiveness. However, with the application of FT, the predicted values come closer to reality, eliminating premature warnings of accelerating aging. By FT only the last few layers of the model, computational demands on onboard devices remain manageable, making it feasible for real-time applications. The RMSE and MAE metrics for the predicted SOH sequences across all testing batteries are notably reduced from 1.334% and 0.912% of the base model to 1.001% and 0.729%, respectively. This approach enhances the model's adaptability and robustness for onboard applications.

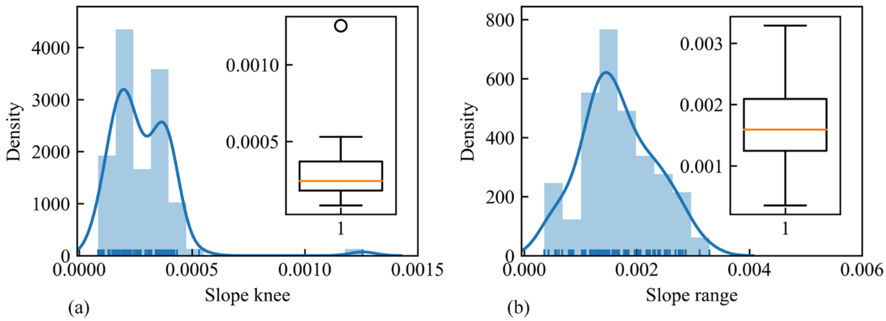

Figure 5-11 Statistic analysis for mean value and ranges of battery knees. Source: [J9]

5.4.4. EXTRAPOLATION TO OTHER BATTERIES

The proposed framework can be extended to other battery types with different aging scenarios, allowing for adaptability to various real-world situations. However, when sufficient batteries for STP predictions are not available, determining the threshold value for the slope is crucial. In this context, a statistical assumption is made, assuming that the relationship between the mean and standard deviation remains consistent for a specific battery. The mean value and standard deviation of slope values within certain distribution ranges are assumed to follow the same overall pattern. The distribution of slope knees and ranges for the publicly available datasets is depicted in Figure 5-11. Notably, these distributions showcase properties of normal distribution. Thus, leveraging the mean values and slope ranges of training and testing batteries, along with their standard deviations, enables the calculation of the required threshold for onboard health assessment. This approach ensures that the framework can be effectively applied to different batteries even when direct STP predictions are not feasible due to limited available data.

$$D\left(m_1 / \left(s_1, \frac{1}{r_1} \right) \right) = D\left(m_2 / \left(s_2, \frac{1}{r_2} \right) \right) \tag{5.6}$$

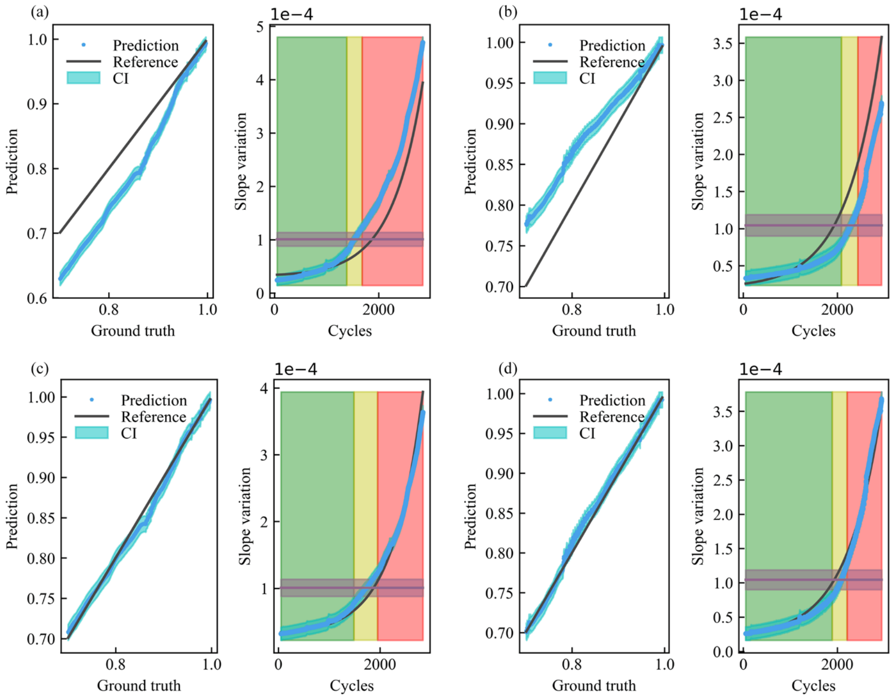

Figure 5-12 Health assessment for second-life batteries (a)/(b) results for cell 2/cell 1 using initial model, (c)/(d) corresponding results after fine-tuning. Source: [J9]

For the application and validation of the proposed framework, two commercial pouch batteries in their second-life are employed. These batteries exhibit an initial capacity that is approximately 73.75% of the nominal capacity, equating to around 5.9 Ah out of an 8 Ah nominal capacity. The two batteries have distinct dynamic working profiles during their first lives and undergo similar testing profiles during their second life. In terms of charging and discharging, a constant current of 2.5 C is applied to the batteries, with the transition to constant voltage charging occurring once the current diminishes to below 0.1 C. The SOH calculation remains consistent with the earlier methodology, involving the division by the 10th cycle, leading to a degradation curve from 1 to approximately 0.7. This data serves as the basis for implementing and validating the proposed approach on different types of batteries.

The outcomes for these two experimental batteries are depicted in Fig. 5-12. Specifically, the results utilizing the base model for predicting Cell 1 and Cell 2 are showcased in Fig. 5-12(a) and Fig. 5-12(b), respectively. Meanwhile, the outcomes employing FT with 30% of the data are exhibited in Fig. 5-12(c) and Fig. 5-12(d), respectively. From the figures, it is evident that the calculated bound for the slope threshold can encompass the actual threshold, considering CI derived from the statistical analysis. With the incorporation of 30% data for FT, the predictions closely converge to the actual degradation curves, exhibiting an RMSE of less than 0.76%, an MAE of less than 0.55%, and a MaxAE of less than 2.85%. The numerical results, as presented in Table 3, showcase significant improvement in prediction accuracy. The depicted trajectories of slope variation prior to FT exhibit early warnings for Cell 2 and late warnings for Cell 1, which align with the overestimation and underestimation of SOH predictions. With the application of fine-tuning, the trajectories of the aging rate become more accurate, furnishing a precise and timely assessment of the anticipated aging rate in future cycles. This enhancement in accuracy will greatly facilitate the health management of BMSs.

Table 5-3 Health assessment performances for the second-life batteries. Source: [J9]

Testing cell	Error (%)	Initial model	10% data for TL	30% data for TL	50% data for TL
Cell 1	RMSE	3.356	2.267	0.623	0.565
	MAE	2.612	1.471	0.405	0.369
	MaxAE	7.942	6.771	2.842	2.531
Cell 2	RMSE	3.915	2.310	0.754	0.736
	MAE	3.024	1.661	0.541	0.511
	MaxAE	7.780	5.020	2.616	2.573

5.5. SUMMARY

This chapter introduces a novel strategy that addresses the crucial need for online health assessment, offering a viable solution for practical applications. The combined early prediction within the proposed framework showcases remarkable accuracy while also optimizing resource utilization by eliminating the need for separate model constructions. The synergistic information sharing across associated tasks yields benefits for each task, paving the way for an encouraging avenue in the integration of distinct yet interconnected prognostic tasks within future BMS.

Furthermore, the incorporation of sequence predictions within the multi-task framework is a notable advancement. This includes the simultaneous prediction of future SOH and degradation rates. The obtained results illustrate the adaptability of the STS prediction for varying prediction horizons, aligning with practical requirements. The predictions are characterized by an RMSE of less than 1.41% and an MAE of less than 0.96%, with a majority of the prediction errors falling below 5%. The prediction of degradation rates, rather than calculating them from predicted SOH, aids in avoiding improper detection stemming from local variations. The provision of probabilistic regression helps in establishing prediction boundaries that segregate regions of degradation, allowing the identification of periods most susceptible to accelerating aging. This approach holds promise for real-world applications, as it predicts probabilistic ranges of the accelerating aging process rather than focusing on single specific points that may exhibit large errors.

Moreover, the integration of the cloud-edge concept, coupled with flexible TL, offers a robust approach for performance enhancement during battery cycling. The base model is trained on a powerful server and subsequently transferred to user-edge devices, where it can be fine-tuned to cater to diverse aging patterns. The online prediction effectively detects accelerating regions, with performance improvements demonstrated during the aging process through FT. The framework's applicability is further demonstrated through its application to two retired batteries, showcasing satisfactory assessment capabilities with maximum errors of less than 3% after 30% of the battery's lifetime.

CHAPTER 6. CONCLUSION AND OUTLOOK

6.1. CONCLUSIONS

Battery health prognostics are essential to guide safe operation and optimal control while challenging especially under diverse conditions and limited labels. This Ph.D. project focuses on TL-based SOH estimation and prediction using only sparsely labeled data to improve performance under various conditions. The key findings and main contributions are summarized as follows.

- **Various application scenarios cause diverse aging patterns.**
  Battery aging patterns are influenced by coupling factors including battery types, loading profiles, and working temperatures, which are illustrated by the experimental results. Dynamic loadings and pulse currents have the potential to help extend the lifetime, while highway loadings and variable temperatures that correlate to different seasons accelerate the aging process.

- **Sequential features from partial *Q-V* curve enable aging characterization.**
  HIs extracted from partial *Q-V* curve have high correlations with both battery SOH and EOL while enabling practical applications. Data cleaning by filtering the rest period ensures effective extraction under different charging profiles. These features can be used for all three main battery health prognostics including SOH estimation, EOL prediction, and future trajectory predictions.

- **Sparsely and limited data ensure accurate and reliable SOH estimation.**
  Fine-tuning-based TL strategies are fast and effective for model improvement by updating the model from the source domain using only sparsely labeled data. Limited labels ensure the accurate and reliable estimation of SOH for the whole aging process. In addition, the reconstructed capacity curves by the sparsely labeled data can serve the pseudo values for the following SOH prediction model FT to improve the degradation trajectory predictions. Therefore, in practical applications, it is not essentially required to obtain continuous labeled data, which is also very challenging, while those sparse labels obtained from regular maintenance could help improve the SOH estimations.

- **Learning from unlabeled data improves SOH estimation and prediction.**
  In real-world applications, the obtained data are most unlabeled. Although the expected capacity or lifetime labels are not directly available for modeling, aging information contained in the unlabeled data is valuable to boost the model performance. By constructing a self-supervised framework, where the unlabeled

data are used for the pre-text learning to learn the aging characteristics from the partial *Q*-*V* curves, the downstream SOH estimation model can be quickly converged by leveraging limited labels for FT the model learned from the unlabeled data, and the model performance is improved by comparing to pure labeled data trained models.

- **DA and CL increase generalization of the SOH estimation model.**
  Aligning the hidden states of the neural network from the source batteries and testing batteries can help learn the domain adaptative features that reduce the domain discrepancies to improve the model accuracy on the target batteries. In addition, the CL is supposed to take into consideration to avoid catastrophic forgetting when upgrading the models using the labeled samples from the target domains. By the post-hoc analysis of the learned model, the model performance can be interpreted to understand the intrinsic reasons for the model working under different scenarios. By the DA and CL strategies, the model generalization can be continuously improved during usage without requirement of establishing several models for different battery types and working conditions.

- **MTL improves accuracy and integration by combining different related prognostic tasks.**
  Different health prognostic tasks are demanded in different applications while constructing specific models for each task consumes huge amounts of resources. MTL integrates different related prognostic tasks that provide prognostics for different tasks via one model. The performance can be also improved by leveraging information among related tasks. The early predictions of battery lifetime, knee, and so on can be obtained together, and the online sequence predictions for future SOH and degradation rates can be also integrated. In addition, the feature extrapolation for recursive predictions is easy to combine with the SOH trajectory prediction task, which solves the problem with dependencies on the historical capacities for future SOH predictions.

- **Long-term prediction requires regularization to ensure stability.**
  Long-term prediction of battery degradation trajectories is valuable while challenging. The long-term prediction performance needs to be regularized during the training of the prediction model since the long-term prediction via a recursive process is not stable. By adding an additional regularization penalty, the learned model remains stable during recursive predictions for the future degradation trajectory. Thus, the model can be used both for short-term and long-term predictions of future SOH.

- **Predictive health assessment detects accelerating aging and guides better maintenance.**
  Typical degradation curves experience a process from slow aging to fast aging, divided by the knee on the degradation curve. The detection of accelerating aging

is significant to the downstream predictive health management control strategies for the extension of battery lifetime. By leveraging the collaboration of probabilistic point prediction and sequence predictions, the accelerating aging progress can be detected early to provide key insights into future degradation to guide proper maintenance. The concept of could-edge collaboration can also be adapted for online applications.

6.2. FUTURE WORK

Comprehensive TL technologies for battery health prognostics have been investigated in this Ph.D. project and promising results have been obtained. However, it is still on the pure data level and running on the computer. Future works are mainly looking at the implementation of algorithms onboard and combining more with physical mechanisms. Several aspects are summarized as follows.

- **Onboard implementation with cloud-edge platform**
  The developed algorithms for battery health prognostics and assessment are supposed to be implemented onboard BMS to play their roles in the PHMs of batteries. The base model can be trained on the cloud with powerful computing resources while the FT process can be conducted on the onboard BMSs. In addition, the data can also be stored on the cloud to reduce the storage burden of onboard BMSs. To come up with the idea, the edge devices will be used to implement the prognostic methods and verify the performance with the hardware in-loop device. Then the developed devices can be explored to be implemented in real energy storage systems. With the hardware support, the author will conduct this implementation in his future work.

- **Aging mode prognostics**
  Battery capacity and power fade are the macroscopic behaviors of battery aging, while the internal aging modes are the key factors affecting the degradation patterns. Detecting the loss of active materials, loss of lithium inventory, and the increase of impedance are important and be more physically reliable to tell the aging of batteries. Therefore, the prognostics of aging modes via measurements are worth more investigations. Similarly, advanced TL strategies such as domain adaptative learning will also perform important roles in the prognostic performance improvements under various scenarios in which different aging modes exist due to different loadings and environmental conditions.

- **Physics-guided ML for battery health prognostics.**
  Features from measured data are easy to extract while influenced hugely by the usage conditions and are hard to understand the physical meanings. Therefore, future works will focus more on the extraction of physical information-enabled features from EMs that characterize the exact internal aging mechanisms. For example, the average concentrations of solids and electrolytes can be used to

describe the degradations of batteries. By using those physical features for the ML model, the model performance can be better interpreted, and the prognostic results are more trusted.

- **Health management and control strategies**
  Health prognostics tell the customers the aging status of their batteries and guide their maintenance and recycling behaviors. The more important role of battery health prognostics should be the guidance of downstream health management strategies. By considering the current aging status and future degradation trend, control strategies such as by-pass, balancing, circuit reconfiguration, and new charging profiles can be performed to help avoid accelerating aging to improve the battery lifetime. By taking into consideration the accurate and reliable health prognostic results, the downstream control strategies will be more reliable and play the most valuable roles in battery health management.

LITERATURE LIST

[1] J. Cho, S. Jeong, and Y. Kim, “Commercial and research battery technologies for electrical energy storage applications,” *Progress in Energy and Combustion Science*, vol. 48, pp. 84–101, 2015, doi: 10.1016/j.pecs.2015.01.002.

[2] X. Hu, Z. Deng, X. Lin, Y. Xie, and R. Teodorescu, “Research directions for next-generation battery management solutions in automotive applications,” *Renewable and Sustainable Energy Reviews*, vol. 152, no. August, p. 111695, 2021, doi: 10.1016/j.rser.2021.111695.

[3] M. M. Thackeray, C. Wolverton, and E. D. Isaacs, “Electrical energy storage for transportation - Approaching the limits of, and going beyond, lithium-ion batteries,” *Energy and Environmental Science*, vol. 5, no. 7, pp. 7854–7863, 2012, doi: 10.1039/c2ee21892e.

[4] M. A. Hannan, M. S. H. Lipu, A. Hussain, and A. Mohamed, “A review of lithium-ion battery state of charge estimation and management system in electric vehicle applications: Challenges and recommendations,” *Renewable and Sustainable Energy Reviews*, vol. 78, no. May, pp. 834–854, 2017, doi: 10.1016/j.rser.2017.05.001.

[5] C. Zhao, P. B. Andersen, C. Træholt, and S. Hashemi, “Grid-connected battery energy storage system: a review on application and integration,” *Renewable and Sustainable Energy Reviews*, vol. 182, no. September 2022, p. 113400, 2023, doi: 10.1016/j.rser.2023.113400.

[6] T. M. Gür, “Review of electrical energy storage technologies, materials and systems: Challenges and prospects for large-scale grid storage,” *Energy and Environmental Science*, vol. 11, no. 10, pp. 2696–2767, 2018, doi: 10.1039/c8ee01419a.

[7] Y. Wang *et al.*, “A comprehensive review of battery modeling and state estimation approaches for advanced battery management systems,” *Renewable and Sustainable Energy Reviews*, vol. 131, no. March, p. 110015, 2020, doi: 10.1016/j.rser.2020.110015.

[8] R. Xiong, Y. Pan, W. Shen, H. Li, and F. Sun, “Lithium-ion battery aging mechanisms and diagnosis method for automotive applications: Recent advances and perspectives,” *Renewable and Sustainable Energy Reviews*, vol. 131, no. 5, p. 110048, 2020, doi: 10.1016/j.rser.2020.110048.

[9] X. Hu, Y. Che, X. Lin, and Z. Deng, “Health Prognosis for Electric Vehicle

Battery Packs: A Data-Driven Approach," *IEEE/ASME Transactions on Mechatronics*, vol. 25, no. 6, pp. 2622–2632, 2020, doi: 10.1109/TMECH.2020.2986364.

[10] Y. Che, A. Foley, M. El-Gindy, X. Lin, X. Hu, and M. Pecht, "Joint Estimation of Inconsistency and State of Health for Series Battery Packs," *Automotive Innovation*, vol. 4, no. 1, pp. 103–116, 2021, doi: 10.1007/s42154-020-00128-8.

[11] M. R. Palacín and A. De Guibert, "Batteries: Why do batteries fail?," *Science*, vol. 351, no. 6273, 2016, doi: 10.1126/science.1253292.

[12] X. Han *et al.*, "A review on the key issues of the lithium ion battery degradation among the whole life cycle," *eTransportation*, vol. 1, p. 100005, 2019, doi: 10.1016/j.etran.2019.100005.

[13] K. Liu, Q. Peng, H. Sun, M. Fei, H. Ma, and T. Hu, "A Transferred Recurrent Neural Network for Battery Calendar Health Prognostics of Energy-Transportation Systems," *IEEE Transactions on Industrial Informatics*, vol. 3203, no. c, 2022, doi: 10.1109/TII.2022.3145573.

[14] H. Rahimi-Eichi, U. Ojha, F. Baronti, and M. Y. Chow, "Battery management system: An overview of its application in the smart grid and electric vehicles," *IEEE Industrial Electronics Magazine*, vol. 7, no. 2, pp. 4–16, 2013, doi: 10.1109/MIE.2013.2250351.

[15] S. T. Hung, D. C. Hopkins, and C. R. Mosling, "Extension of Battery Life via Charge Equalization Control," *IEEE Transactions on Industrial Electronics*, vol. 40, no. 1, pp. 96–104, 1993, doi: 10.1109/41.184826.

[16] X. Huang *et al.*, "Lifetime Extension of Lithium-ion Batteries with Low-Frequency Pulsed Current Charging," *IEEE Journal of Emerging and Selected Topics in Power Electronics*, vol. 6777, no. c, 2021, doi: 10.1109/JESTPE.2021.3130424.

[17] K. Liu, K. Li, Q. Peng, and C. Zhang, "A brief review on key technologies in the battery management system of electric vehicles," *Frontiers of Mechanical Engineering*, vol. 14, no. 1, pp. 47–64, 2019, doi: 10.1007/s11465-018-0516-8.

[18] S. Yang, C. Zhang, J. Jiang, W. Zhang, L. Zhang, and Y. Wang, "Review on state-of-health of lithium-ion batteries: Characterizations, estimations and applications," *Journal of Cleaner Production*, vol. 314, no. June, p. 128015, 2021, doi: 10.1016/j.jclepro.2021.128015.

[19] V. Sulzer *et al.*, “The challenge and opportunity of battery lifetime prediction from field data,” *Joule*, vol. 5, no. 8, pp. 1934–1955, 2021, doi: 10.1016/j.joule.2021.06.005.

[20] H. Rauf, M. Khalid, and N. Arshad, “Machine learning in state of health and remaining useful life estimation: Theoretical and technological development in battery degradation modelling,” *Renewable and Sustainable Energy Reviews*, vol. 156, no. August 2021, p. 111903, 2022, doi: 10.1016/j.rser.2021.111903.

[21] Q. Wang, B. Mao, S. I. Stoliarov, and J. Sun, “A review of lithium ion battery failure mechanisms and fire prevention strategies,” *Progress in Energy and Combustion Science*, vol. 73, pp. 95–131, 2019, doi: 10.1016/j.pecs.2019.03.002.

[22] X. Hu, L. Xu, X. Lin, and M. Pecht, “Battery Lifetime Prognostics,” *Joule*, vol. 4, no. 2, pp. 310–346, 2020, doi: 10.1016/j.joule.2019.11.018.

[23] X. Hu, F. Feng, K. Liu, L. Zhang, J. Xie, and B. Liu, “State estimation for advanced battery management: Key challenges and future trends,” *Renewable and Sustainable Energy Reviews*, vol. 114, no. April, p. 109334, 2019, doi: 10.1016/j.rser.2019.109334.

[24] J. Tian, R. Xiong, and W. Shen, “A review on state of health estimation for lithium ion batteries in photovoltaic systems,” *eTransportation*, vol. 2, p. 100028, 2019, doi: 10.1016/j.etran.2019.100028.

[25] A. Guha and A. Patra, “State of Health Estimation of Lithium-Ion Batteries Using Capacity Fade and Internal Resistance Growth Models,” *IEEE Transactions on Transportation Electrification*, vol. 4, no. 1, pp. 135–146, 2017, doi: 10.1109/TTE.2017.2776558.

[26] Z. Song *et al.*, “The sequential algorithm for combined state of charge and state of health estimation of lithium-ion battery based on active current injection,” *Energy*, vol. 193, p. 116732, 2020, doi: 10.1016/j.energy.2019.116732.

[27] B. Liu, X. Tang, and F. Gao, “Joint estimation of battery state-of-charge and state-of-health based on a simplified pseudo-two-dimensional model,” *Electrochimica Acta*, vol. 344, p. 136098, 2020, doi: 10.1016/j.electacta.2020.136098.

[28] Y. Li *et al.*, “Model Order Reduction Techniques for Physics-Based Lithium-Ion Battery Management: A Survey,” *IEEE Industrial Electronics Magazine*,

no. September, 2021, doi: 10.1109/MIE.2021.3100318.

[29] H. Shi *et al.*, "On-line adaptive asynchronous parameter identification of lumped electrical characteristic model for vehicle lithium-ion battery considering multi-time scale effects," *Journal of Power Sources*, vol. 517, no. September 2021, p. 230725, 2022, doi: 10.1016/j.jpowsour.2021.230725.

[30] J. Bi, T. Zhang, H. Yu, and Y. Kang, "State-of-health estimation of lithium-ion battery packs in electric vehicles based on genetic resampling particle filter," *Applied Energy*, vol. 182, pp. 558–568, 2016, doi: 10.1016/j.apenergy.2016.08.138.

[31] S. Tong, M. P. Klein, and J. W. Park, "On-line optimization of battery open circuit voltage for improved state-of-charge and state-of-health estimation," *Journal of Power Sources*, vol. 293, pp. 416–428, 2015, doi: 10.1016/j.jpowsour.2015.03.157.

[32] F. Zhu and J. Fu, "A Novel State-of-Health Estimation for Lithium-Ion Battery via Unscented Kalman Filter and Improved Unscented Particle Filter," *IEEE Sensors Journal*, vol. 21, no. 22, pp. 25449–25456, 2021, doi: 10.1109/JSEN.2021.3102990.

[33] X. Hu, H. Jiang, F. Feng, and B. Liu, "An enhanced multi-state estimation hierarchy for advanced lithium-ion battery management," *Applied Energy*, vol. 257, no. September 2019, p. 114019, 2020, doi: 10.1016/j.apenergy.2019.114019.

[34] Z. Chen, C. C. Mi, Y. Fu, J. Xu, and X. Gong, "Online battery state of health estimation based on Genetic Algorithm for electric and hybrid vehicle applications," *Journal of Power Sources*, vol. 240, pp. 184–192, 2013, doi: 10.1016/j.jpowsour.2013.03.158.

[35] C. Fleischer, W. Waag, H. M. Heyn, and D. U. Sauer, "On-line adaptive battery impedance parameter and state estimation considering physical principles in reduced order equivalent circuit battery models part 2. Parameter and state estimation," *Journal of Power Sources*, vol. 262, pp. 457–482, 2014, doi: 10.1016/j.jpowsour.2014.03.046.

[36] Y. Zhang and Y. F. Li, "Prognostics and health management of Lithium-ion battery using deep learning methods: A review," *Renewable and Sustainable Energy Reviews*, vol. 161, no. February, p. 112282, 2022, doi: 10.1016/j.rser.2022.112282.

[37] X. Hu, Y. Che, X. Lin, and S. Onori, "Battery Health Prediction Using Fusion-

Based Feature Selection and Machine Learning," *IEEE Transactions on Transportation Electrification*, vol. 7, no. 2, pp. 382–398, 2021, doi: 10.1109/TTE.2020.3017090.

[38] Z. Deng *et al.*, "Health Evaluation for Lithium-Ion Batteries," *Ieee/Asme Transactions on Mechatronics*, vol. 26, no. 3, pp. 1295–1306, 2021.

[39] Y. Zhang, T. Wik, J. Bergstrom, and C. Zou, "State of health estimation for lithium-ion batteries under arbitrary usage using data-driven multi-model fusion," *IEEE Transactions on Transportation Electrification*, vol. PP, p. 1, 2023, doi: 10.1109/TTE.2023.3267124.

[40] C. Zhao, P. B. Andersen, C. Træholt, and S. Hashemi, "Data-driven battery health prognosis with partial-discharge information," *Journal of Energy Storage*, vol. 65, no. December 2022, p. 107151, 2023, doi: 10.1016/j.est.2023.107151.

[41] J. Meng *et al.*, "An Automatic Weak Learner Formulation for Lithium-Ion Battery State of Health Estimation," *IEEE Transactions on Industrial Electronics*, vol. 69, no. 3, pp. 2659–2668, 2022, doi: 10.1109/TIE.2021.3065594.

[42] D. Roman, S. Saxena, V. Robu, M. Pecht, and D. Flynn, "Machine learning pipeline for battery state-of-health estimation," *Nature Machine Intelligence*, vol. 3, no. 5, pp. 447–456, 2021, doi: 10.1038/s42256-021-00312-3.

[43] C. She, L. Zhang, Z. Wang, F. Sun, P. Liu, and C. Song, "Battery State of Health Estimation Based on Incremental Capacity Analysis Method: Synthesizing from Cell-Level Test to Real-World Application," *IEEE Journal of Emerging and Selected Topics in Power Electronics*, vol. PP, no. c, p. 1, 2021, doi: 10.1109/JESTPE.2021.3112754.

[44] Z. Wang, C. Yuan, and X. Li, "Lithium Battery State-of-Health Estimation via Differential Thermal Voltammetry with Gaussian Process Regression," *IEEE Transactions on Transportation Electrification*, vol. 7, no. 1, pp. 16–25, 2021, doi: 10.1109/TTE.2020.3028784.

[45] D. Wang, Q. Zhang, H. Huang, B. Yang, H. Dong, and J. Zhang, "An electrochemical–thermal model of lithium-ion battery and state of health estimation," *Journal of Energy Storage*, vol. 47, no. October 2021, p. 103528, 2022, doi: 10.1016/j.est.2021.103528.

[46] Y. Zhang, T. Wik, J. Bergström, M. Pecht, and C. Zou, "A machine learning-based framework for online prediction of battery ageing trajectory and

lifetime using histogram data," *Journal of Power Sources*, vol. 526, no. October 2021, p. 231110, 2022, doi: 10.1016/j.jpowsour.2022.231110.

[47] X. Li, Z. Wang, L. Zhang, C. Zou, and D. D. Dorrell, "State-of-health estimation for Li-ion batteries by combing the incremental capacity analysis method with grey relational analysis," *Journal of Power Sources*, vol. 410–411, no. November 2018, pp. 106–114, 2019, doi: 10.1016/j.jpowsour.2018.10.069.

[48] S. B. Vilsen and D. I. Stroe, "Battery state-of-health modelling by multiple linear regression," *Journal of Cleaner Production*, vol. 290, p. 125700, 2021, doi: 10.1016/j.jclepro.2020.125700.

[49] C. She, Y. Li, C. Zou, T. Wik, Z. Wang, and F. Sun, "Offline and Online Blended Machine Learning for Lithium-Ion Battery Health State Estimation," *IEEE Transactions on Transportation Electrification*, vol. 8, no. 2, pp. 1604–1618, 2022, doi: 10.1109/TTE.2021.3129479.

[50] X. Li, Z. Wang, and J. Yan, "Prognostic health condition for lithium battery using the partial incremental capacity and Gaussian process regression," *Journal of Power Sources*, vol. 421, no. March, pp. 56–67, 2019, doi: 10.1016/j.jpowsour.2019.03.008.

[51] L. Cai, J. Meng, D. I. Stroe, G. Luo, and R. Teodorescu, "An evolutionary framework for lithium-ion battery state of health estimation," *Journal of Power Sources*, vol. 412, no. December 2018, pp. 615–622, 2019, doi: 10.1016/j.jpowsour.2018.12.001.

[52] Q. Gong, P. Wang, and Z. Cheng, "An encoder-decoder model based on deep learning for state of health estimation of lithium-ion battery," *Journal of Energy Storage*, vol. 46, no. September 2021, p. 103804, 2022, doi: 10.1016/j.est.2021.103804.

[53] J. Lu, R. Xiong, J. Tian, C. Wang, F. Sun, and J. Tian, "Deep learning to estimate battery state of health without additional degradation experiments," *Nature Communications*, pp. 1–13, 2023, doi: 10.1038/s41467-023-38458-w.

[54] G. Ma *et al.*, "Real-time personalized health status prediction of lithium-ion batteries using deep transfer learning," *Energy and Environmental Science*, 2022, doi: 10.1039/d2ee01676a.

[55] K. A. Severson *et al.*, "Data-driven prediction of battery cycle life before capacity degradation," *Nature Energy*, vol. 4, no. 5, pp. 383–391, 2019, doi: 10.1038/s41560-019-0356-8.

[56] P. M. Attia, K. A. Severson, and J. D. Witmer, "Statistical Learning for Accurate and Interpretable Battery Lifetime Prediction," *Journal of The Electrochemical Society*, vol. 168, no. 9, p. 090547, 2021, doi: 10.1149/1945-7111/ac2704.

[57] Z. Fei, F. Yang, K. L. Tsui, L. Li, and Z. Zhang, "Early prediction of battery lifetime via a machine learning based framework," *Energy*, vol. 225, p. 120205, 2021, doi: 10.1016/j.energy.2021.120205.

[58] S. Shen, V. Nemani, J. Liu, C. Hu, and Z. Wang, "A hybrid machine learning model for battery cycle life prediction with early cycle data," *2020 IEEE Transportation Electrification Conference and Expo, ITEC 2020*, pp. 181–184, 2020, doi: 10.1109/ITEC48692.2020.9161647.

[59] Y. Yang, "A machine-learning prediction method of lithium-ion battery life based on charge process for different applications," *Applied Energy*, vol. 292, no. October 2020, 2021, doi: 10.1016/j.apenergy.2021.116897.

[60] Q. Zhang *et al.*, "A deep learning method for lithium-ion battery remaining useful life prediction based on sparse segment data via cloud computing system," *Energy*, vol. 241, p. 122716, 2022, doi: 10.1016/j.energy.2021.122716.

[61] P. G. Anselma, P. Kollmeyer, J. Lempert, Z. Zhao, G. Belingardi, and A. Emadi, "Battery state-of-health sensitive energy management of hybrid electric vehicles: Lifetime prediction and ageing experimental validation," *Applied Energy*, vol. 285, no. December 2020, p. 116440, 2021, doi: 10.1016/j.apenergy.2021.116440.

[62] N. Omar *et al.*, "Lithium iron phosphate based battery - Assessment of the aging parameters and development of cycle life model," *Applied Energy*, vol. 113, pp. 1575–1585, 2014, doi: 10.1016/j.apenergy.2013.09.003.

[63] M. Ecker *et al.*, "Development of a lifetime prediction model for lithium-ion batteries based on extended accelerated aging test data," *Journal of Power Sources*, vol. 215, pp. 248–257, 2012, doi: 10.1016/j.jpowsour.2012.05.012.

[64] G. Suri and S. Onori, "A control-oriented cycle-life model for hybrid electric vehicle lithium-ion batteries," *Energy*, vol. 96, pp. 644–653, 2016, doi: 10.1016/j.energy.2015.11.075.

[65] L. Yan *et al.*, "A hybrid method with cascaded structure for early-stage remaining useful life prediction of lithium-ion battery," *Energy*, vol. 243, p. 123038, 2022, doi: 10.1016/j.energy.2021.123038.

[66] W. Gu, Z. Sun, X. Wei, and H. Dai, “A capacity fading model of lithium-ion battery cycle life based on the kinetics of side reactions for electric vehicle applications,” *Electrochimica Acta*, vol. 133, pp. 107–116, 2014, doi: 10.1016/j.electacta.2014.03.186.

[67] C. Kupper and W. G. Bessler, “ Multi-Scale Thermo-Electrochemical Modeling of Performance and Aging of a LiFePO 4 /Graphite Lithium-Ion Cell ,” *Journal of The Electrochemical Society*, vol. 164, no. 2, pp. A304–A320, 2017, doi: 10.1149/2.0761702jes.

[68] J. M. Reniers, G. Mulder, and D. A. Howey, “Review and Performance Comparison of Mechanical-Chemical Degradation Models for Lithium-Ion Batteries,” *Journal of The Electrochemical Society*, vol. 166, no. 14, pp. A3189–A3200, 2019, doi: 10.1149/2.0281914jes.

[69] Y. Che, Z. Deng, X. Lin, and L. Hu, “Predictive Battery Health Management With Transfer Learning and Online Model Correction,” *IEEE Transactions on Vehicular Technology*, vol. 70, no. 2, pp. 1269–1277, 2021.

[70] Y. Che, Z. Deng, X. Tang, X. Lin, X. Nie, and X. Hu, “Lifetime and Aging Degradation Prognostics for Lithium-ion Battery Packs Based on a Cell to Pack Method,” *Chinese Journal of Mechanical Engineering*, vol. 35, no. 1, 2022, doi: 10.1186/s10033-021-00668-y.

[71] W. Li, N. Sengupta, P. Dechent, D. Howey, A. Annaswamy, and D. U. Sauer, “One-shot battery degradation trajectory prediction with deep learning,” *Journal of Power Sources*, vol. 506, p. 230024, 2021, doi: 10.1016/j.jpowsour.2021.230024.

[72] P. M. Attia *et al.*, “Closed-loop optimization of fast-charging protocols for batteries with machine learning,” *Nature*, vol. 578, no. 7795, pp. 397–402, 2020, doi: 10.1038/s41586-020-1994-5.

[73] J. Zhu *et al.*, “Data-driven capacity estimation of commercial lithium-ion batteries from voltage relaxation,” *Nature Communications*, vol. 13, no. 1, pp. 1–10, 2022, doi: 10.1038/s41467-022-29837-w.

[74] “Oxford Battery Degradation Dataset 1,” 2017. https://ora.ox.ac.uk/objects/uuid:03ba4b01-cfed-46d3-9b1a-7d4a7bdf6fac.

[75] R. Xiong *et al.*, “A data-driven method for extracting aging features to accurately predict the battery health,” *Energy Storage Materials*, vol. 57, no. January, pp. 460–470, 2023, doi: 10.1016/j.ensm.2023.02.034.

[76] A. Zaknich, “Probabilistic Neural Network Classifier,” *Neural Networks for Intelligent Signal Processing*, vol. 9, no. 2, pp. 157–189, 2003, doi: 10.1142/9789812796851_0007.

[77] G. Dong, W. Han, and Y. Wang, “Dynamic Bayesian Network-Based Lithium-Ion Battery Health Prognosis for Electric Vehicles,” *IEEE Transactions on Industrial Electronics*, vol. 68, no. 11, pp. 10949–10958, 2021, doi: 10.1109/TIE.2020.3034855.

[78] H. Yao, D. lai Zhu, B. Jiang, and P. Yu, “Negative Log Likelihood Ratio Loss for Deep Neural Network Classification,” *Advances in Intelligent Systems and Computing*, vol. 1069, pp. 276–282, 2020, doi: 10.1007/978-3-030-32520-6_22.

[79] X. Liu *et al.*, “Self-supervised Learning: Generative or Contrastive,” *IEEE Transactions on Knowledge and Data Engineering*, vol. 35, no. 1, pp. 857–876, 2021, doi: 10.1109/TKDE.2021.3090866.

[80] M. Noroozi, A. Vinjimoor, P. Favaro, and H. Pirsiavash, “Boosting Self-Supervised Learning via Knowledge Transfer,” *Proceedings of the IEEE Computer Society Conference on Computer Vision and Pattern Recognition*, pp. 9359–9367, 2018, doi: 10.1109/CVPR.2018.00975.

[81] W. J. Murdoch, C. Singh, K. Kumbier, R. Abbasi-Asl, and B. Yu, “Definitions, methods, and applications in interpretable machine learning,” *Proceedings of the National Academy of Sciences of the United States of America*, vol. 116, no. 44, pp. 22071–22080, 2019, doi: 10.1073/pnas.1900654116.

[82] X. Feng, M. Ouyang, X. Liu, L. Lu, Y. Xia, and X. He, “Thermal runaway mechanism of lithium ion battery for electric vehicles: A review,” *Energy Storage Materials*, vol. 10, no. December 2016, pp. 246–267, 2018, doi: 10.1016/j.ensm.2017.05.013.

[83] J. Tian, R. Xiong, and W. Shen, “State-of-Health Estimation Based on Differential Temperature for Lithium Ion Batteries,” *IEEE Transactions on Power Electronics*, vol. 35, no. 10, pp. 10363–10373, 2020, doi: 10.1109/TPEL.2020.2978493.

[84] R. Xiong, L. Li, and J. Tian, “Towards a smarter battery management system: A critical review on battery state of health monitoring methods,” *Journal of Power Sources*, vol. 405, no. 5, pp. 18–29, 2018, doi: 10.1016/j.jpowsour.2018.10.019.

[85] S. Wang, H. Miao, J. Li, and J. Cao, "Spatio-Temporal Knowledge Transfer for Urban Crowd Flow Prediction via Deep Attentive Adaptation Networks," *IEEE Transactions on Intelligent Transportation Systems*, vol. 23, no. 5, pp. 4695–4705, 2022, doi: 10.1109/TITS.2021.3055207.

[86] M. Ghifary, W. Bastiaan Kleijn, and M. Zhang, "Domain adaptive neural networks for object recognition," *Lecture Notes in Computer Science (including subseries Lecture Notes in Artificial Intelligence and Lecture Notes in Bioinformatics)*, vol. 8862, pp. 898–904, 2014, doi: 10.1007/978-3-319-13560-1.

[87] E. Tzeng, J. Hoffman, N. Zhang, K. Saenko, and T. Darrell, "Deep Domain Confusion: Maximizing for Domain Invariance," 2014, [Online]. Available: http://arxiv.org/abs/1412.3474.

[88] T. Han, Z. Wang, and H. Meng, "End-to-end capacity estimation of Lithium-ion batteries with an enhanced long short-term memory network considering domain adaptation," *Journal of Power Sources*, vol. 520, no. December 2021, p. 230823, 2022, doi: 10.1016/j.jpowsour.2021.230823.

[89] X. Li, C. Yuan, Z. Wang, and J. Xie, "A data-fusion framework for lithium battery health condition Estimation Based on differential thermal voltammetry," *Energy*, vol. 239, p. 122206, 2022, doi: 10.1016/j.energy.2021.122206.

[90] R. Cipolla, Y. Gal, and A. Kendall, "Multi-task Learning Using Uncertainty to Weigh Losses for Scene Geometry and Semantics," *Proceedings of the IEEE Computer Society Conference on Computer Vision and Pattern Recognition*, pp. 7482–7491, 2018, doi: 10.1109/CVPR.2018.00781.

[91] P. M. Attia *et al.*, "'Knees' in Lithium-Ion Battery Aging Trajectories," *Journal of The Electrochemical Society*, 2022, doi: https://doi.org/10.1149/1945-7111/ac6d13.

[92] H. You *et al.*, "Nonlinear health evaluation for lithium-ion battery within full-lifespan," *Journal of Energy Chemistry*, vol. 72, pp. 333–341, 2022, doi: 10.1016/j.jechem.2022.04.013.

[93] Z. Mao, M. Farkhondeh, M. Pritzker, M. Fowler, and Z. Chen, "Calendar Aging and Gas Generation in Commercial Graphite/NMC-LMO Lithium-Ion Pouch Cell," *Journal of The Electrochemical Society*, vol. 164, no. 14, pp. A3469–A3483, 2017, doi: 10.1149/2.0241714jes.

[94] Y. Chen *et al.*, "A review of lithium-ion battery safety concerns: The issues,

strategies, and testing standards," *Journal of Energy Chemistry*, vol. 59, pp. 83–99, 2021, doi: 10.1016/j.jechem.2020.10.017.

[95] W. Diao, J. Kim, M. H. Azarian, and M. Pecht, "Degradation modes and mechanisms analysis of lithium-ion batteries with knee points," *Electrochimica Acta*, vol. 431, no. September, p. 141143, 2022, doi: 10.1016/j.electacta.2022.141143.

[96] V. Satopää, J. Albrecht, D. Irwin, and B. Raghavan, "Finding a 'kneedle' in a haystack: Detecting knee points in system behavior," *Proceedings - International Conference on Distributed Computing Systems*, pp. 166–171, 2011, doi: 10.1109/ICDCSW.2011.20.

[97] X. Jia, C. Zhang, Y. Li, C. Zou, L. Y. Wang, and X. Cai, "Knee-Point-Conscious Battery Aging Trajectory Prediction Based on Physics-Guided Machine Learning," *IEEE Transactions on Transportation Electrification*, vol. PP, p. 1, 2023, doi: 10.1109/TTE.2023.3266386.

PART II PUBLICATIONS

ISSN (online): 2446-1636
ISBN (online): 978-87-7573-582-2

AALBORG UNIVERSITY PRESS